

Università degli studi della Calabria

Dipartimenti di Chimica e di Fisica

Dottorato di Ricerca in

Scienze e Tecnologie delle Mesofasi e dei Materiali Molecolari

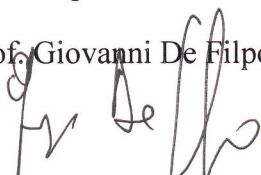
XXI Ciclo

Settore disciplinare CHIM/02

Study of composite systems of polymers and liquid crystals with homeotropic orientation

Supervisore

Prof. Giovanni De Filpo



Coordinatore

Prof. Carlo Versace



Candidato

Dott.ssa Maria Caterina Gallucci



Anno Accademico 2008 – 2009

To Chiara..

... Andrea, my mom and daddy

INDEX

| | |
|--|-----------|
| Introduction | i |
| | |
| CHAPTER 1: Liquid Crystals | |
| <i>1.1 The history</i> | <i>1</i> |
| <i>1.2 Liquid crystals as fourth state of matter</i> | <i>2</i> |
| <i>1.3 Liquid crystal phases</i> | <i>6</i> |
| 1.3.1 <i>Nematic liquid crystal phase</i> | <i>6</i> |
| 1.3.2 <i>Smectic liquid crystal phase</i> | <i>7</i> |
| 1.3.3 <i>Chiral nematic liquid crystal phase</i> | <i>10</i> |
| 1.3.4 <i>Chiral smectics liquid crystal phase</i> | <i>11</i> |
| 1.3.5 <i>Columnar liquid crystals phases</i> | <i>13</i> |
| <i>1.4 Physical properties of liquid crystals</i> | <i>13</i> |
| 1.4.1 <i>Orientational order parameter</i> | <i>13</i> |
| 1.4.2 <i>Dielectric anisotropy</i> | <i>14</i> |
| 1.4.3 <i>Diamagnetic anisotropy</i> | <i>16</i> |
| 1.4.4 <i>Optical anisotropy</i> | <i>18</i> |
| 1.4.5 <i>Elastic constants</i> | <i>19</i> |
| 1.4.6 <i>Anchoring energy</i> | <i>20</i> |
| References | 22 |
| | |
| CHAPTER 2: PDLC | |
| <i>2.1 Introduction</i> | <i>23</i> |
| <i>2.2 Nematic configurations within droplets</i> | <i>23</i> |
| <i>2.3 Preparation methods for PDLC films</i> | <i>25</i> |

| | | |
|--------------|---|-----------|
| 2.3.1 | <i>Encapsulation</i> | 25 |
| 2.3.2 | <i>Phase separation methods</i> | 26 |
| 2.3.2.1 | <i>TIPS</i> | 26 |
| 2.3.2.2 | <i>SIPS</i> | 27 |
| 2.3.2.3 | <i>PIPS</i> | 27 |
| 2.4 | <i>Polymer networks</i> | 28 |
| 2.5 | <i>Aspect of film structure</i> | 29 |
| 2.6 | <i>Liquid crystal/polymer phase separation</i> | 30 |
| 2.6.1 | <i>Phase diagrams for LC/monomer mixtures</i> | 30 |
| 2.6.2 | <i>Phase separation in the binodal and spinodal regimes</i> | 32 |
| 2.7 | <i>Electro-optical effects</i> | 33 |
| 2.7.1 | <i>Light scattering and index matching</i> | 33 |
| 2.7.2 | <i>PDLC film operating voltage</i> | 35 |
| 2.7.3 | <i>Switching times</i> | 38 |
| 2.8 | <i>Reverse mode devices</i> | 39 |
| | References | 43 |

CHAPTER 3: Alignment technologies

| | | |
|------------|--|-----------|
| 3.1 | <i>Introduction</i> | 46 |
| 3.2 | <i>Liquid crystal alignments</i> | 46 |
| 3.3 | <i>Rubbing Technologies</i> | 50 |
| 3.3.1 | <i>The rubbing process</i> | 50 |
| 3.3.2 | <i>Alignment materials and mechanisms of the rubbing process</i> | 51 |
| 3.4 | <i>Non-rubbing Methods</i> | 54 |
| 3.4.1 | <i>Introduction</i> | 54 |
| 3.4.2 | <i>Ion beam alignment.</i> | 56 |
| 3.4.3 | <i>Photoalignment</i> | 57 |

| | | |
|-------------------|--|-----------|
| 3.4.3.1 | <i>Alignment materials and mechanisms for the photoalignment</i> | |
| 3.4.3.2 | <i>Influence of UV light on display device characteristics</i> | 58 |
| 3.4.4 | <i>Oblique Evaporation Method</i> | 59 |
| 3.4.4.1 | <i>Alignment mechanism</i> | 59 |
| 3.4.5 | <i>LB membranes for the alignment layer</i> | 61 |
| 3.5 | <i>Liquid Crystalline Alignment on Chemically Treated Surfaces</i> | 63 |
| 3.5.1 | <i>Addition of surface active agents into liquid crystalline materials</i> | |
| 3.5.2 | <i>Treatment of the substrate surface by active surface agents</i> | 64 |
| 3.5.3 | <i>Pyridinium salts</i> | 67 |
| References | | 68 |

CHAPTER 4: Impurities characterization in the bis{4-[(6-acryloxy)hexyloxy]benzoate}-1,4-phenylene (C6H) LC monomer

| | | |
|------------|--|-----------|
| 4.1 | <i>Introduction</i> | 71 |
| 4.2 | <i>The history of our interest for C6H</i> | 72 |
| 4.3 | <i>Synthesis of bis{4-[(6acryloxy)hexyloxy]benzoate}1,4-phenylene(C6H)</i> | 73 |
| 4.4 | <i>Characterization of the monomer</i> | 75 |
| 4.4.1 | <i>DSC</i> | 76 |
| 4.4.2 | <i>TLC</i> | 78 |
| 4.4.3 | <i>SEM/EDS microanalysis</i> | 79 |
| 4.4.4 | <i>FTIR</i> | 80 |
| 4.4.5 | <i>MALDI TOF-MS</i> | 83 |
| 4.4.6 | <i>¹H-NMR</i> | 85 |
| 4.5 | <i>Impurities generation mechanisms</i> | 92 |
| 4.6 | <i>Reproduction of aligning “impurities” in C6H monomer</i> | 93 |
| 4.7 | <i>Characterization of the products of reaction between commercial C6H and DMAP</i> | 96 |

| | | |
|-------|--------------------------------|------------|
| 4.7.1 | <i>FTIR</i> | 96 |
| 4.7.2 | <i>MALDI MS-MS experiments</i> | 99 |
| 4.7.3 | <i>¹H - NMR</i> | 103 |
| 4.7.4 | <i>¹³C - NMR</i> | 112 |
| | 4.8 Conclusions | 116 |
| | References | 118 |

Chapter 5: High contrast Reverse Mode PDLC Films: morphologic and electro-optical studies

| | | |
|-----|--|------------|
| 5.1 | <i>Reverse mode PDLC</i> | 120 |
| 5.2 | <i>Films preparation methodology</i> | 122 |
| 5.3 | <i>Electro-optical measurements</i> | 124 |
| 5.4 | <i>Morphologic analysis of PDLC films</i> | 129 |
| 5.5 | <i>Model for E_{th} and response times t_{off}</i> | 134 |
| 5.6 | <i>Conclusions</i> | 137 |
| | References | 139 |

Acknowledgments

Introduction

This work is related to the optimization of methodologies to obtain electro-optical devices like PDLC Reverse Mode, obtained by photo-polymerization of a mixture of diacrylates monomers and a liquid crystal with negative dielectric anisotropy, developed at Calabria Universityⁱ.

Previous works demonstrate the possibility to obtain PDLC electro-optical Reverse Mode film by using the bis{4-[(6-acryloxy)hexyloxy]benzoate}-1,4-phenylene (C6H) and bis{4-[6-(acryloxy)hexyloxy]benzoate}-4,4'-bicyclohexyl (AHBB) Liquid Crystal monomers, synthesized at Calabria University. Even if the precursor Liquid Crystal mixtures contained only 16-20% of the above mentioned monomers, a very good homeotropic orientation of the precursor liquid crystal mixture could be achieved without pre-treating of the glass substrate. The alignment process within liquid crystal devices is very important and influence the cost, time and technology required for the production of composite systems, i.e. PDLC and PSLC, and technology displays.

The very lucky behavior encountered in the case of C6H and AHBB behavior was attributed to the presence of small percentages of “impurities” generated during the synthesis process, since the spontaneous homeotropic alignment of PDLC precursor was not observed when C6H commercial LC monomer, was used. The nature of the aligning impurities, however, was not identified.

The aim of this thesis, was, from one side, to give further insight with respect to the morphology and electro-optical response of the PDLC Reverse Mode system realized at Calabria University, and, from another point of view, to clarify the role of possible synthesis impurities, with respect to the generation of uniform homeotropic alignment into PDLC precursor mixtures. The presentation has been divided into the following parts:

First off all, the product employed in the C6H monomer synthesis, as well as the synthesis intermediate products, were characterized. This characterization work was performed by using Spectroscopic, Chromatographic, electron and optical Microscopy techniques.. The results obtained from the interpretation of

these experimental data converge towards a common display of sub-products, and are illustrated in the chapter 4 of this thesis.

As second step, the mechanisms of formation of the identified impurities were studied. Experimental work has been performed in order to reproduce the impurity formation in the pure commercial C6H monomer. The variation in the aligning capacity on glass of the C6H was determined, after inducing, through chemical reactions, the formation of given impurities. The base idea was to develop a simple and reproducible method to obtain LC monomer mixtures, showing a homeotropic spontaneous alignment on ITO coated glass support, without recurring to surface pretreatment. This argument is also treated in chapter 4.

The electro-optical and Morphologic properties of Reverse Mode PDLC film, obtained by using the above mentioned aligning methodologies, in comparison with those of analogous films obtained through surface pre-treatments, were investigated. To complete the analysis, PDLC with higher LC monomer content and PDLC with only AHBB monomer, were studied in order to establish systems with optimal electro-optical contrast, lower operational voltages and faster response time.

Finally, a simple model to account for the threshold voltages and switching times of reverse Mode PDLC films, as a function of morphologic parameters, has been developed. These items are reported in chapter 5.

For completeness, three chapters were added to present the state of art on the research argument treated in this thesis. In particular: Chapter 1 reports a general overview of liquid crystal materials; Chapter 2 concerns the properties of PDLC films and Chapter 3 summarize the alignment methodologies useful for the LC device preparation.

ⁱ *G. Chidichimo, G. De Filpo, European Patent n° WO9816865 (1997) ; G. Chidichimo, G. De Filpo, European Patent n°WO9900464 (1997), U.S. Patent n°6,383,577 B1 (2002)*

CHAPTER 1: Liquid Crystals

1.1 The history

The discovery of liquid crystals is thought to have occurred nearly 150 years ago although its significance was not fully understood until over a hundred years later. Around the middle of the last century Virchow, Mettenheimer and Valentin found that the nerve fiber they were studying formed a fluid substance when left in water, which exhibited a strange behavior when viewed using polarized light. They did not realize this was a different phase but they are attributed with the first observation of liquid crystals.

Later, in 1877, Otto Lehmann used a polarizing microscope with a heated stage to investigate the phase transitions of various substances. He found that one substance would change from a clear liquid to a cloudy liquid before crystallizing but he thought that this was simply an imperfect phase transition from liquid to crystalline. In 1888 Reinitzer ⁽¹⁾ observed that a material known as cholesteryl benzoate had two distinct melting points. In his experiments, Reinitzer increased the temperature of a solid sample and watched the crystal change into a hazy liquid. As he increased the temperature further, the material changed again into a clear, transparent liquid. Because of this early work, Reinitzer is often credited with discovering a new phase of matter. He has consequently been given the credit for the discovery of the liquid crystalline phase. Up till 1890 all the liquid crystalline substances that had been investigated, had been naturally occurring and it was then that the first synthetic liquid crystal, p- azoxyanisole, was produced by Gatterman and Ritschke. Subsequently more liquid crystals were synthesized and it is now possible to produce liquid crystals with specific predetermined material properties.

In the beginning of this century George Freidel conducted many experiments on liquid crystals and he explained the orienting effect of electric fields and the presence of defects in liquid crystals. In 1922 he proposed a classification of liquid crystals based upon the different molecular orderings of each substance. It was between 1922 and the World War II that Oseen and Zocher developed a

mathematical basis for the study of liquid crystals⁽²⁾⁽³⁾.

After the start of the war many scientists believed that the important features of liquid crystals had been already discovered and it was not until the 1950's that work by Brown in America, Chistiakoff in the Soviet Union and Gray and Frank in England led to a revival of interest in liquid crystals. Maier and Saupe⁽⁴⁾ formulated a microscopic theory of liquid crystals; Frank⁽⁵⁾ and later Leslie⁽⁶⁾ and Ericksen⁽⁷⁾ developed continuum theories for static and dynamic systems and in 1968 scientists from RCA first demonstrated a liquid crystal display.

The interest in the study of liquid crystals has grown ever since, partly due to the great variety of phenomena exhibited by liquid crystals and partly because of the enormous commercial interest and importance of liquid crystal displays. As research on this field continues and as new applications are developed, the role of liquid crystals in modern technology will continue to grow.

1.2 Liquid crystals as fourth state of matter

The three common states of the matter: solid, liquid and gas, are different because the molecules in each state have a different degree of order.

In the solid state there exists a rigid arrangement of molecules, which stay in fixed positions and orientations with a small amount of variation due to molecular vibrations. To maintain this arrangement, large attractive forces are required to hold the molecules in piece and therefore a solid is difficult to deform.

In the liquid phase the molecules have no fixed positions or orientations and are free to move in a random fashion; consequently, the liquid state has less order than the solid state. The random motions of the molecules mean that the intermolecular attractive forces are not strong as in solids but are only strong enough to keep the liquid molecules fairly close together. A liquid can therefore be easily deformed.

In the gas state the random motion of the molecules overcomes the intermolecular forces, and the molecules spread out to fill any container that holds them. The order in a liquid, which derives from the closeness of the molecules, is lost in a gas. The probability of molecules in a certain region being in a rigid arrangement, and having the same orientation can be used to define a positional

and orientational order. These parameters have the greatest value in the solid state and the least one in the gaseous state.

A liquid crystalline phase occurs in some substances in a temperature region between the solid and liquid states. In this state the substance possesses properties of both liquids and solids. A liquid crystal is a fluid like a liquid but it is anisotropic, in its optical and electro-magnetic characteristics, like a solid. When the liquid crystal is formed from the isotropic state, some amount of positional or orientational order is gained. It is this order that accounts for the anisotropies of the substance. The distinguishing characteristic of the liquid crystalline state is the tendency of the molecules (mesogens) to point along a common axis, called the director. This is in contrast to molecules in the liquid phase, which have no intrinsic order. In the solid state, molecules are highly ordered and have little translational freedom. The characteristic orientational order of the liquid crystal state is between the traditional solid and liquid phases and this is the origin of the term mesogenic state, used synonymously with liquid crystal state. Note the average alignment of the molecules for each phase (Fig.1.1):

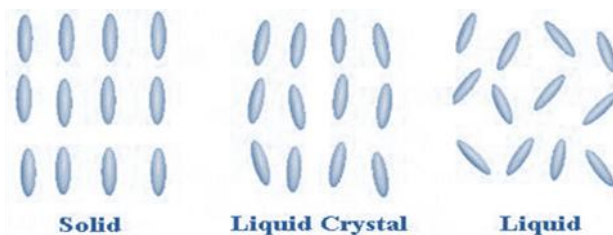


Fig.1.1 Average alignment of the molecules: a) solid phase, b) liquid crystal phase, c) liquid phase.

It is sometimes difficult to determine whether a material is in a crystal or liquid crystal state. Crystalline materials demonstrate long range periodic order in three dimensions ⁽⁸⁾. By definition, an isotropic liquid has no orientational order. Substances that are not as ordered as a solid, yet have some degree of alignment, are thus properly called liquid crystals. Liquid crystals can be classified into two main categories:

- thermotropic liquid crystals;
- lyotropic liquid crystals.

While these two types of liquid crystals are distinguished by the mechanisms that drive their self-organization, they are similar in many ways. Thermotropic transitions occur in most liquid crystals, and they are defined by the fact that the transitions to the liquid crystalline state are thermally induced. That is, one can arrive at the liquid crystalline state by raising the temperature of a solid *and/or* lowering the temperature of a liquid. Thermotropic liquid crystals can be classified into two types: enantiotropic liquid crystals, which can be changed into the liquid crystal state from either lowering the temperature of a liquid or raising of the temperature of a solid, and monotropic liquid crystals, which can only be changed into the liquid crystal state from either an increase in the temperature of a solid or a decrease in the temperature of a liquid, but not both. In general, thermotropic mesophases occur because of anisotropic dispersion forces between the molecules and because of packing interactions⁽⁹⁾⁽¹⁰⁾.

There are mainly two types of mesogenic molecules which can originate thermotropic liquid crystals: discotics and rod-shaped molecules.

Discotics are flat disc-like molecules consisting of a core of adjacent aromatic rings. This allows for two-dimensional columnar ordering. Rod-shaped molecules have an elongated, anisotropic geometry, which allows for preferential alignment along one spatial direction.

As showed in Fig 1.2, rod-like molecules (a) organize themselves into layers, whereas disc-like molecules (b) form columns that can be arranged parallel to each other in a two-dimensional lattice.

A bend introduced in the rigid core leads to 'banana-shaped' molecules (c). The rotation of these molecules around their long axis is restricted and they adopt a directed order within the layers. Depending on the bending direction in adjacent layers, either antiferroelectric or ferroelectric smectic phases may result.

Molecules with a conical shape (d) can lead to a polar order within columns. The polar direction of neighbouring columns may be parallel or anti-parallel.

Sawamura⁽¹¹⁾ have made a 'shuttlecock-shaped' molecule (e) based on the C₆₀ molecule, whose distinctive shape leads to directed organization in columns⁽¹²⁾.

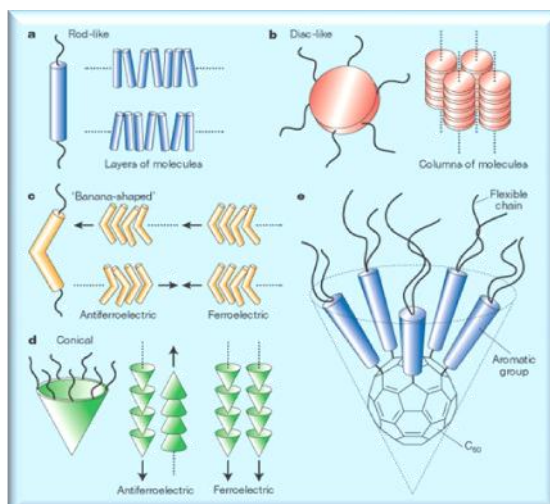


Fig.1.2 Shape-dependent organization of Liquid crystal molecules

In contrast to thermotropic mesophases, lyotropic liquid crystal transitions occur both by the influence of solvents, and by change in temperature (Fig 1.3). Lyotropic mesophases occur as a result of solvent-induced aggregation of the constituent mesogens into anisotropic micellar structures. Lyotropic mesogens are typically amphiphilic, meaning that they are composed of both lyophilic (solvent-attracting) and lyophobic (solvent-repelling) parts. This causes them to form micellar structures in the presence of a solvent, since the lyophobic ends will collect together, out of the solvent environment. As the concentration of the solution is increased and the solution is cooled, the micelles increase in size and eventually coalesce. This process separates the newly formed liquid crystalline state from the solvent. A very large number of chemical compounds are known to exhibit one or several liquid crystalline phases. Despite significant differences in chemical composition, these molecules have some common features such as anisotropy of molecular shape and physical properties⁽¹³⁾.

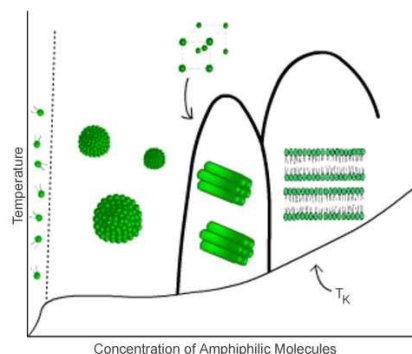


Fig 1.3 Lyotropic mesophases depending on the Temperature and amphiphile concentration

1.3 Liquid crystal phases⁽¹⁴⁾

Most liquid crystal compounds exhibit polymorphism, or a condition where more than one phase is observed in the liquid crystalline state. The term mesophase is used to describe the "subphases" of liquid crystal materials. Mesophases are formed by changing the amount of order in the sample, either by imposing order in only one or two dimensions, or by allowing the molecules to have a degree of translational motion⁽¹⁵⁾

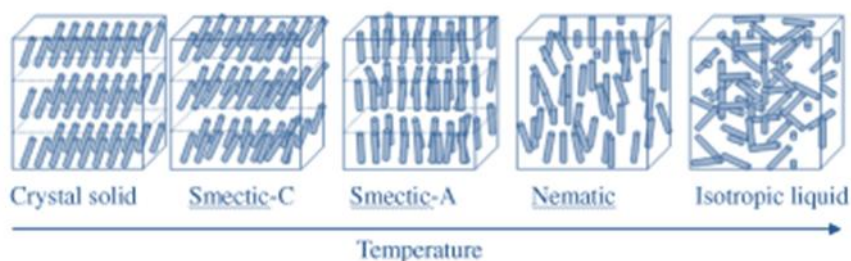


Fig.1.4 Schematic representation of the liquid crystal phases for rod-like molecules

1.3.1 Nematic liquid crystal phase

It is characterized by molecules that have no positional order but tend to point in the same direction (see Fig 1.5). This reordering is thought to be due to the packing constraints of the molecules. This claim is supported by the fact that most liquid crystal molecules tend to be long thin molecules with a rigid central region.

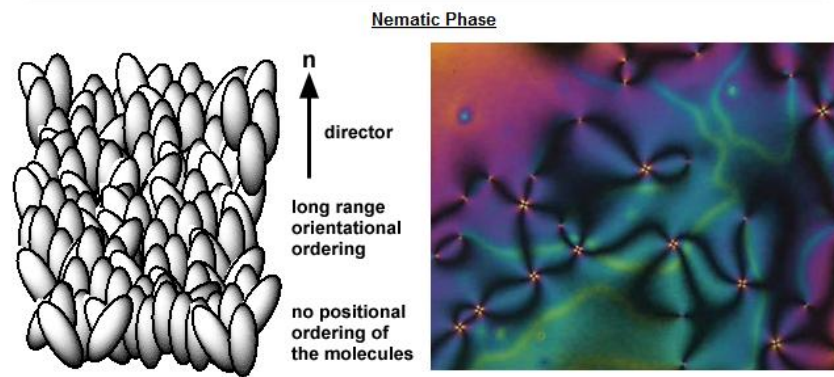


Fig 1.5 Schematic representation of the nematic mesophase(left) and typical texture corresponding, showed by Polarized Optical Microscopy(right)

Molecules in this phase possess three degree of translational freedom, and they can move in all the directions. The viscosity of the nematic liquid crystals is similar to that of the isotropic liquid.

1.3.2 Smectic liquid crystal phase

The smectic state is another distinct mesophase present in some liquid crystal substances. Molecules in this phase show a degree of translational state not present in the nematic. In the smectic state, the molecules maintain the general orientational order of nematics, but in addition tend to align themselves in layers or planes. Motion is restricted to within these planes, and separate planes are observed to flow past each other. Within each layer the liquid crystal is essentially a two dimensional nematic liquid crystal. The increased order means that the smectic state is more "solid-like" than the nematic. This positional ordering may be described in terms of the density of the mass centers of the molecules:

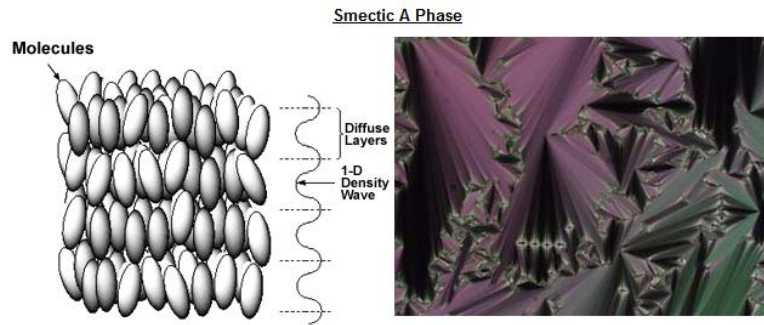
$$\rho(z) = \rho_o [1 + \psi \cos(2\pi z/d)] \quad (1.1)$$

where z is the coordinate parallel to the layer normal; the average density of the fluid is ρ_o , d is the distance between layers and ψ is the order parameter. When $|\psi|=0$ there is no layering and the material is nematic, but if $|\psi|>0$ then some amount of sinusoidal layering exists and the material is smectic. There are many

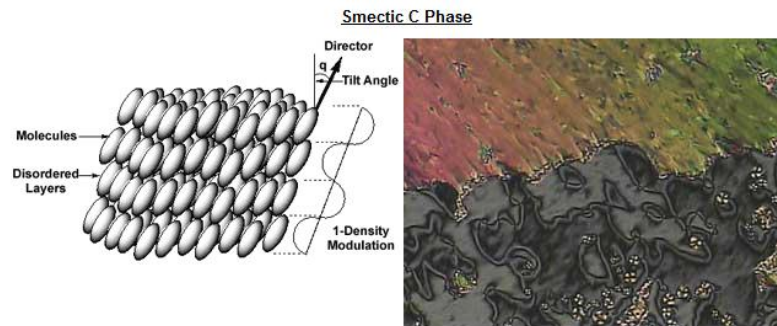
types of smectic materials ⁽¹⁶⁾. In particular, in the smectic-A mesophase, the director is perpendicular to the smectic plane, and there is no particular positional order in the layer (Fig.1.6 a).

In the smectic-C mesophase (Fig.1.6 b), molecules are arranged as in the smectic-A mesophase, but the director is at a constant tilt angle measured normally to the smectic plane. In some smectic materials, called Sm-CA (Fig 1.6 c) or Anti-Ferroelectric Liquid Crystal (AFLC), the direction of this tilt may alternate to form a so called "herringbone structure". Smectic materials have potential advantages over nematics when used in liquid crystal displays. They exhibit better viewing angle characteristics, contrast ratio and can operate at high speed.

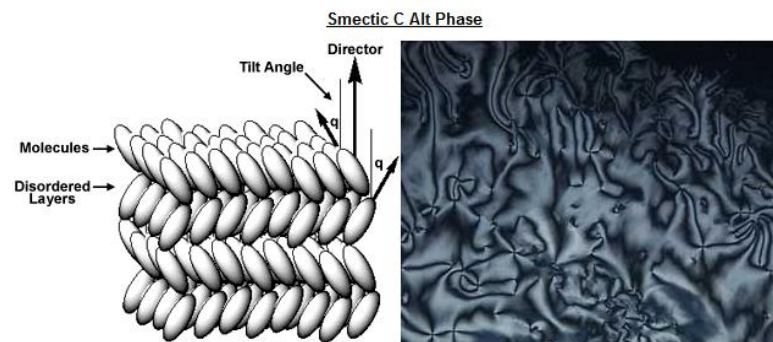
Similarly, the smectic-B mesophase (fig 1.6 d) orients with the director perpendicular to the smectic plane, but the molecules are arranged into a network of hexagons within the layer.



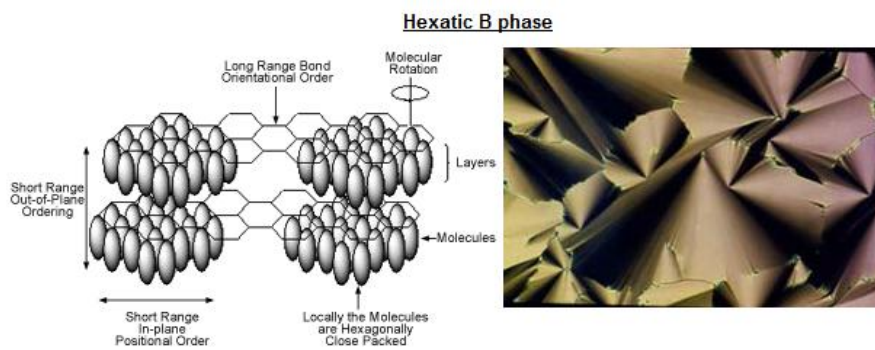
a



b



c



d

Fig.1.6 From the top: Smectic A (a), Smectic C(b), Smectic CA (c) and (Hexatic) Smectic B phases (d)

1.3.3 Chiral nematic liquid crystal phase

This phase is typically composed of nematic mesogenic molecules containing a chiral center which produces intermolecular forces that favor alignment between molecules at a slight angle to one another. This leads to the formation of a structure which can be visualized as a stack of very thin 2-D nematic-like layers with the director in each layer twisted with respect to those above and below. This induces a helical director configuration in which the director rotates through the material (Fig.1.7). The molecules shown are merely representations of the many chiral nematic mesogens lying in the slabs of infinitesimal thickness with a distribution of orientation around the director. This is not to be confused with the planar arrangement found in smectic mesophases.

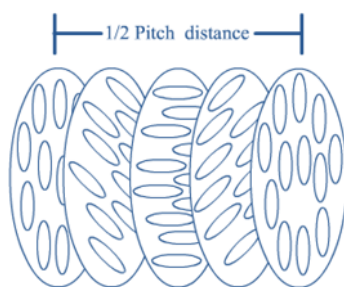


Fig.1.7 Schematic view of the helical director configuration.

Mesophases having this type of structure are called cholesteric mesophases. An important characteristic of the cholesteric mesophase is the pitch, p , which is defined as the distance the director rotates one full turn in the helix (see Fig 1.9) A by-product of the helical structure of the chiral nematic phase is its ability to selectively reflect light of wavelengths equal to the pitch length, so that a color will be reflected when the pitch is equal to the corresponding wavelength of light in the visible spectrum. Due to this phenomena, cholesterics change color when the temperature changes. The effect is based on the temperature dependence of the gradual change in director orientation between successive layers, which modifies the pitch length resulting in an alteration of the wavelength of reflected light according to the temperature. The angle at which the director changes, can be made larger, and thus tighten the pitch, by increasing the temperature of the

molecules, hence giving them more thermal energy.

Similarly, decreasing the temperature of the molecules increases the pitch length of the chiral nematic liquid crystal. This makes it possible to build a liquid crystal thermometer that displays the temperature of its environment by the reflected color. Mixtures of various types of these liquid crystals are often used to create sensors with a wide variety of responses to temperature change. Such sensors are used for thermometers often in the form of heat sensitive films. In the fabrication of films, since putting chiral nematic liquid crystals directly on a black background would lead to degradation and perhaps contamination, the crystals are micro-encapsulated into particles of very small dimensions. The particles are then treated with a binding material that will shrink upon curing so as to flatten the microcapsules and produce the best alignment for brighter colors. Adjusting the chemical composition can also control the wavelength of the reflected light, since cholesterics can either consist of exclusively chiral molecules or of nematic molecules with a chiral dopant dispersed throughout. In this case, the dopant concentration is used to adjust the chirality and thus the pitch.

1.3.4 Chiral smectics liquid crystal phase

In a similar way to chiral nematics there are chiral forms of smectic phases. Fig.1.8 shows schematically a chiral smectic C material, denoted by smectic-C*. Consistent with the smectic-C, the director makes a tilt angle with respect to the smectic layer. The difference is that this angle rotates from layer to layer forming a helical structure. In other words, the director of the smectic-C* mesophase is not parallel or perpendicular to the layers, and it rotates from one layer to the next (see Fig 1.10).



Fig. 1.8-Director tilt in smectic-C phase*

This helix may be suppressed by placing the liquid crystal in a cell where the material is sandwiched between two glass plates. Such systems are said to be

surface stabilized. Once the helix is suppressed and the directors in each layer are forced to lie in the plane of the glass plates the chiral nature of the molecules creates a spontaneous polarization within each layer.

In some smectic mesophases, the molecules are affected by the various layers above and below them. Therefore, a small amount of three-dimensional order is observed. The Smectic-G phase is an example demonstrating this type of arrangement (Fig 1.11)

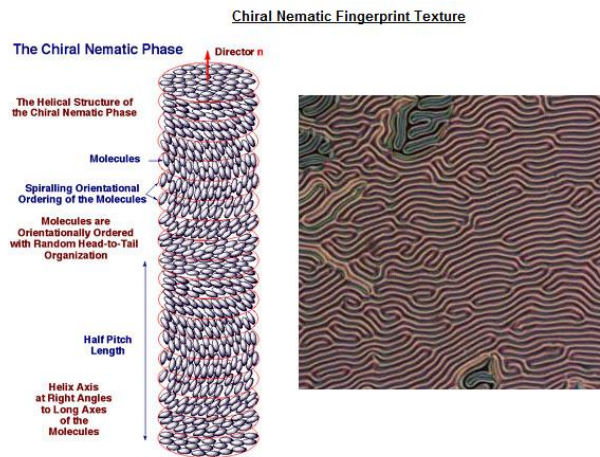


Fig 1.9 Chiral nematic phase

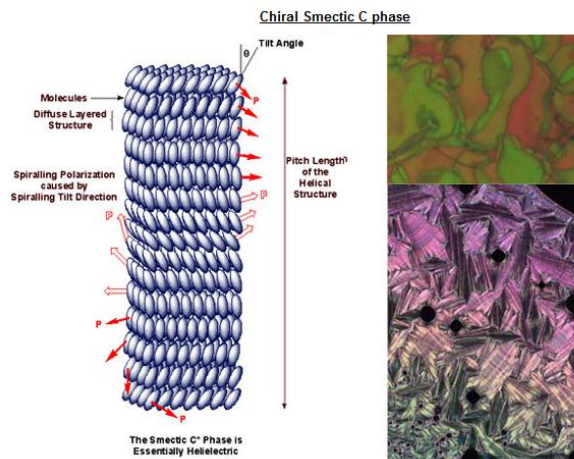


Fig 1.10 Chiral smectic C mesophases

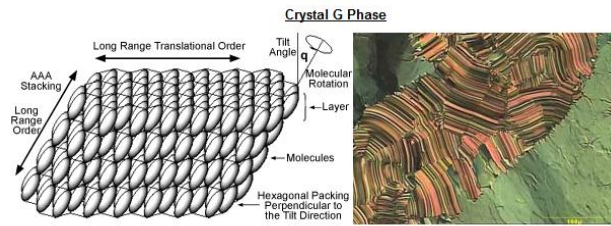


Fig 1.11 Smectic G phase

1.3.5 Columnar liquid crystals phases

These phases are different from the previous types because they are shaped like disks instead of long rods. This mesophase is characterized by stacked columns of molecules (Fig.1.12). The columns are packed together to form a two-dimensional crystalline array. The arrangement of the molecules within the columns and the arrangement of the columns themselves leads to new mesophases.

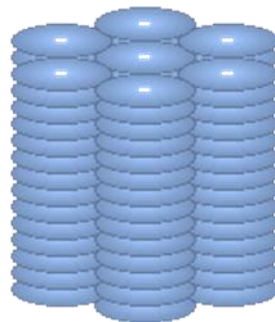


Fig. 1.12 Columnar liquid crystal phase.

1.4 Physical properties of liquid crystals

The physical behavior of liquid crystals can be divided into scalar and non scalar properties. A typical scalar property is the orientational order parameter S . Important non scalar properties are the dielectric, diamagnetic, optical, and elastic coefficients.

1.4.1 Orientational order parameter

To quantify just how much order is present in a liquid crystal material, an order parameter (S) is defined⁽¹⁷⁾. Traditionally, the order parameter is given as follows:

$$S = \frac{1}{2} \langle 3 \cos^2 \theta - 1 \rangle \quad (1.2)$$

In this equation θ is the angle between the axis of an individual molecule and the director of the liquid crystal. The brackets denote an average over all of the molecules in the sample (Fig.1.13).



Fig. 1.13 Tilt angle between the molecular axis and the director n .

In an isotropic liquid, where all the orientations are possible, the average of the cosine terms is zero, and therefore the order parameter is equal to zero. For a perfect crystal, the order parameter evaluates to one. Typical values for the order parameter of a liquid crystal range between 0.3 and 0.9, with the exact value a function of temperature, as a result of kinetic molecular motion.

When the molecular symmetry is not perfectly cylindrical, as in a real nematic liquid crystal, the order parameter becomes a matrix whose generic element is⁽¹⁸⁾:

$$S_{ij}^{\alpha\beta} = \frac{1}{2} \langle 3 \cos \theta_{ij} \cos \theta_{j\beta} - \delta_{ij} \delta_{\alpha\beta} \rangle \quad (1.3)$$

where ij and $\alpha\beta$ are respectively the coordinates of the fixed and molecular system; $\theta_{j\beta}$ is the angle between the j axis and the β axis; δ_{ij} and $\delta_{\alpha\beta}$ are Kroenecker's delta functions.

1.4.2 Dielectric anisotropy

The response of liquid crystal molecules to an electric field is the major characteristic utilized in industrial applications. The ability of the director to align along an external field is caused by the electric nature of the molecules.

Permanent electric dipoles result when one end of a molecule has a net positive charge while the other end has a net negative charge, giving an unbalanced distribution of charge. A liquid crystal molecule containing a permanent dipole might or might not be polar, depending on the symmetry of the dipoles within or attached to the main molecular body. When an external electric field is applied to the liquid crystal, the dipole molecules tend to orient themselves along the direction of the field. In the Fig.1.14, the black arrows represent the electric field vector and the red arrows show the electric force on the molecule.

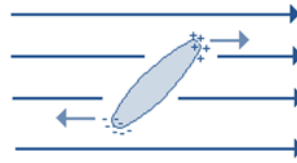


Fig. 1.14 Effect of the applied electric field on the dipole molecules

Even if a molecule does not form a permanent dipole, it can still be influenced by an electric field. In some cases, the field produces slight rearrangement of electrons and protons in molecules such that an *induced electric dipole* results. While not as strong as permanent dipoles, orientation with the external field still occurs. By applying an electric field along the long axis of the liquid crystal, the permittivity ϵ_{\parallel} (i.e. parallel to the director) is observed. However, the application of an electric field perpendicular to this axis results in a permittivity ϵ_{\perp} . The anisotropy of the dielectric permittivity $\Delta\epsilon$ is given by

$$\Delta\epsilon = \epsilon_{\parallel} - \epsilon_{\perp} \quad (1.4)$$

the dielectric anisotropy can be positive or negative depending by the orientation (respectively parallel or perpendicular) of the molecular dipole respect to the molecular axis. The electric energy density for volume unit depends on the electrical displacement according to the following equation:

$$E_{elctr} = -\frac{1}{4} \int DdE = -\left(\frac{\epsilon_{\perp}}{8\pi}\right)E - \left(\frac{\Delta\epsilon}{8\pi}\right)(n \cdot E)^2 \quad (1.5)$$

when $\Delta\varepsilon$ is positive there is a minimum in the energy if n and E are parallel, while when $\Delta\varepsilon$ is negative the energy reaches a minimum if n is perpendicular to E . Values for $\Delta\varepsilon$ of technically useful material range from between -6 to +50. The mean dielectric permittivity $\bar{\varepsilon}$ for a nematic liquid crystal can be described by ⁽¹⁹⁾:

$$\bar{\varepsilon} = \frac{\varepsilon_{\parallel} + 2\varepsilon_{\perp}}{3} \quad (1.6)$$

1.4.3 Diamagnetic anisotropy

The effects of magnetic fields on liquid crystal molecules are analogous to electric fields. Because magnetic fields are generated by moving electric charges, permanent magnetic dipoles are produced by electrons moving about atoms. When a magnetic field is applied, the molecules will tend to align along or opposite the field. The macroscopic magnetization M is given by:

$$M = \chi_{\alpha\beta} H_{\beta} \quad (1.7)$$

where ε and β are the axis of the molecular reference system; χ is the magnetic susceptibility. The diamagnetic properties of nematogenic liquid crystal can be described by two susceptibilities χ_{\parallel} and χ_{\perp} . The diamagnetic anisotropy $\Delta\chi$ is defined as

$$\Delta\chi = \chi_{\parallel} - \chi_{\perp} \quad (1.8)$$

using the above equation, the magnetization can be written as follows:

$$M = \chi_{\perp} H + (\chi_{\parallel} - \chi_{\perp})(H \cdot n)n \quad (1.9)$$

and the corresponding density of magnetic energy far volume unit is then given by (20):

$$E_{magn} = - \int_0^H \mathbf{M} \cdot d\mathbf{H} = -\frac{1}{2} \chi_{\perp} H^2 = -\frac{1}{2} \Delta\chi (n \cdot H)^2 \quad (1.10)$$

Usually $\Delta\chi > 0$; for this reason the minimum of the energy is reached when n has the same orientation of the field. The director orientation also depends on surface interactions: for a nematic liquid crystal tangentially oriented respect to the surface and subjected to a strong surface interaction, the director reorientation increases with the distance from the surface, until it become parallel to the field direction. It has been calculated that the angle between the director and the magnetic field is described by the following expression⁽²¹⁾:

$$\theta = \frac{1}{r} \cdot \exp - \left\{ \frac{r}{\xi(H)} \right\} \quad (1.11)$$

S is the length of magnetic coherence, and assuming $K=K_{11}=K_{22}=K_{33}$ it is expressed by the following equation:

$$\xi = \left(\frac{K}{\mu_0 \Delta\chi} \right)^{\frac{1}{2}} \cdot \frac{1}{H} \quad (1.12)$$

A magnetic field H is able to induce an elastic deformation over a length scale ξ ; over a nematic liquid crystal with diamagnetic anisotropy $\Delta\chi$ and elastic constant K (μ_0 is the magnetic permeability constant). This equation provides an order of magnitude estimate for the field required to reorient the liquid crystal director. Intuitively ξ ; can be defined as the thickness of the nematic liquid crystal layer where the orientation depends more on the surface interaction than on the field action.

The diamagnetic anisotropy is linked to the order parameter S by⁽¹⁸⁾:

$$S = \frac{\chi_{\parallel} - \chi_{\perp}}{\chi_{\parallel} + \chi_{\perp}} \quad (1.13)$$

where χ_{\parallel} and χ_{\perp} are the susceptibilities of the nematic liquid crystal parallel

and perpendicular to the magnetic field and χ_i and χ_t are the susceptibilities of the liquid crystal molecule parallel and perpendicular to the molecular longitudinal axis.

1.4.4 Optical anisotropy

Liquid crystals are found to be birefringent, due to their anisotropic nature: they exhibit double refraction (having two indices of refraction). Light polarized parallel to the director has a different index of refraction (that is to say it travels at a different velocity) than light polarized perpendicular to the director.

Thus, when light enters a birefringent material, such as a nematic liquid crystal sample, the process is modeled in terms of the light being broken up into the fast (called the ordinary ray) and slow (called the extraordinary ray) components (Fig. 1.15).

Because the two components travel at different velocities, the waves get out of phase. When the light rays are recombined as they exit the birefringent material, the polarization state has changed because of this phase difference⁽²²⁾.

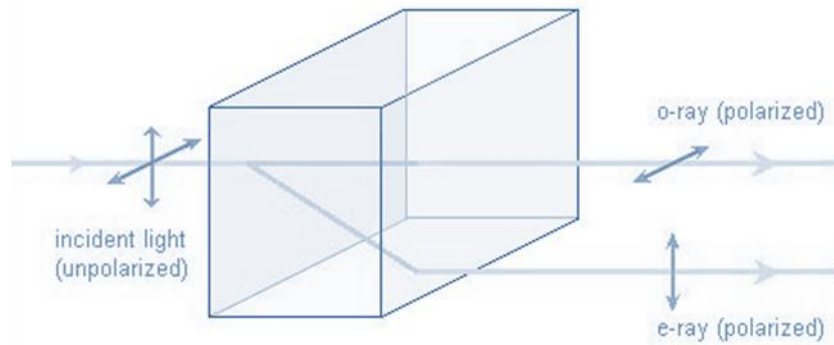


Fig. 1.15 Light traveling through a birefringent medium.

The birefringence of a material is characterized by the difference, Δn , in the indices of refraction for the ordinary and extraordinary rays.

Quantitatively, since the index of refraction of a material is defined as the ratio of the speed of light in vacuum to that in the material, we have for this case:

$$n_e = c/v_{\parallel} \quad \text{and} \quad n_o = c/v_{\perp} \quad (1.14)$$

for the velocities of a wave traveling perpendicular to the director. The maximum value for the birefringence is given by:

$$\Delta n = n_e - n_o = n_{\parallel} - n_{\perp} \quad (1.15)$$

where n_{\parallel} and n_{\perp} are the refraction index of the light polarized having the electrical vector respectively parallel and perpendicular to the director. Δn varies from zero to the maximum value, depending on the travel direction. In the general case of a wave traveling in an arbitrary direction relative to the director in a liquid crystal sample, n_o is coincident with n_{\parallel} and n_e is given by⁽²³⁾:

$$n_e = \frac{n_{\parallel}n_{\perp}}{\sqrt{n_{\parallel}^2 \cos^2 \theta + n_{\perp}^2 \sin^2 \theta}} \quad (1.16)$$

where θ is the angle between the incident ray and the director.

The condition $n_e > n_o$ describes a positive uniaxial material, so that nematic liquid crystals are in this category. For typical nematic liquid crystals, n_o is approximately 1.5 and the maximum difference, Δn , may range between 0.05 and 0.5. The Δn value depends on the wavelength of the light and the temperature.

1.4.5 Elastic constants

Liquid crystals respond to an external stimulus with an elastic reaction, varying only the molecules orientation. The elastic reaction for volume unit in apolar, achiral, nematic liquid crystal with cylindrical symmetry depends on three elastic constant K_{11} , K_{22} and K_{33} as follow⁽²⁴⁾:

$$F = \frac{1}{2} [K_1 (\nabla \cdot \mathbf{n})^2 + K_2 (\mathbf{n} \cdot \nabla \times \mathbf{n})^2 + K_3 (\mathbf{n} \cdot \nabla \mathbf{n})^2] \quad (1.17)$$

Each term in this equation is related to a particular deformation: splay

(K_{11}), twist (K_{22}) and bend (K_{33}) (see Fig.1.16).

The elastic constants are strongly temperature dependent.

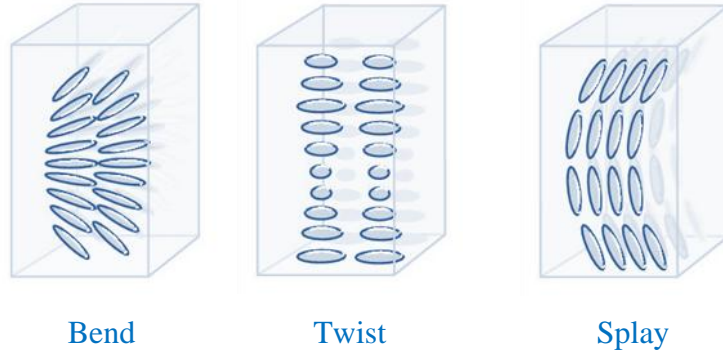


Fig.1.16 Elastic deformations of a liquid crystal

1.4.6 Anchoring energy

The director orientation in a nematic liquid crystal at the interface with a solid surface can be defined by two angles: the polar angle α , and the azimuthal angle φ . The orientation is homeotropic when $\theta=0$, while $\theta = \frac{\pi}{2}$ gives a planar or homogenous orientation (Fig.1.17).

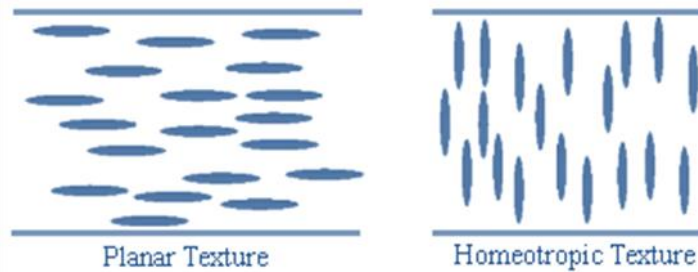


Fig. 1.17 Planar and homeotropic orientation of the director.

The surface energy F^S it is composed by two terms: the isotropic superficial energy F_i^S , and the anchoring energy. The latter is expressed by the following equation⁽¹⁷⁾:

$$F_a^S = \frac{1}{2} W \sin^2 \delta\theta \quad (1.18)$$

Where W is the angular anchoring and F_a^S is the necessary energy to turn the

director by an angle $\delta\theta$ from the equilibrium direction.

The alignment of liquid crystal molecules, was from the begin a problem of main importance, in order to obtain macroscopically mono-oriented liquid crystal films to be employed in the display technology.

Because of their importance, the alignment methodologies will be discussed in another chapter (the third), while in the next theoretical chapter we will discuss one of their most interesting applications of liquid crystals, such as polymer dispersed liquid crystals (PDLC), that are of main importance in the fabrication of optical devices, like the intelligent windows, to be employed in several useful applications.

References

1. F. Reinitzer, *Monatsh. Chem.*, 9, 421 (1888).
2. C. Oseen, *Trans. Faraday Soc.*, 29, 883 (1933).
3. H. Zocher, *Ibid.*, 29, 945 (1933).
4. W. Maier, and A. Saupe: *Eine einfache molekulare Theorie des nematischen kristallinussigen Zustandes*, *Z. Naturforschung, A* 13, 564-566 (1958).
5. F.C. Frank, *Discussions Faraday Soc.*, 25, 19 (1958).
6. F. M. Leslie, *Quart. J. Mech. Appl. Math.*, 19,357 (1966).
7. J. L. Ericksen, *Arch. Ratl. Mech. Anal.*, 4, 231 (1960); 9, 371 (1962).
8. I. C. Khoo, *Liquid Crystals*, 2Ed, Wiley (2007).
9. D. Demus, J. Goodby, *Handbook of Liquid Crystals, Vol.1 - Fundamentals*, Wiley-VCH, (1998).
10. S. Singh, *Liquid Crystals Fundamentals*, WSP (2002).
11. M. Sawamura et al., *Nature*, 419, 702 (2002).
12. T. Kato, *Liquid Crystalline Functional Assemblies and Their Supramolecular Structures*, Springer (2008).
13. A. M. Neto, *The Physics of Lyotropic Liquid Crystals - Phase Transitions and Structural Properties*, Oxford (2005).
14. I. Dierking, *Textures of Liquid Crystals*, Wiley-VCH, (2003).
15. S. Chandrasekhar, *Liquid Crystals*, 2th Ed, Cambridge (1992).
16. H. Sackmann, and D. Demus, *Mol. Cryst.*, 2,81 (1996).
17. P. G. De Gennes, J. Prost, *The physics of liquid crystals*, 2th Ed., Oxford University Press, (1993).
18. W. Maier, and A. Saupe, *Z. Naturf.*, 13 A, 564 (1958), 14 A, 882 (1959), 15 A, 287 (1960).
19. W. Maier, and G. Meier, *Z. Naturf.*, 16 A, 262 (1961).
20. E. A. Guggenheim, *Thermodynamics*, 5th ed., North-Holland (Amsterdam), (1967).
21. F. Brochard, and P.G. de Gennes, *J. Phys (Fr.)*, 21,691 (1970).
22. T. Scharf, *Polarized Light In Liquid Crystals And Polymers*, Wiley (2007).
23. K. Kondo, M. Arakawa, A. Fukuda, and E. Kuze, *Jpn. J. Appl. Phys.*, 22, 394 (1983).
24. A. Rapini, and M. J. Papoular, *J. Phys. (Paris) Colloq.*, C4 30, C4-C5 (1969).

CHAPTER 2: PDLC

2.1 Introduction

Polymer dispersed liquid crystals (PDLC) consist of micron-sized droplets of a low-molecular-weight nematic liquid crystal in a polymer matrix. These materials are able to modulate light through a controllable scattering⁽¹⁾.

In the absence of an electric field (zero field state) the director in the nematic droplets has a random orientation and the material strongly scatters light (Fig.2.1a).

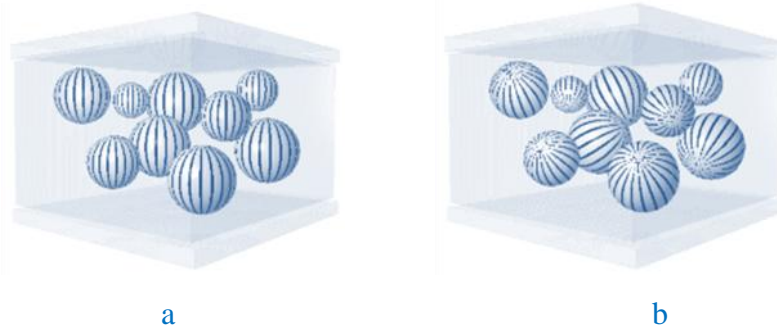


Fig.2.1 PDLC devices, a) ON state, with droplets aligned by an applied electric field, b) OFF state, with randomly oriented nematic liquid crystal droplets.

Droplets alignment is obtained applying an electric field such that the droplets refractive index nearly matches that of the polymer, and the material become transparent (fig. 2.1b). If the applied electric field is turned off, the droplets return to their original scattering orientation.

2.2 Nematic configurations within droplets

When liquid crystals are confined to small cavities such as in PDLC droplets, elastic deformations act on the director structure creating particular director configurations. The factors determining the director configuration adopted by a droplet include properties intrinsic (physical and chemical) to the liquid crystal, anchoring characteristics of the liquid crystal at the droplet interface, the presence

of external fields, and the size and the shape of the droplets.

The most common droplet alignment in PDLC films is the bipolar configuration ^{(2) (3)} (Fig.2.2a). In this configuration the director field is anchored parallel at the interface. The director field possesses cylindrical symmetry, with the symmetry axis defined by two point defects, named "boojums", which lie at the opposite ends of the droplets. These point defects are regions, in which there is a distributed orientation of the director. In a spherical droplet there is no preferred alignment of the droplet symmetry axis, as all the orientations are equally energetically favorable.

When the symmetry of the cavity is reduced, the bipolar configuration is maintained, but the symmetry axis tends to align along the longest distance available in the cavity. This occurs in order to minimize the bend and twist deformation energy. If a sufficiently strong electric or magnetic field is applied to bipolar droplets, the droplet director will reorient to lie parallel to the applied field for positive dielectric anisotropy materials, or perpendicular to the field for negative dielectric anisotropy materials ⁽⁴⁾.

A variation on the structure of bipolar droplets is to add a twist deformation to the director field, while maintaining the point defects of the bipolar structure. A twisted bipolar structure was first observed by Volovik and Lavrentovich ⁽⁵⁾.

Nematic droplets with a line defect running along the diameter possess a concentric (or toroidal) structure; the nematic director field is everywhere perpendicular to this line and arranged in a series of concentric circles. Theoretical considerations have questioned the stability of the concentric configuration, but several experiments showed results consistent with a stable concentric structure.

The configuration of nematic droplets that are possible with perpendicular alignment are quite different from those with parallel alignment. The most common are the radial configuration (see Fig.2.2b), with a point defect at the centre of the droplet, named hedgehog ⁽⁶⁾, and the axial configuration with an equatorial defect line (Fig.2.2c).

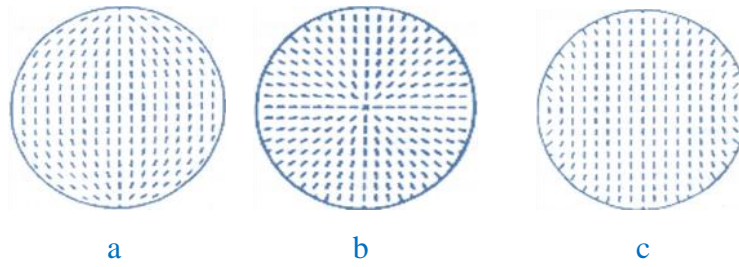


Fig.2.2 Droplet configuration: *a) bipolar, b) radial, and c) axial.*

The stability of these configurations depends on the intensity of the anchoring strength and the droplets size ⁽⁷⁾: large droplets with strong anchoring show radial configuration, while for small droplets in a weak anchoring case the axial configuration is preferred.

2.3 Preparation methods for PDLC films

Two basic methods have been developed for preparing polymer materials which contain a dispersion of droplets: encapsulation and phase separation. Each of these methods is fundamentally different.

2.3.1 Encapsulation

This technique was introduced by Fergason ⁽⁸⁾ as the original method for forming polymer dispersed liquid crystals and it was used by P. S. Drzaic ⁽⁹⁾. In the original formulation an aqueous solution of polyvinyl alcohol (PVA) is mixed with a nematic liquid crystal and then rapidly stirred. The size of the nematic droplets is a function of the stirring speed and time, the viscosity of the PVA solution, and the viscosity of the liquid crystal. The emulsion is coated onto a conductive transparent substrate, such as indium-tin-oxide (ITO) coated polyester, and the film allowed to dry. Once the film is dry, a second conductive substrate is laminated to form the final device. In addition to PVA other materials such as ammonium polyacrylate and gelatine have been used as the encapsulating medium for liquid crystals.

2.3.2 Phase separation methods

The phase separation method involves first forming an homogeneous solution of polymer or pre-polymer with a liquid crystal; the liquid crystal separates from the solution, and droplet formation and finally polymer solidification occur. The use of phase separation processes has been pioneered by Doane and coworkers⁽¹⁰⁾. Doane has coined acronyms for three broad classifications of phase separation process:

- *thermally induced phase separation (TIPS)*
- *solvent induced phase separation (SIPS)*
- *polymerization induced phase separation (PIPS)*

2.3.2.1 TIPS

The TIPS process is useful for thermoplastic polymers. In this process a binary mixture of polymer and liquid crystal forms an homogeneous solution at elevated temperatures. Cooling this solution into the miscibility gap causes phase separation of the liquid crystal; the separation process ends when the polymer viscosity is so high that the droplets do not grow and their size become stable. The thermoplastic polymer has to become a low viscous liquid with the heating; in this way is possible to obtain a homogeneous solution. The liquid crystal has to be completely soluble in the melt polymer.

Polymers such as polymethylmethacrylate (PMMA), polyvinylformal (PVF)⁽¹¹⁾ and polyvinylbutanal (PVB), form droplet dispersions with cyanobiphenyl liquid crystal materials. Thermoplastic materials can also be made from epoxy systems which form extended-chain molecules instead of cross-linked systems⁽¹²⁾. The droplet size is governed by the rate of cooling and depends upon a number of material parameters such as viscosity, chemical potentials, diffusion, etc..

TIPS technique shows some advantages respect to the other phase separations techniques. It could be possible to improve the samples homogeneity with repetitive heating and cooling of the material. The droplet diameter can be varied by adjustment of the rate of cooling: with a high cooling rate the liquid crystal hasn't enough time to separate and samples with low droplets density and size are

obtained, due to the break off of the growth. A low cooling rate produces PDLC with high droplet density and longer droplet diameter. TIPS allows to change easily the droplets shape; if the PDLC is softened without to be melted, it is possible to obtain with low pressures, stretched droplet.

2.3.2.2 SIPS

Phase separation by solvent evaporation is useful with thermoplastics which melt above the decomposition temperature. The liquid crystal and polymer are dissolved in a common solvent, forming a homogeneous solution. The solvent is then removed by evaporation, resulting in phase separation and polymer solidification⁽¹³⁾. The droplet dimension is governed by the evaporation rate: the higher is this rate, the smaller are the droplets. SIPS technique is useful because allows to prepare PDLC without drastic conditions such as high temperature.

2.3.2.3 PIPS

Photopolymerized PIPS systems are a most versatile and common method of creating PDLC films. Phase separation by polymerization is useful when the pre-polymer materials are miscible with the low molecular weight liquid crystal compounds. The process starts with a homogeneous solution made by mixing the pre-polymer with the liquid crystal. Polymerization is induced through a condensation reaction or, in other cases, it may proceed by a free radical polymerization or through a photo-initiated polymerization where phase separation is induced by an UV lamp. The solubility of the liquid crystal decreases in the growing polymer chains until the liquid crystal phase separate, forming droplet. The droplets grow until gelation of the polymer locks in the droplet morphology.

Droplets size is controlled by the rate of polymerization and by the types of liquid crystal and polymer used. The rate of polymerization depends on the curing temperature and the relative concentration of components in thermally cured polymers or by light intensity for photochemical polymerization⁽¹⁴⁾⁽¹⁵⁾.

In photopolymerization processes for the PDLC film formation, acrylate and

methacrylate chemistries have been extensively used⁽¹⁶⁾⁽¹⁷⁾⁽¹⁸⁾.

Many acrylate systems show a droplet morphology although wide variations can be found in droplet sizes, shapes and interconnectivity⁽¹⁹⁾. Dramatic changes in film morphology could be achieved through relatively minor changes in the starting materials. As general trend:

- The starting mixture must show good solubility between the liquid crystal and polymer-forming components
- A multifunctional acrylate can increase the rate of cure and phase separation in the system, which affects both the droplet size and the film morphology.

PDLC systems can be made with a high degree of interconnection between nematic domains. In the extreme can resemble interpenetrating networks of LC and polymer (fig 2.3).

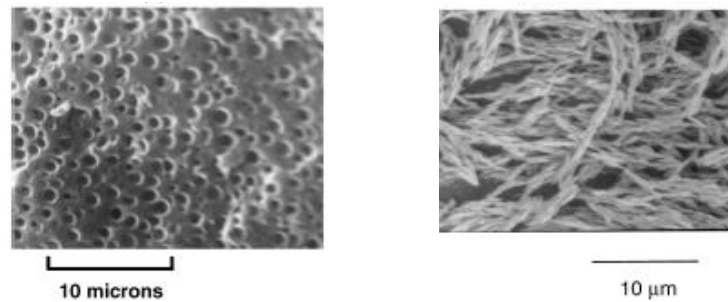


Fig 2.3 Different morphologies in PDLC film

Spatially-varying PIPS structures can be formed by modulating the intensity of the light across the film during cure. For example a mask can be used to expose different portions of the PDLC film to different cure intensities, or we can use the interference of crossed laser beams to form a sinusoidal intensity pattern in the film⁽²⁰⁾⁽²¹⁾. Such films act as an electrically-controllable diffraction grating for light.

2.4 Polymer networks

With “polymer network” is indicate a PDLC system with only a few percent of a highly-crosslinked polymer, like liquid crystalline diacrylates. The orientation of this network can be quite durable, with its structure unaffected by external fields

or change in temperature⁽²²⁾. This polymer mesogenic skeleton can dominate the local orientation of the surrounding low molar mass liquid crystal and consequently the alignment effects of the network can be used to alter the electro-optical properties of conventional liquid crystalline devices.

The morphology of the mesogenic network PDLC systems can vary widely with the ratio of monomer/LC. A high concentration of polymer the diacrylate forms a system with micro-sized domains of polymer and LC⁽²³⁾. Low concentration of polymer reflect in a much fine phase separation (nanometer).

2.5 Aspect of film structure

The microstructure of dispersed nematic films is a critical aspect in the electro-optical performance of the PDLC devices. Despite the large number of methods available to create PDLC systems, the resulting films possess several common structural features of interest, like: PDLC film thickness; sizes and shapes of LC droplets; polymer morphology; degree of cure in polymerized PDLC systems; any preferential alignment of the LC director field; the volume fraction of LC dissolved into polymer matrix etc..

The size and shape of the LC domains are critical factors in controlling droplet alignment and electro-optical properties of the PDLC.

To study the droplets dimension is difficult because in PDLC films the droplets diameters is not constant and the shape of the droplet varies due both to the preparation methods and to the interactions with the surface of the cell electrodes. Every PDLC is characterized, from a morphological point of view, by a medium diameter which generally corresponds to the prevalent measured value in the whole sample. The experimental techniques commonly used are the optical microscopy, when the droplets size is larger than 3 micron, and the scanning electron microscopy (SEM): the first allows to observe directly the PDLC, with the second is possible to observe cavity images obtained after removing the liquid crystal through sublimation or washing with the solvent^{(24) (25) (26) (27) (28)}.

The SEM analysis is the most general method for determining droplet size distributions in phase separation films, but care must be taken, due to the random

spacing between droplets that reflect in slices not in the middle of the droplets, or to the insufficient statistics (somewhat fewer than 1000 droplets were processed by the SEM analysis). The bi-dimensional images, achieved by SEM analysis, don't allow to determine completely the shape and the density of the droplets.

An attempt to optimize the methods for the structural study of the PDLC has been made by *Havens*⁽²⁹⁾: he analyzed the SEM images and used the statistic information collected in order to obtain indications about the actual volume occupied by the droplets. It is also noted that the medium diameter of the droplets in PDLC films can be obtained also using diffusion optical measurements⁽³⁰⁾. Several methods are achieved^{(31) (32) (33)} taking account of problems like the under- or over-counting in the droplet distribution by SEM analysis, helpful in this case is the use of informatics for the data post elaboration.

2.6 Liquid crystal/polymer phase separation

The phase separation of LC and polymer is a crucial feature. Starting from an homogeneous solution, the polymeric components become sufficiently incompatible with the LC to induce the formation of separate fluid and polymer. Depending to the chemical nature of the components and to the kinetics of the process driving the phase separation, this determine the morphology and consequently the electro-optical properties of the resulting PDLC film.

The analysis of Phase separation process found in PDLC films is often simplified by treating the system as a simple binary mixture.

2.6.1 Phase diagrams for LC/monomer mixtures

In PDLC system made by PIPS processes the initial system consist of a mixture of LC, monomers and sometimes low molecular weight oligomers. Plotting temperature versus LC composition the phase diagrams of PIPS systems typically show upper critical solution temperature (UCST) behavior (fig 2.4). A single phase is stable at high temperatures, the miscibility decreases with decreasing temperature and at low temperature we have a phase separation of the mixture.

The temperature at which phase separation is allowed depend on the relative concentration of the LC and monomer/polymer solution and on the relative solubility of the two components of the mixture. At the extremes of the concentration the two components are completely miscible and not phase separate at any temperature. The upper curve in the figure define the temperatures at which the separation is allowed for a solution at a given concentration.

There are two curves which separate single and dual-phase system:

- The lower curve (Spinodal curve) marks the region where the phase separation occurs spontaneously without need of activation
- The upper curve (Binodal curve) defines the point at which the phase separation become energetically possible, but not necessary.

In the region between spinodal and binodal curves the system is metastable, the phase separation is thermodynamically allowed but may occur depending of the size of the activation barrier and if nucleation sites are available.

If phase separation occur in spinodal or binodal regime, controls the kinetics of the phase separation process, affecting the structure of the polymeric matrix.

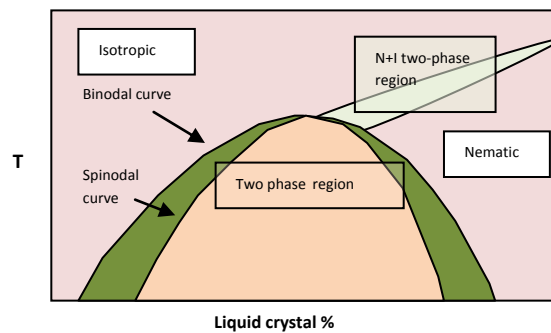


Fig 2.4 Idealized representation of a binary phase diagram between a liquid crystal and an isotropic monomer or polymer

Another important aspect is that, when we have phase separation, the two phases do not simply separate into a pure LC phase and a pure monomer/polymer phase, but the mixture separate into a LC-rich phase and a LC-poor phase. The concentrations of LC in each phase, at a given temperature, are defined by a line,

which connects the opposite sides of bimodal and spinodal curve at the same temperature^{(34) (35)}.

2.6.2 Phase separation in the binodal and spinodal regimes

Phase separation is driven by the thermodynamics of the solution but kinetic processes like nucleation and molecular diffusion often determine the nature of the process⁽³⁶⁾.

Two distinct mechanisms, that can lead to a different types of polymer morphology in the final film, are recognized for the process of phase separation:

- ✚ Nucleation and growth mechanism if the system requires an activation energy for the initiation of a new phase. This occur under the binodal curve in the metastable portion of the phase diagram,

- ✚ Under the spinodal curve if the activation energy is not required (without activation barriers).

The lack of activation barriers changes significantly the nature of the process and lead to a spinodal decomposition mechanism. In this process concentration gradients spontaneously appear in an interconnected network structure, and these concentration gradients grow sharper and larger as phase separation proceeds. In contrast, the nucleation and growth process phase separation begin in random, unconnected spots which grow over time and these phase separated area do not change in concentration^{(37) (38)}.

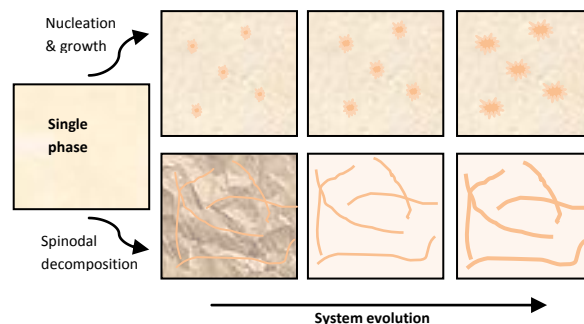


Fig 2.5 Two-dimensional representation of the phase structure in a nucleation and growth phase separation process and in a spinodal decomposition.

2.7 Electro-optical effects

2.7.1 Light scattering and index matching

The contrast in a PDLC display is defined as the ratio between the transmitted light in the transparent state and that transmitted in the opaque state⁽³⁹⁾. PDLC are never completely transparent. For example, an object observed through a PDLC in the on state, is darkened due to the residual scattering⁽⁴⁰⁾. The intensity of the transmitted light is expressed by the following equation:

$$I_t = I_0 e^{-\beta d \sigma} \quad (2.1)$$

where β is the volume density of the droplets, d the path length through the shutter ($d = d_0 \cos \alpha$, where d_0 is the PDLC thickness), α is the angle that the incident light makes with the normal to the cell surface, σ is the scattering capability of a droplet. In the transparent state ideally there is not light scattering and $\sigma = 0$. For nematic droplets of radius R used in PDLC light shutters in the visible region, the cross section σ can be approximated by the following equation⁽⁴¹⁾:

$$\sigma = 2\sigma_0 (KR)^2 \left[\frac{n(\alpha)}{n_p} - 1 \right]^2 \quad (2.2)$$

where σ_0 is the geometrical cross section of the droplet, $K = 2\pi/\lambda$, λ is the wavelength of the light; n_p is the refraction index of the polymer matrix, $n(\alpha)$ is the refraction index of a nematic droplet with a positive dielectric anisotropy which has been aligned by an applied field at the angle α , and given by:

$$n(\alpha) = \frac{n_o n_e}{[n_e^2 \cos^2 \alpha + n_o^2 \sin^2 \alpha]^{1/2}} \quad (2.3)$$

where n_o and n_e are the ordinary and extraordinary refractive indices of the aligned droplet, respectively. The most transparent condition exists when $\alpha = 0$, $n(\alpha) = n_p$ (normally incident light); when the refraction index of the polymer is

equal to the ordinary refraction index of the liquid crystal, but at finite angle α when $n_p > n_o$. The angular dependence of the light transmitted through the shutter falls off faster at larger angles than those calculated with the previous equations due to the reflections from the air-glass surface of the cell⁽⁴²⁾.

The intensity of the transmitted light and, consequently, the contrast, depends on the temperature. This feature was studied by Vaz et al^{(43) (44) (45) (46)}.

From the experimental data results at temperatures above T_{NI} , the refractive indices of the liquid crystal and the polymer matrix decrease with temperature at nearly the same rate so that the index difference between liquid crystal and polymer is nearly independent of temperature. In the nematic phase, as the temperature decreases, the ordinary refractive index decreases while the extraordinary refractive index increases; this means that the OFF state scattering will increase and the OFF state transmittance will decrease with decreasing temperature. In the ON state, the transmittance will initially increase as the temperature is lowered below T_{NI} , it will reach a maximum value at the temperature for which the refraction index of the polymer is equal to the ordinary refraction index of the liquid crystal, and will decrease monotonically as the temperature is decreased further. To maximize the PDLC ON state transmittance over a given operating temperature range, the polymer should be index-matched to the liquid crystal at some temperature within the operating range. Diffuse light incident on a PDLC device causes haze effect in the transparent state, limiting the contrast of the shutter⁽⁴⁷⁾. The contrast depends on the entity of the PDLC opacity in the OFF state. Haze is defined as the fraction of light which is scattered out of at $\pm 2.5^\circ$ aperture, normalized to the total light transmitted by the sample. Zumer⁽⁴⁸⁾ has made theoretical studies of the light scattering from a single nematic droplet for various director configurations. Scattering profile, as well as the total and differential cross sections, were calculated in the Rayleigh-Gans (small droplet) and Anomalous Diffraction (large droplet) regimes. The RG approximation is an approach to light scattering appropriate to systems in which the induced phase shift of the light is weak. The Rayleigh-Gans (RG) approximation assumes that the maximum phase shift induced by the scattering object is small, on the order of

$$2kR \left| \frac{n_{ic}}{n_p} - 1 \right| \ll 1 \quad (2.4)$$

The anomalous diffraction (AD) approximation assumes that

$$KR \gg 1 \text{ and } \frac{n_{ic}}{n_p} \gg 1 \quad (2.5)$$

Light scattering for PDLC light shutters lies intermediate between these two theoretical regimes where there is some overlap. In the opaque state single scattering calculations can describe the attenuation of light by PDLC films provided multiple scattering does not significantly change the fraction of the incident power scattered out of the acceptance solid angle of the detection system⁽⁴⁹⁾. Attenuation measurements are not sensitive to change in the angular distribution of the scattered light produced by multiple scattering outside the detector acceptance cone.

2.7.2 PDLC film operating voltage

Liquid crystals dispersed in a polymer matrix have been object of great interest over the last several years due to two principal reasons:

- These systems allow to study the behavior of nematic phases confined in small cavities and while subject to hard surface interactions;
- They can be easily utilized in the production of electro-optical shutters.

One of the most important electro-optical parameters of PDLC films is the voltage required to achieve an electro-optical effect. From a material point of view, it is more appropriate to discuss the reorientation field (voltage/film thickness) of a PDLC film. Like in other liquid crystal devices, this reorientation field is determined by the balance of the elastic forces (which resist orientation) and electric forces (which induce orientation).

In the normal condition a PDLC film is opaque (OFF state), but it can become

transparent (ON state) after application of an electric or magnetic field of suitable intensity. The opaque-transparent transition (OFF-ON) induced by the field is known as "switching". The switching voltage of a PDLC light shutter depends upon a variety of factors: it depends on the nematic director configuration of the droplet, on the shape, the size and the density of the droplet, on the thickness of the PDLC cell. Perhaps the dominating factors for the response voltage are the resistive and the dielectric properties of the nematic liquid crystal and the polymer.

The electric field inside the droplets of PDLC shutters is not the same as the applied electric field, $E = V/d$, where V is the applied voltage and d the thickness of the PDLC film. Considering an isolated spherical droplet in a polymeric material, the electric field inside the droplet, E' , is related to the applied field by the expression⁽⁵⁰⁾:

$$E' = \frac{3E}{(\varepsilon_{lc}/\varepsilon_p + 2)} \quad (2.6)$$

Where ε_{lc} and ε_p are the dielectric constants of the liquid crystal and the polymer, respectively. The dielectric constant for materials with nonzero conductivity can be written as

$$\varepsilon = \varepsilon' + j/\rho\omega \quad (2.7)$$

where ε' is the real component, ρ is the resistivity and ω is frequency of the applied voltage.

In the resistive regime $\varepsilon'\rho\omega \ll 1$: such is the case in PDLC light shutters where the liquid crystal inside the droplet can be slightly contaminated with the polymer and the polymer can be plasticized with the liquid crystal, lowering the resistivity of both ρ_{lc} and ρ_p , the field inside the droplet can be expressed as⁽³⁹⁾ :

$$E' = \frac{3V}{d_0 \left(\frac{\rho_p}{\rho_{lc}} + 2 \right)} \quad (2.8)$$

Where V is the voltage applied to the electrodes and d_0 the interelectrode spacing.

To determine the threshold voltage for an electro-optic PDLC switch is necessary to consider the specific director configurations involved. In the case of a radial configuration, droplets will switch at a threshold voltage, V_R , according to the expression:

$$V_R = \frac{1}{40} \frac{d_0}{d_s} \left(\frac{\rho_p}{\rho_{lc}} + 2 \right) \left| \frac{K}{\varepsilon_0 \Delta \varepsilon} \right|^{1/2} \quad (2.9)$$

Where d_e is the surface extrapolation length, and K is the elastic constant (in the single constant approximation $K=K_{11}=K_{22}=K_{33}$). In the case of a bipolar configuration, choosing a simple elongated model, the switching voltage of a bipolar droplet is given by:

$$V_B = \frac{d}{3\alpha} \left(\frac{\rho_p}{\rho_{lc}} + 2 \right) \left(\frac{K(l^2-1)}{\varepsilon_0 \Delta \varepsilon} \right)^{1/2} \quad (2.10)$$

where l describe the extend of the elongation of the cavity defined as $l=a/b$, the ratio of the length of the semi-major axis, a , to the length of the semi-minor axis b .

The electro-optical response is determined studying the variation of the PDLC transmittance versus the applied electric field, whose values are calculated from the applied voltage normalized with respect to the film thickness. Two values of the electric field are particularly relevant: $E_{10\%}$, which is the electric field value able to increase the transparency to 10%, and $E_{90\%}$, the electric field value which induces an increase in the PDLC transmission of 90%. $E_{10\%}$ is also known as the threshold field and $E_{90\%}$ is known as the switching field. Other important

parameters for the PDLC characterization are the response times, τ_{rise} and τ_{decay} . τ_{rise} is the time necessary to obtain a transmission change from 10% to 90%, while τ_{decay} is the time related to a variation of the transmission from 90% to 10%. The experimental determination of these two parameters are obtained using pulses with suitable length, amplitude and shape.

2.7.3 Switching times

The response times depend on the droplets shape and the viscoelastic property of the liquid crystals^{(30) (51) (52)}. The relevant lowering of the response time in sheared PDLC light shutters with elongated droplet, observed by Erdmann, has been explained by including a viscous torque density which opposes the elastic torque in returning the droplet director to its equilibrium orientation upon removal of the field.

Summing these two torque densities and considering the inertial term to be negligible, the expression of decay time is given by:

$$\tau_{\text{decay}} = \frac{\gamma a^2}{K(l^2 - 1)} \quad (2.11)$$

Where γ is the rotational viscosity of the liquid crystal. An elliptical droplet of $l = 1.1$ yields a decay time of about 10 ms. The small value of l illustrates the large effect of the droplet shape on the relaxation time. This expression accounts only for the droplet shape and it is valid only for elliptical droplet because in the case of spherical droplet $l=1$ and decay time is undefined. However, the above expression can be considered valid in general, due to the impossibility to prepare PDLC films with perfectly spherical droplet. The rise time, τ_{rise} , has been calculated by balancing all three torque densities, electric, elastic and viscous, with the following result:

$$\tau_{\text{rise}}^{-1} = \frac{1}{\gamma} \frac{9\epsilon_0 \Delta\epsilon E_{90\%}^2}{d^2 \left(\frac{\rho}{\rho_{lc}} + 2\right)^2} + \frac{K(l^2 - 1)}{\gamma a^2} \quad (2.12)$$

2.8 Reverse mode devices

PDLC may be used in very interesting industrial applications like solar light shutters used for the production of car windows. However, for this purpose, PDLC are limited by the necessity of an electric field to obtain the transparent state. Several research groups turned their attention at the possibility to obtain PDLC working in "reverse mode", that is, transparent OFF state and opaque ON state devices. Different methodologies have been developed to realize PDLC reverse mode: in 1992 a group at Kent State University (USA) invented a composite material named "Polymer Stabilized Cholesteric Texture (PSCT)"⁽⁵³⁾, composed by 90% of a nematic liquid crystal, 8% of a cholesteric liquid crystal and 2% of a polymer. When this material is confined between two surfaces pre-treated with polyimide, a planar alignment of the liquid crystal is obtained, with the helical pitch normal to the confining surface; this is the transparent state. When an electric field is applied, the planar uniformity is destroyed and a disordered, scattering state is created. Other kinds of "reverse mode" electro-optical materials are obtained by changing the superficial energy of the droplets in the PDLC⁽⁵⁴⁾, and by using "dual frequency" liquid crystals⁽⁵⁵⁾⁽⁵⁶⁾.

Another possibility can be the realization of mesogenic networks with a high content of liquid crystal, also known as polymer stabilized liquid crystal polymer (PSLC)⁽⁵⁷⁾⁽⁵⁸⁾⁽⁵⁹⁾⁽⁶⁰⁾⁽⁶¹⁾. PSLC cells are generally prepared by dissolving and photo-polymerizing monomers (typically an amount varying from 2 to 10 wt%) in a liquid crystal matrix to form a polymer network. Hudson, et al.⁽⁶²⁾⁽⁶³⁾ chose to study network formation in a nematic liquid crystal matrix (solvent) of homogeneous aligned nematic liquid crystal.

Moreover, homeotropically aligned PDLCs or PSLC working in "reverse mode" can be obtained by photo-induced cross linking of a liquid crystalline mixture containing the diacrylate monomer bis{ 4-[(6-acryloxy)hexyloxy]benzoate}-1,4-phenylene (C6H) and conventional liquid crystal molecules with negative dielectric anisotropy; N-dimethyl-N-octadecylaminopropyltrimethoxysilyl chloride (DMOAP) has been used for inducing homeotropic orientation of the molecules⁽⁶⁴⁾.

The above mentioned methodologies showed several disadvantages as poor optical contrast, weak anchoring to the supports, high switching field, chemical instability and long response times.

To overcome those limitations, another kind of electro-optical device working in reverse mode, has been realized by the Liquid Crystal Group of the University of Calabria ⁽⁶⁵⁾ ⁽⁶⁶⁾ . This is characterized by micro-droplets of uniformly aligned nematic liquid crystal with a negative dielectric anisotropy, dispersed in a solid polymeric matrix: aligning permanently the mesogenic molecules inside to the droplets normal to the glass supports with the aid of an oriented polymerization in magnetic field, a perfectly transparent material is obtained with the condition that the refraction index of the polymeric matrix, n_p is the same of the ordinary refraction index of the liquid crystal, n_o . In this way, there is not light scattering, Fig. 2.6a.

Applying an external electric field of suitable intensity induces the reorientation of the droplets director perpendicular to the electric field direction. The difference between the refraction index n_p , and the extraordinary refraction index of the liquid crystal, n_e results in the scattering of light, Fig. 2.6b.

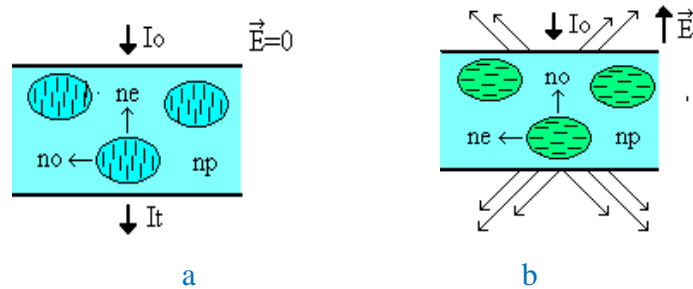


Fig.2.6 Schematic view of an electro-optical cell working in reverse mode:
a) OFF state, b) ON state.

The liquid crystal alignment in the micro-droplets it was firstly obtained by starting from Liquid Crystal organic emulsion ⁽⁶⁷⁾ ⁽⁶⁸⁾ composed by an acrylic monomer and a liquid crystal; the mesogenic molecules in the emulsion could be oriented in the homeotropic direction using an external magnetic field. The

polymerization of the acrylic monomer, freezes in a permanent way the liquid crystal in a uniformly aligned state, yielding a perfectly transparent film. To understand how this permanent alignment occurs, two different hypothesis have been formulated: it is possible that to minimize the free energy of the liquid crystal, the shape of the droplets in the emulsion is slightly distorted, with the major semi-axis on the direction of the phase director. This deformation is frozen during the polymerization process of the surrounding in water or water in oil. Such system are generally metastable and considerable efforts have been devoted to get stable emulsions by choosing or adding specific molecules⁽⁵⁵⁾. In particular, Nematic emulsions have been widely investigated in the past^{(69) (70) (71) (72)} as well as more recently⁽⁷³⁾.

Recent studies of emulsions characterized by micro-droplets of nematic liquid crystal found that they exhibited good stability (74). The monomers used to obtain this systems have several -OH groups and they are characterized by an high value of viscosity. As in the common PDLC, a nematic emulsion at room temperature appears white and opaque but, with the application of an electric or magnetic field, it becomes transparent.

To form a nematic emulsion, it is enough to use a smaller amount of liquid crystal than that generally used to obtain a traditional PDLC: a mixture containing only 10 wt% of liquid crystal suffices to obtain phase separation. Nematic emulsions are obtained adding the liquid crystal to the organic monomer. To obtain homogeneous emulsions, a solution of the component is made by heating the system above the emulsion critical point. The temperature is then lowered below this critical temperature, and can be enough to induce a permanent alignment in the liquid crystal. Alternatively, it can be assumed that the oriented liquid crystal molecules induce the orientation of the monomer at the interface. Since the polymerization of the sample takes place in an ordered system the polymer matrix will keep a certain degree of orientation. The surface interaction between this polymer ordered structure and the liquid crystal molecules could be enough strong to stabilize a uniform alignment of the mesogenic molecules. This new process is different from the traditional methodologies as TIPS, SIPS e PIPS because liquid crystal droplets exist in the organic phase before the

polymerization.

Comparing with existing films working in the reverse mode, this new composite material has several advantages including good adhesion strength between the electro-optical film and the glass supports, a low content of liquid crystal (30-40%), fast response times and good optical contrast.

Moreover, to prepare reverse mode PDLC films, another methodology was applied by the Calabrian research group which opens the possibility to produce in very simple way large size reverse mode intelligent windows. It was found that diacrylic liquid crystal monomers mixed with other nematic liquid crystals can be spontaneously oriented on glass support in such a way that a full homeotropic oriented liquid crystal film can be prepared and turned in a reverse mode PDLC film by UV polymerizing the diacrylic monomer ^{(75) (76) (77) (78)}.

The interesting feature of these device, that allow their use as large, not expensive, intelligent windows is that the homeotropic orientation was achieved without pre-treating of the glass substrate. This spontaneous homeotropic alignment, which was previously highlighted but not fully explained ⁽⁷⁹⁾, will be discussed in the experimental section of this work..

References

1. S. Zumer, J.L. West, J.W. Doane, *J. Appl. Phys.*, 58, 529 (1988).
2. S. Zumer, J.W. Doane, *Phys. Rev.*, A 34, 3373 (1986).
3. S. Candau, P. Le Roy, F. Debeauvais, *Mol. Cryst. Liq. Cryst.*, 23, 283 (1973).
4. S. Zumer, D. Allender, *Bull. Am. Phys. Soc.*, 31, 691 (1986).
5. G.E. Volovik, O.D. Lavrentovich, *Sov. Phys. JETP Lett.*, 58, 1159 (1983).
6. AV. Koval'chuk, MV.Kurik, O.D.Lavrentovich, VV.Sergan, *Zh. Eksp. Teor. Fiz.*, 94, 359 (1988).
7. J. Erdmann, S. Zumer, J.W. Doane, *Phys. Rev. Lett.*, 64, 1907 (1990).
8. J.L. Ferguson, *SID Digest of Technical Papers*, 16,68 (1985).
9. P.S. Drzaic, *J. Appl. Phys.*, 60, 2142 (1986).
10. J.W. Doane, G. Chidichimo, N.A Vaz, *U.S. Patent No.4688900* (1987).
11. B.G. Wu, J.L. West, J.W. Doane, *J. Appl. Phys.*, 62, 3925 (1987).
12. J.L. West, *Mol. Cryst. Liq. Cryst.*, 157,427 (1988).
13. J.W. Doane, A. Golemme, J.L. West, J.S. Whitehead, B.G. Wu, *Mol. Cryst. Liq. Cryst.*, 165, 511 (1988).
14. J.West, A Golemme, J.W. Doane, *U.S. Patent No.4.673.255*(1987).
15. Z. Huang, G. Chidichimo, A Golemme, H. A Hakemi, M. Santangelo, F. P. Nicoletta, *Liq. Cryst.*, 23,519 (1997).
16. Y.Hirai, S.Niiyama et al, *Phase diagram and phase separation in LC/prepolymer mixture*, in *Proc. SPIE*, 1257, 2-8, (1990).
17. D. Coates, S. Greenfield, M. Goulding et al., *Recent developements in materials for TFT/PDLC devices*, in *Proc. SPIE*, 1911, 2-14 (1993).
18. T. Fujisawa, H. Ogawa, K. Muruyama, *electro-optic properties and multiplexibility of polymer network liquid crystal display*, *Japan Display*, (1989).
19. C.H. Noh et al., *A study on the morphology and electrooptic properties of liquid crystal-polymer composite films*. *Mol. Cryst. Liq. Cryst. Sci. Tec. A*, 237, 299-309, (1993).
20. A.M. Lacner, J. D. Margerum, et al. *Droplet size control in polymer dispersed liquid crystal film*, in *Proc SPIE*, 1080, 53-61, (1989).
21. R.L. Sutherland, V.P. Tondiglia, et al. *Bragg gratings in an acrylate polymer consisting of periodic polymer dispersed liquid crystal planes*, *Chem. Mater*, 5, 1533-1538, (1993).
22. R. Stannarius et al., *Nematic director orientation in a liquid crystal dispersed polymer: a deuterium nuclear magnetic resonance approach*, *J. Appl. Phys*, 70, 135-143, (1991).
23. S.Niiyama, Y.Hirai, et al. *A hysteresis-less LCPC device for a projection display*, in *SID Digest*, 575-8, (1992).
24. S. Zumer, J.W. Doane, *Phys. Rev.*, A 34, 3373 (1986).
25. P.S. Drzaic, *Mol. Cryst. Liq. Cryst.*, 154,239 (1988); H. Yang, D.W. Allender, and M.A. Lee, *Bull. Am. Phys. Soc.*, 33, 275 (1988).

26. AV. Koval'chuk, MV. Kurik, O.D. Lavrentovich, VV. Sergan, *Zh. Eksp. Teor. Fiz.*, 94, 359 (1988); J. Erdmann, S. Zumer, and J.W. Doane, *Phys. Rev. Lett.*, 64, 1907 (1990);.
27. J.W. Doane, J.L. West, J.B. Whitehead, and D.S. Fredley, *Society for Information Display Digest*, 21, 224 (1990); N.A. Vaz, *Proc. SPIE*, 1080, 2 (1989).
28. R Ondris-Crawford, E.P. Boyko, B.G. Wagner, J.H. Erdmann, S. Zumer, and J.W. Doane, *J. Appl. Phys.*, 69,6380 (1991).
29. J.R Havens, D.B. Leong, and K.B. Reimer, *Mol. Cryst Liq. Cryst.*, 178, 89 (1990).
30. A. Golemme, S. Zumer, J.W. Doane, and M.E. Neubert, *Phys. Rev. A*, 37,559 (1988).
31. N. Vaz, G.W. Smith, G.P. Montgomery, *PDLC film formed by electron-beam cure*, *Mol. Cryst Liq. Cryst.*, 197, 83-101, (1991).
32. J. R. Havens, D. B. Leong, K. B. Reamer, *Quantitative SEM characterization of PDLC films*, *Mol. Cryst Liq. Cryst*, 178, 89-101, (1990).
33. R.T. De Hoff, *The determination of the size distribution of ellipsoidal particles from measurements made on random plane samples*, *Trans. Met. Soc. AIME*, 224, 474-477, (1992).
34. O. Olabisi, L. M. Robenson, M. T. Shaw, *Polymer-polymer miscibility*, New York Academic Press (1979).
35. J. W. Cahn, *Spinodal decomposition*, *Trans. Met. Soc. AIME*, 242, 166-180, (1968).
36. T.Nishi, *Experimental aspects of compatible polymer mixtures*, *J. Macromol. Sci. Phys*, B17, 517-542, (1980).
37. W. D. McIntyre, D. S. Soane, *Controlled phase separation of polymer-liquid crystal mixtures for reversible data storage*, *Appl. Optics*, 29, 1658-1665, (1990).
38. W. D. McIntyre, D. S. Soane, *Optical data storage using phase separation polymer-liquid crystals mixtures*, in *Polymer Inc. Storage Tech*, Plenum, 21-50, (1988).
39. G.Chidichimo, G.Arabia, A.Golemme, J.W. Doane, *Electro-optic properties of polymer dispersed liquid crystals*, *Liq. Cryst.*, 5, 1443-52, (1989).
40. P. van Konynenburg, RT. Wipfler, and J.L. Smith, *Proc. SPIE*, 1080, 62 (1989).
41. S. Zumer, A. Golemme, and J.W. Doane, *J. Opt. Soc. Am.*, 6, 1102 (1989).
42. J.W. Doane, A Golemme, J.L. West, J.S. Whitehead, and B.G. Wu, *Mol. Cryst. Liq. Cryst.*, 165, 511 (1988).
43. N.A. Vaz, *Proc. SPIE*, 1080, 2 (1989).
44. G.P. Montgomery, N.A. Vaz, and G.W. Smith, *Proc. SPIE*, 958, 104 (1988).
45. N.A. Vaz, and G.P. Montgomery, *J. Appl. Phys.*, 62, 3161 (1987).
46. G.P. Montgomery, and N.A. Vaz, *Applied Optics*, 26, 738 (1987).
47. P. van Konynenburg, RT. Wipfler, and J.L. Smith, *Proc. SPIE*, 1080, 62 (1989).
48. S. Zumer, J.W. Doane, *Phys. Rev. A*, 34, 3373 (1986); S. Zumer, *Phys. Rev. A*, 37,4006 (1988).
49. G.P. Montgomery, *J. Opt. Soc. Am. B*, 5,774 (1988).
50. J. Erdmann, J.W. Doane, S. Zumer, and G. Chidichimo, *Proc. SPIE*, 1080, 32 (1989).
51. P.S. Drzaic, *Liq. Cryst.*, 3, 1543 (1988).
52. B.G. Wu, J.H. Erdmann, and J.W. Doane, *Liq. Cryst.*, 5, 1453 (1989).
53. O.K. Yang, L.C. Chien, and J.W. Ooane, *Appl. Phys. Lett.*, 60, 3102 (1992).

54. Y. O. Ma, S. G. Wu, and G. Xu, *Proc. SPIE*, 1257,46 (1990).
55. P. Nolan, and O. Coates, *Mol. Cryst. Liq. Cryst., Lett.*, 8, 75 (1991).
56. T. Gotoh, and H. Murai, *Appl. Phys. Lett.*, 60,392 (1992).
57. R. A. M. Hikmet, *J. Appl. Phys.*, 68, 1 (1990).
58. R. A. M. Hikmet, B. H. Zwerver, *Liq. Cryst.*, 12,319 (1992).
59. R. A. M. Hikmet, *Mol. Cryst. Liq. Cryst.*, 213, 117 (1992).
60. R. A. M. Hikmet, *Liq. Cryst.*, 9,405 (1991).
61. R. A. M. Hikmet, *Mol. Cryst. Liq. Cryst.*, 198, 357 (1991).
62. C.V. Rajaram, S.O. Hudson, and L.C. Chien, *Chem. Mater.*, 8, 2451, (1996).
63. C.V. Rajaram, S.O. Hudson, and L.C. Chien, *Polymer*, 39, 5315, (1998).
64. R. A. M. Hikmet, *Mol. Cryst. Liq. Cryst.*, 213, 117 (1992).
65. G. Chidichimo and G. De Filpo, *Reverse mode electro-optical cell made of liquid crystals encapsulated in a polymeric layer and method for manufacturing it, European patent n° WO9816865 (1997).*
66. F.P. Nicoletta, G. De Filpo, J.Lanzo, G. Chidichimo, *Appl. Phys. Lett.*, 74, 3945 (1999).
67. F. P. Nicoletta, G. De Filpo, J. Lanzo, G. Chidichimo, *J. Appl. Phys.*, 84, 3581 (1998).
68. G. De Filpo, J. Lanzo, F. P. Nicoletta, G. Chidichimo, *J. Appl. Phys.* 85,2894 (1999).
69. P. Le Roy, F. Oebeauvais, S. Candau, *C. R. Acad. Sci. Paris*, 274, 419 (1972);
70. S. Candau, P. Le Roy, F. Oebeauvais, *Mol. Cryst. Liq. Cryst.*, 23, 283 (1973).
71. G.E. Volovik, O. D. Lavrentovich, *Sov. Phys. JETP*, 58, 1159 (1983).
72. O.D. Lavrentovich, *Sov. Tech. Phys. Lett.*, 14,73, (1988).
73. P. Poulin, H. Stark, TG. Lubensky, O.A. Weitz, *Science*, 275, 1770 (1997); E.M. Oe Groot, and G.G. Fuller, *Liq. Cryst.*, 23,113 (1997).
74. J. Lanzo, *Emulsioni Elettroottiche Liquido Cristalline: Proprietà e Stabilità Termodinamica*, 1996-1997.
75. G. De Filpo, G. Chidichimo, "Reverse mode electro-optical film composed of one mutual dispersion of polymers and liquid crystals", *European patent n° WO 9900464 (1997)*, *U.S. Patent n° 6,383,577 81 (2002)*.
76. M. Macchione, O.Cupelli, G. DeFilpo, F.P. Nicoletta, G. Chidichimo, *Liq. Cryst*, 27, 917 (2000).
77. M. Macchione, G. De Filpo, F. lemma, F.P. Nicoletta, N. Picci, and G. Chidichimo, *Mol. Cryst. Liq. Cryst.*, 363, 137 (2000).
78. M. Macchione, O.Cupelli, G. DeFilpo, F.P. Nicoletta, G.Chidichimo, *Liq.Cryst.*, 27, 1337(2000).
79. L. Tortora, *Optical Shutters by liquid crystal organic dispersions*", *PhD thesis 2003-2004*.
80. P. Le Roy, F. Oebeauvais, S. Candau, *C. R. Acad. Sci. Paris*, 274, 419 (1972);
81. M. Macchione, G. De Filpo, F. lemma, F.P. Nicoletta, N. Picci, and G. Chidichimo, *Mol. Cryst. Liq. Cryst.*, 363, 137 (2000).

CHAPTER 3: Alignment technologies

3.1 Introduction

One of the most important problems in the fabrication of liquid crystal devices, is the surface alignment of the liquid crystal molecules. It is required that the liquid crystals are aligned uniformly and in an orderly manner between the two substrates and this is achieved by means of the chosen alignment processing method.

In this chapter we discussed the typical alignment technologies for nematic liquid crystals, distinguishing between rubbing and non-rubbing methods.

The non rubbing methods include photoalignment and the use of surface active agents, the latter method is of main interest for this thesis work.

3.2 Liquid crystal alignments

In LCD devices, liquid crystal materials are usually sandwiched between two glass substrates carrying alignment film with a gap of 1-10 μm . By the influence of the alignment film on the substrates, liquid crystal molecular orientations are determined.

Typical orientations are shown in Fig. 3.1. These orientations are classified into two groups. The directors of the liquid crystal molecules in the Homogeneous (or Planar), Tilted and Homeotropic cases are aligned in one fixed direction, while, the director of the liquid crystal molecules in the Splay, Twist, Bend, Hybrid and Super-twisted nematic cases are not fixed in one direction. In the latter orientations, the liquid crystals are under stress.

The liquid crystal molecules align parallel to the substrates in the Homogeneous and align perpendicular to the substrates in the Homeotropic alignments. Tilted alignment is an intermediate state between Homogeneous and Homeotropic, and the molecules are tilted at a certain pretilt angle. Actually, the Tilted alignment with low pretilt angle (less than about 10°) is often called Homogeneous. In the Hybrid alignment, the liquid crystals on one substrate have Homogeneous alignment and those on the other substrate Homeotropic alignment.

In practical application, a small tilt from parallel and perpendicular, namely, pretilt is important for obtaining domain-free orientation under electric field.

For smectic LC cells, there are three fundamental alignments (planar, homeotropic and focal conic), while in cholesteric LC cells, there are three corresponding alignments: planar, quasi-planar and focal conic.

One of the most important problems with Ferroelectric Liquid Crystals (FLC) is to obtain homogenous and/or bistable alignment.

Because chiral smectic C phases are difficult to align with a unique molecular axis (bookshelf texture), the phase sometime shows unfavorable defect lines (zig-zag defects) or chevron (a heraldic ornament in the form of a wide inverted V-shape) structure. In order to remove zig-zag defects, uniform tilt alignment is achieved by obliquely evaporated SiO and antiparallel sealed cell. The bistable surface stabilized FLC requires weak surface anchoring. In practical, FLCs can be made to form bookshelf structures by lowering the surface energy and applying voltage.

In nematic liquid crystal cells, there are six commonly used combinations of surface alignment: Homogenous, Homeotropic, Twisted, Hybrid, 180° Super-twisted nematic (STN) and 270° Super birefringence effect (SBE).

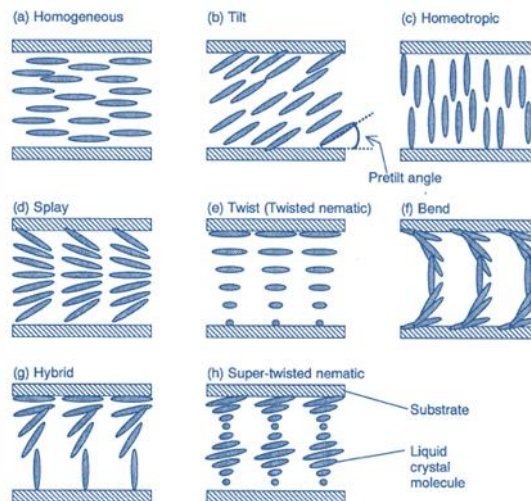


Fig 3.1 Typical orientation in nematic liquid crystals

Parallel, homogeneous, alignment is usually obtained as long as the surface is microscopically flat and liquid crystal does not contain amphiphilic impurity as well as surface polarity is too low to absorb the impurity.

In order to obtain Homogeneous alignment (including the Tilted alignment with less than about 10° pretilt angle), rubbed polyimide films are usually used in mass production, but also non-rubbing methods such as photoalignment and those using microgrooves have been developed.

There are three proposed alignment mechanisms to obtain perpendicular alignment. Amphiphilic materials (surfactants) assisted alignment, i.e., amphiphilic material absorbs perpendicular to the polar surface and LC aligns according to the amphiphilic material. Homeotropic alignment is also obtained by substrates coated with hydrophobic films. Recently, polyimide films with hydrophobic side chains have been developed and used in the multi-vertical aligned nematic (MVA) mode. This second mechanism involve the use of surface coupling agents such as silanes with long alkyl chains.

The third mechanism is microscopic columnar structure-assisted alignment which is obtained by SiO-rotatively oblique evaporation as reported by Hiroshima et al. ⁽¹⁾. The SiO evaporation align method can give any of the Homogeneous, Homeotropic and Tilted alignments by changing the evaporation angle.

These alignment mechanisms are discussed in the next paragraphs.

The reason why hydrophobic surfaces give Homeotropic alignment is explained by the FCK model ⁽²⁾ (see par 3.5).

In general, as the polarity of various metal oxides increases, the tendency of perpendicular alignment of LCs increase. Weak surface polarity of metal oxides favors the parallel alignment.

The liquid crystal molecules near the substrate surface affect the liquid crystal orientation in the bulk (in the middle of a liquid crystal cell) by molecular-molecular interactions, and the orientation in the entire liquid crystal cell is so determined. In most cases, the interaction between the substrate surface (alignment layer) and the liquid crystal molecules near the surface is very strong.

By the application of electric or magnetic fields, the alignment of the liquid crystals near the substrate is hardly changed. Such a relationship between the substrate surface and the liquid crystals is called “strong anchoring”.

In the case of the strong anchoring, after removing the electric or magnetic field, the liquid crystal orientation recovers to that of the initial orientation. In contrast, when the liquid crystal orientation after removing the field is different from the initial orientation, the relationship is called “weak anchoring”.

Mechanism and method to obtain stable surface alignment have been studied by many researchers ⁽³⁾ ⁽⁴⁾ ⁽⁵⁾. Kahn empirically described the alignment as determined by the competition between the surface tensions of liquid crystal and substrate ⁽⁶⁾ ⁽⁷⁾ ⁽⁸⁾, which is based on the relation between surface energies of the substrates and liquid crystal.

The most common methodologies to obtain the parallel, perpendicular and tilted homogenous alignments are argument of the next sections.

3.3 Rubbing Technologies

3.3.1 The rubbing process

Rubbing is still the dominant alignment process, although it has been a long time since Mauguin ⁽⁹⁾ reported this method to align liquid crystals ninety years ago.

The present rubbing process in the manufacture of liquid crystal displays (LCDs) is to rub an organic polymer coated substrate using a rotating drum which is covered by a cloth with short fibers (Fig 3.2). This process has many problems, for example the generation of dust and static electricity, but LCDs cannot be manufactured without it, because it is a short, simple LC alignment process, and can be applied to a large area at low cost.

Although the process is simple, it has large effects on the image quality and reliability of the LCDs. The rubbing controls both the azimuthal and polar angles of the liquid crystal alignment. Irregularities in the rubbing process causes alignment defects. These defects harm the optical characteristics of the LCDs, because the LCDs use the light modulation phenomena that depend on the LC's alignment.

Not only the rubbing itself, but also the alignment materials affect the quality of the LCDs. In the early stages of liquid crystal manufacturing, polyvinyl alcohol, acrylic polymers, and vinyl polymers were tested as alignment materials for rubbing. Finally, a high temperature polyimide was used.

The development of a low temperature polyimide allowed a colored liquid crystal display using color filters. The reason why polyimide became the dominant alignment material is its stability and superior electric characteristics.

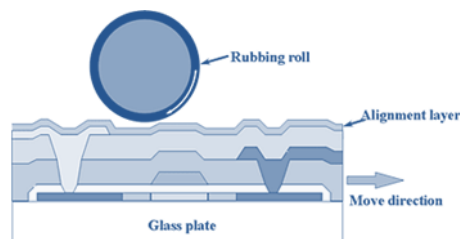


Fig 3.2 Schematic representation of the Rubbing process

3.3.2 *Alignment materials and mechanisms of the rubbing process*

The dominant material for display devices using rubbing alignment processes is a polyimide, not only because of the alignment characteristics, but also for stability, together with its electrical properties, such as resistivity, which are suitable for these devices. Many types of polyimide were synthesized for this purpose⁽¹⁰⁾.

Two types of polyimide are used for actual devices; solvent soluble pre-imidized polyimide and polyamic acid type. A baking process is required for both types of polyimide.

The alignment related process consists of a coating of polyimide, a baking step, rubbing, and cleaning of the substrates. The sensitivity of the alignment material to the manufacturing process conditions is one of the important issues when selecting it for manufacturing use. Stability of the pretilt angle and alignment in the face of normal variations in the processing conditions is required.

Major process parameters are the rubbing process strength, the baking conditions for the alignment material, and the annealing conditions of the panels. Nishikawa et al. reported that a soluble pre-imidized polyimide shows better stability against process instabilities⁽¹¹⁾.

For the perpendicular alignment (that is of fundamental importance in Reverse mode PDLC), at the present, are on the market two types of alignment material: polyimides and organosiloxanes. The polyimide used for this kind of alignment has long side chains.

To examine the alignment mechanisms of the rubbing process, many studies have been made by using modern surface observation techniques such as AFM observations for the surface structure, polarized UV and IR absorption spectral measurements for molecular anisotropy. Table 3.1 summarizes the characteristics of the principal observation methods.

| Method | Subject | Depth | Target of analysis |
|----------------------------------|---------|--------------------------|---------------------|
| AFM | Surface | 0.5-0.8 nm | Morphology |
| UV absorption | Volume | Whole | Molecular direction |
| IR absorption | Volume | Whole | Molecular direction |
| X-ray scattering | Surface | 5 nm | Molecular direction |
| X-ray absorption | Surface | 1 nm | Molecular direction |
| Second Harmonic Generation (SHG) | Surface | Several molecular layers | Molecular direction |
| Water contact angle | Surface | | Polarity |
| Optical retardation | Volume | | Anisotropy |

Tab 3.1 Observation methods for the rubbing process

The main alignment mechanism of the rubbed polyimide is the epitaxial growth of the LC due to the reorientation of polymer molecules ⁽¹²⁾. This reorientation of polymers which gives the anisotropic characteristics caused by rubbing was confirmed by spectral observations.

The buffing of the polymer, induces alignment of its molecular chains, and the orientational order of the liquid crystal then grows epitaxially from the oriented polymer surface ⁽¹³⁾.

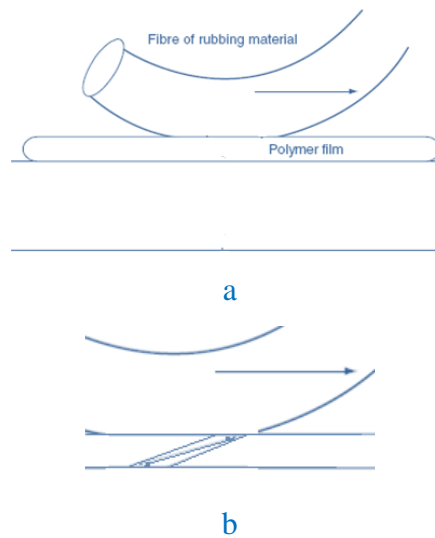


Fig.3.3 a) Cross sectional view of a polymer film in contact with a moving fibre of buffing material and b) enlarged contact region, showing the effect of large shear deformation

The alignment mechanism of the rubbed polyimide, can be expressed by calculation of the anchoring energy. The undulated surface, defined by the depth A and the frequency $\lambda=2\pi/q$, show the azimuthal anchoring energy, W_{\square} , calculated as ⁽¹⁴⁾:

$$W_{\square} = \frac{1}{4}K_{11}(A_q)^2q \quad (3.1)$$

where K_{11} is a splay elastic constant of the LC. By using this equation, we can calculate the relationship between the groove frequency and the anchoring energy, as shown in Fig 3.4:

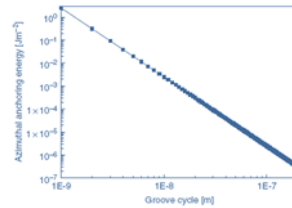


Fig 3.4 Azimuthal anchoring energy as a function of the groove frequency, calculated based on the elastic energy.

The surface grooves caused by rubbing play an important role in the alignment of the LC.

Two alignment mechanisms, a short range interaction by the reorientation of the polymers and a long range interaction caused by the elastic energy induced in the rubbed surface are proposed ⁽¹⁵⁾. The surface reorientation of the polymers, rubbed by cloth, might be the dominant mechanism ^{(16) (17)}.

3.4 Non-rubbing Methods

3.4.1 Introduction

The rubbing based alignment technology is already established for use at actual production sites. However, there remain some problem issues that are yet to be solved., such as unevenness, lack of controllability, failure to achieve multiple domain alignment, and difficulties of status monitoring, all related to its mechanical contact operating principle.

To overcome these problems caused by the buffing mechanism, several liquid crystal (LC) alignment methods have been developed. Previously developed LC alignment methods are summarized in Table 3.2.

These methods can be divided into two categories. One uses surface alignment caused by the anisotropy of the surface. The other method aligns the LCs based on an electric or magnetic field coming from outside the cell, and the surface of the substrate becomes joined to the aligned LC. After the electric or magnetic field is removed, the aligned LC on the surface aligns the bulk of the LC.

Nematic LCs can be easily aligned by a small anisotropy of the surface. However, when the order parameter of the surface alignment or the anchoring energy is small, this alignment tendency is comparable to other causes of anisotropy, e.g. the flow effect of the injection, and many disclination faults can appear. In this specific case, the influence of flow can be eliminated by using an isotropic phase injection of the LC.

Recently, studies of stabilized LC alignment obtained by using polymer networks have been reported. A photo-curable monomer is added to the LC, and it is polymerized by UV exposure after the LC has been aligned either by the surface method or by using electric or magnetic forces. An application for an FLC was reported based on this approach, and good alignment of the FLC was reported

(18).

| Method | Description | Characteristics |
|--|---|--|
| Oblique evaporation (19) | Obliquely evaporate SiO onto a substrate. Alignment direction depends on incident angle. | High tilt angles near 80° can be generated. |
| Micro-groove (20) | Make photolithographic micro-grooves on a substrate. | |
| Stretched polymer film (21) | Attach a stretched polymer film to the substrate. | |
| Dip-coat | Dip a substrate into a polymer solution, and pull it up slowly. | Alignment strength is even weaker than flow alignment. |
| Transcription (22) | Transcribe a rubbing surface structure onto the resin surface. | Multiple domains can be obtained easily by using a prefabricated multiple domain master. |
| Surface stripped film | Strip a polymer film from the substrate. | Tilt angle depends on strip direction and speed. |
| LB film (23) | Stack LB films on a substrate. | Tilt angle depends on pull up speed of the LB film. |
| Photo isomerization (24) (25) | Isomerization | Reversible |
| Photo dimerization (26) (27) | Dimerization | Stable |
| Photo decomposition (28) | Decomposition | Wide selection of materials |
| Photocrosslinking (29) | Crosslinking | Stable |
| Combination of photocrosslinking and photodecomposition (30) | Combination of crosslinking and decomposition. | |
| Magnetic field (31) (32) | Inject LC into a cell in the isotropic phase, apply a magnetic field, and cool down to the nematic phase. | High tilt angles can be established. |
| Flow alignment | Inject LC into a cell with a homogeneous alignment layer in the nematic phase | Weak anchoring |
| Temperature gradient (33) | Inject LC into a cell with a homogeneous alignment layer in the isotropic phase, and cool following a temperature gradient. Polymer edge is used in the cells for nucleation of the alignment | Used for FLC |
| Shear (34) | Put FLC polymer between film, and apply shear stress. | Used for FLC polymer alignment. |
| Amorphous (35) | Inject LC with chiral agent in the isotropic phase into a cell with a homogeneous alignment layer, and cool down. | TN configurations having multiple domains can be established. |
| Ion beam (36) (37) | Substrate covered with polymer exposed to low energy argon ion beam. | |

Tab 3.2 Summary of alignment methods

3.4.2 Ion beam alignment

The ion beam alignment technology is a new alignment technology that is designed to replace the traditional rubbing technology for LC ⁽³⁸⁾.

In this process ⁽³⁹⁾, the alignment films are not rubbed with rollers but are exposed to irradiation from the oblique direction of the ion beam (Argon ions, for example) which is accelerated in an electric field. A diamond-like carbon is deposited on the glass substrate, and exposed to the Ar^+ ion beam that anisotropically decomposes bonds in the diamond-like carbon layer, providing the alignment film surfaces ⁽⁴⁰⁾.

Both the coating of the alignment material and the alignment processes can be freed from any mechanical contacts by using this technique.

While the diameter of the tissues used for the buffing cloths of the ordinary rubbing rollers is of the order of some tens of micrometers, the diameter of the Ar^+ ion is much lower, so this technology can process surfaces at an extremely accurate level and at a high density. The process is therefore attracting attention as a technology that will not leave scratches on the alignment film surfaces and offers high contrast and smooth black images without roughness or irregularities ^{(41) (42)}. In Fig. 3.5 are showed schematically the two processes.

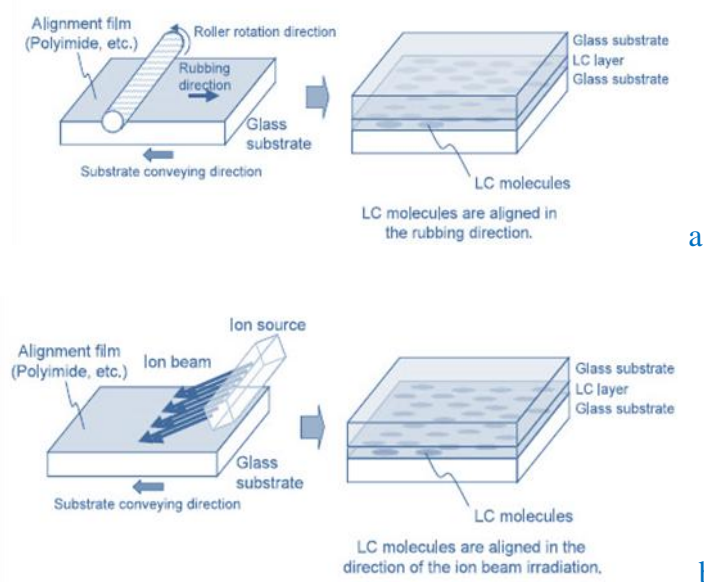


Fig 3.5 Liquid crystal alignment using a) the rubbing process, b) the ion beam process.

3.4.3 Photoalignment

Photoalignment has been a focus of research since, in 1991⁽⁴³⁾, described an azobenzene-mixed polyimide exposed to linearly polarized UV light that aligned the LC. Other authors reported photoalignment by dimerization of poly-vinyl cinnamate⁽⁴⁴⁾ or by isomerization of azobenzene⁽⁴⁵⁾. In these projects, special photochemical reactions, such as dimerization or isomerization, were used, and only a few limited types of photoalignment materials were involved.

In 1994, it was found that polyimide exposed to linearly polarized deep UV light showed LC alignment, and that a wider variety of materials could be used for photoalignment⁽⁴⁶⁾.

Today many types of photoalignment have been developed, and the choices of materials have increased. All ranges of pretilt angles can be established by photoalignment. Not only linearly polarized light, but also a non-polarized light can be used as the light source for photoalignment⁽⁴⁷⁾.

This technique has been applied to the TN cells resulting hybrid LCD with high resolution of alignment pattern. Its hybrid molecular configuration is operable in a black and white mode as well as in color.



Fig.3.6 Photo induced alignment of liquid crystals with polarized light.

3.4.3.1 Alignment materials and mechanisms for the photoalignment

The most common technique for photoalignment involves the generation of an anisotropic distribution of the molecules of the alignment materials by using the dependence of the polarization direction of the absorption of light by the molecules⁽¹⁰⁾.

When the electric vector of the photons coincides with the transition moment of the molecule, the molecule absorbs light strongly, and a photochemical reaction occurs. The creation of anisotropy by using polarized light is called the *Weigert effect*, and has been known since 1920. However, the photo-alignment mechanisms in some materials are not yet understood because the photochemical reactions are different in each photo-alignment material. In some cases, the LC alignment direction depends on the exposure energy of the light on the photo-aligning material.

Two similar LC alignment mechanisms coexist, one caused by residual molecules not affected by the light, and the other relying on photochemically produced structural changes ⁽⁴⁸⁾. The photochemical reaction type can be categorized as photodimerization, photodecomposition, photolinking, and a combination of decomposition and linking.

3.4.3.2 Influence of UV light on display device characteristics

Degradation of the polymer by deep UV exposure generate many radicals ⁽⁴⁹⁾ and causes various problems on the photo-aligned LC devices.

Image sticking, or other residual image phenomena, is one of the big problems. The offset voltage, which causes the image sticking, increases linearly with dosage. The radicals generated by the UV exposure absorb ions or impurities in the LC, and generate an electrical double layer. This double layer generates an internal voltage inside the cell ⁽⁵⁰⁾.

3.4.4 *Oblique Evaporation Method*

Practically, liquid crystal alignment is required on an active matrix like an Amorphous Si-TFT array or on microstructures like colour filters. Therefore a surface contact treatment like the rubbing method tends to be dangerous because of substrate surface damage like electrostatic damage, chemical contamination and mechanical damage of the patterns on the substrate surface. Thus a non-contact alignment treatment has advantages compared with the conventional rubbing method. Oblique evaporation of SiO is one of the few methods in this category⁽⁵¹⁾ in which device quality alignment is realized other than by rubbing.

3.4.4.1 *Alignment mechanism*

In the oblique evaporation process, a micro columnar structure is realized on the substrate surface, due to the self shadowing effect. When a nematic liquid crystal contacts such a surface, elastic deformation of the liquid crystal along the surface induces an interaction energy between the surface and the nematic material. This is thought to be the driving force for alignment of the nematic director.

The surface structure of the oblique evaporated film changes with the evaporation angle (the angle between evaporation beam and substrate normal). The structure of stepwise grooves and the array of columns change their angle and density. The surface structure of the oblique evaporated film is illustrated schematically as in Fig 3.7. There are many grooves and columns, the features of which vary with evaporation angle and change in the nematic alignment direction and pretilt angle.

A homogeneous alignment is realized by an evaporation angle less than 20° , but the in-plane direction of the alignment is not determined uniquely. At an evaporation angle of ca. 50° , homogeneous alignment with a 0° pretilt angle is realized due to the grooves perpendicular to the beam plane (the plane made by the substrate normal and the evaporating beam)⁽⁵²⁾.

Using materials other than SiO attains nematic alignment by oblique evaporation, but a well grown columnar structure is essential.

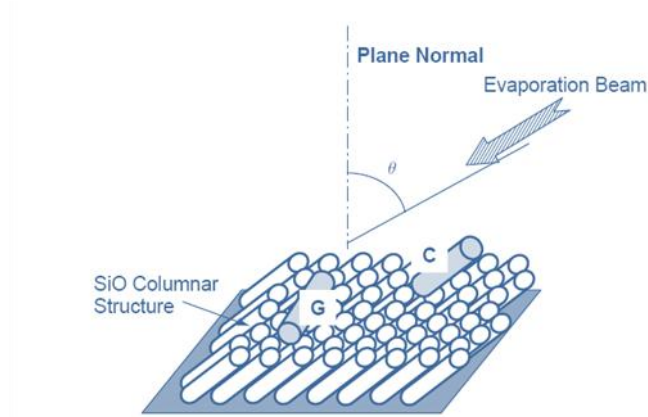


Fig 3.7 The surface structure of the oblique evaporated film. The Liquid crystal molecules lie in the position G (along the groves) or C (along the columns) according to the evaporation angle θ , as indicated.

Generally the oblique evaporation film has a large surface area and is chemically active, i.e., in gas adsorption. Detailed information about the chemical interaction between the surface and the liquid crystalline materials on it is not fully clarified at present, and therefore there might be many unknown factors involved in achieving the reliability of alignment required in device application.

3.4.5 LB membranes for the alignment layer

It is well known that surface active agents with hydrophobic groups such as long alkyl chains with hydroxy or carboxy groups form monomolecular films on the surface of water. By removing the formed film onto a substrate, the monomolecular film can exist on the substrate. Monomolecular layers can also be stacked to form multilayers with several molecular layers. The monomolecular film is named a Langmuir-Blodgett film (or LB film) after the names of the inventors.

Ikeno et al. ⁽⁵³⁾ demonstrated the utility of polyimide-LB films for orienting LCs without performing rubbing. Monomolecular films of amphiphilic compounds were transferred to hydrophilic substrates by dipping a cleaned glass plate into and out of a solution with constant surface pressure by means of a motor drive.

To move the monomolecular film from the water surface to the substrate, there are several possibility. For example, the substrate can be moved up or down perpendicular to the water surface. In another method, the substrate surface is held parallel to the water surface and touches onto the monomolecular film parallel to the water surface so shifting the film to the substrate.

The LB films formed, depending if there is a transfer when the substrate is lifted upwards (pressure is added to the edge of the monomolecular film on the water surface), moved downwards or moved both upwards and downwards, are called 'Z-type', 'X-type' or 'Y-type'.

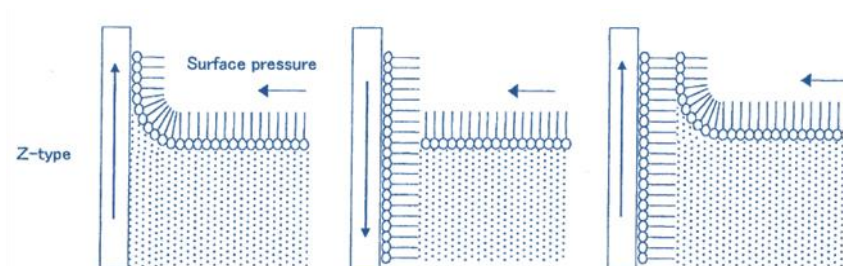


Fig 3.8 Formation of a LB film.

It is well known that liquid crystalline materials align in the extension direction on an extended polymer film surface. The polymer LB film formed by moving the substrates perpendicularly is considered to be a uniaxially extended polymer film, and therefore, liquid crystal alignment on the surface of such a polymer LB film can be expected.

Homeotropic alignment is obtained at low packing density. Using this technique it is possible to build up monolayer or multilayer functional films of organic materials. The polyamidic acid LB films for LC alignment are the most extensively studied material. The polyamidic acid LB film were prepared from alkylamine salt and then removed the alkylamine to obtain the polyamidic acid LB film.

However, twisted nematic (TN) and supertwisted nematic (STN) LCDs using these LB films have alignment defects, such as reverse twist and reverse tilt caused by the fact the use of LB films does not result in pretilting of liquid crystal molecules ⁽⁵⁴⁾. The quality of LB film is high in microscopic region but is poor in macroscopic areas.

Indeed, smectic Liquid crystals are aligned by the alignment layer of polyimide, by rubbing, and photoalignment. The zigzag-free alignment layer of ferroelectric LC is fabricated by photodegradation and photocyclization.

3.5 Liquid Crystalline Alignment on Chemically Treated Surfaces

Surface active agents are often used in industry to form homogeneous polymer layers or to increase adhesion for paints and adhesives. In the case of liquid crystalline materials, surface active agents like silicone compounds are used to obtain homeotropic alignment.

In the case of polymer materials, surface active agents are used both for surface treatment of the substrates and as additives to the polymer materials.

When using surface active agents for liquid crystal materials, two methods are again reported to control the liquid crystal alignment:

- Addition of surface active agents to the liquid crystalline materials
- Treatment of the surface of substrates with surface active agents

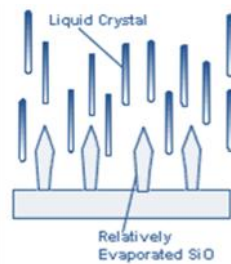


Fig 3.9 Alignment on Silane treated surface

3.5.1 Addition of surface active agents into liquid crystalline materials

In this case, a solution of surface active agents in an appropriate solvent is added to the liquid crystalline materials and then the solvent is removed under reduced pressure. In Table 3.3, the relationship between the surface active agent concentration and the liquid crystal alignment are shown when the surface active agent, cetylammmonium bromide is added to a nematic liquid crystalline material (5).

Low concentrations of the surface active agent result in homogeneous alignment, and high concentrations result in homeotropic alignment.

| %CTAB | 0 | 0.01 | 0.1 | 0.25 | 0.5 | 1 |
|--------------|-----------------------|---------------------|-----------|----------------------|----------------------|----------------------|
| σ | 1.8×10^{-10} | 2×10^{-10} | 10^{-9} | 1.7×10^{-9} | 2.9×10^{-9} | 7.4×10^{-8} |
| LC alignment | | | | — | ⊥ | ⊥ |

Tab 3.3 Alignment and conductivity, σ , of the nematic mixture TN103, with added CTAB (cetyltrimethylammonium bromide)⁽⁵⁾

In Table 3.3, an ionic surface active agent is used. However, when ionic materials are mixed into liquid crystalline materials, several LCD driving problems are known to occur. Saturated voltage increases because of the decrease in the electrical resistance of the liquid crystalline layer. During driving of the LCDs, the absorption of ionic materials onto the substrate surface occurs depending on the magnitude of the signal voltage. The absorption increase or decrease of the threshold voltage compared to that of the initial state causes the defect known as the, ‘sticking phenomenon’. In this phenomenon, the signal information remains after the signal on the liquid crystal disappears.

In the injection process of liquid crystalline materials, ionic compounds are also absorbed onto the surface near the injection point, and this causes an inhomogeneous threshold voltage. Although the application of ionic surfactants in the dynamic scattering (DS) mode was examined, potential use is limited for the above reasons.

3.5.2 Treatment of the substrate surface by active surface agents

To obtain homeotropic alignment by surface active agent treatment of the substrate surface, silicon compounds are usually used as the surface active agent. Silicon compounds, such as alkoxysilanes or chlorosilanes, react with the substrate surface following the scheme in Fig 3.10, and polymerize to form polysiloxane structures near the surface.

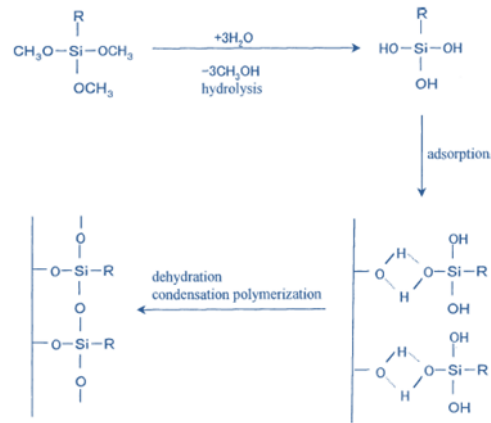


Fig 3.10 Scheme for the reaction between a silicon compound and the substrate

In practice, the surface treatments are carried out by:

- 1) dipping the substrates into a 1-5% aqueous or organic solution of the silane compounds,
- 2) exposing the substrate surface to the vapour of pure silane compounds or of a toluene solution,
- 3) spreading silane compounds on the substrate surface.

In the case of polymer materials, such as paints or adhesives, the wetting properties can be anticipated by using the critical surface γ_c . Let the surface tension of the polymer material γ_1 .

- If $\gamma_1 > \gamma_c$, it is difficult for the surface to become wetted
- If $\gamma_1 < \gamma_c$, the surface can be easily wetted

Thus, the critical surface tension, γ_c , can be used to measure the ease of wetting of the solid surface.

When homologous series of liquids like alcohols or alkyl halides give a contact angle θ on some solid surface and surface tension is γ , $\cos\theta$ can be expressed as:

$$\cos\theta = 1 - b(\gamma - \gamma_c) \quad (3.2)$$

where b is a constant, usually 0.03-0.04. The surface tension of the liquid for which $\cos\theta$ is equal to 1, or θ is equal to 0, is the critical surface tension γ_c .

Liquid crystalline materials also give a similar relationship, and, the critical surface tension, γ_c , is used as the criterion for homeotropic or homogeneous alignment.

Where γ_{lc} is the surface tension of a liquid crystalline material,

- if $\gamma_{lc} > \gamma_c$; the liquid crystalline material shows homeotropic alignment
- if $\gamma_{lc} < \gamma_c$; the liquid crystalline material shows homogeneous alignment

In another expression, by using the solid surface tension, γ_s :

- if $\gamma_{lc} > \gamma_s$; liquid crystalline materials show homeotropic alignment
- if $\gamma_{lc} < \gamma_s$; liquid crystalline materials shows homogeneous alignment

These experimental rules are called the “*Friedel-Creagh-Kmetz (FCK)*” rule. In most cases, this rule can be confirmed, with some exceptions.

A strong relationship between the alkyl chain length of surface active agents and the surface tension and critical surface tension of the treated surface can be observed. Generally speaking, a surface treated by a surface active agent with short alkyl chain shows a large surface tension value and vice versa. This suggests that to obtain homeotropic alignment, surface active agents with long alkyl chains should be applied.

Usually, N, N-dimethyl-N-octyl-N-3-trimethoxysilylpropylammoniumchloride (DMOAP) is generally selected to obtain homeotropic alignment.

Polynuclear complex salts of chromium, aluminum, iron and cobalt are reported to have been used to form the alignment layers for liquid crystalline materials^{(55) (56)}. In Fig. 3.11 are the structures of layers on glass surfaces treated by carboxylato-chromium complexes of both alkanolic and alkandioic acid. Glass surfaces treated by n-alkanoic acids with more than 3 carbon atoms induce homeotropic liquid crystalline alignment as indicated in Fig. 3.11(a).

On the other hand, Fig. 3.11(b) shows the structure of glass surfaces treated by carboxylato-chromium complexes of an alkandioic acid. These surfaces show homogeneous liquid crystalline alignment. In the above cases, the alkyl group

conformation of the carboxylic acid determines the alignment of the liquid crystalline materials.

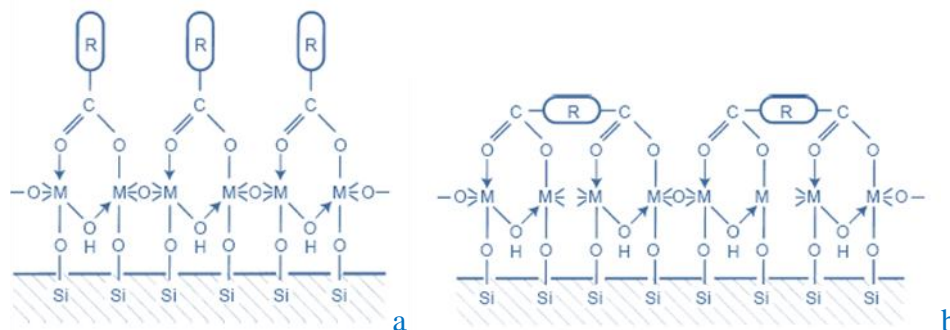


Fig 3.11 Schematic representation of polymerized layers of carboxylatochromium complexes chemisorbed on glass surfaces: a) monocarboxylatochromium complex; b) dicarboxylatochromium complex.

The method of obtaining homeotropic alignment by processing the substrate surface with a surface active agent is well used as a basic laboratory procedure. Trials continue an adding special functions into the alignment layers by using functional groups instead of alkyl groups in active surface agents. By introducing the azo group whose structure can be reversibly changed by light, homogeneous alignment or homeotropic alignment can be changed by irradiation with two different wavelengths of light.

In tab 3.4 are summarized ⁽⁵⁷⁾ (divided into anionic, cationic, non ionic and amphoteric surfactants) a series of surface-active molecules known to induce homeotropic orientation in nematic liquid crystals. Most of these molecules were studied in years of 1970-1990, but there are also works published in recent years, as Takahashi in 2007, about pyridine salts ⁽⁵⁸⁾.

3.5.3 Pyridinium salts

We conclude this chapter with a brief mention of a particular type of Ionic Liquid crystals ⁽⁵⁹⁾, the pyridinium salts.

Thermotropic mesomorphism of pyridinium salts was noticed as early as 1938 by Knight and Shaw ⁽⁶⁰⁾. The authors observed mesophases for N-(n-alkyl)-pyridinium chorides and iodides. Several authors studied other molecules of this

kind and in all cases smectic A phases was found. The smectic A phase (it is uniaxial) is the most common texture for ionic liquid crystals, have a strong tendency to align homeotropically (the homeotropic texture is observed as a dark field between crossed polarizer). The model proposed for the molecules in the smectic A phase is one in which the molecules within one layer are oriented on average perpendicularly to the layer plane in alternate head-to-tail fashion. The “halogen” ions are positioned in such a way that they are sandwiched between the pyridinium ring of neighboring molecules. If in the 4 position of the ring is positioned a group with a strong dipole moment (like the ciano group) it is possible the formation of an ordered smectic B phase.

Recently, Takahashi ⁽⁵⁸⁾ claimed a procedure to obtain LC molecules with a pyridinium ring to which a dialkylamino group is attached as a substituent group at 4-position. This kind of molecules are capable of controlling the angle of aligned liquid crystal molecules. The synthesis involves the reaction of DMAP with a suitable molecule. Similar molecules, but with a different procedure for their formation, were object of this thesis work.

| <i>anionic</i> | <i>cationic</i> | <i>Non-ionic</i> | <i>Anphoteric</i> |
|---|--|--|--|
| acyclic carboxylic acids; aromatic carboxylic acids; | Alkyl-ammonium salts Alkyl-pyridine salts Alkyl-isoquinoline salts; | aliphatic esters complexes; | Lecithin; α -leucine |
| carboxylic acids with LC structure: Derivates of Schiff's bases (-C=NR) Derivates of azo-structured liquid crystals Azo-oxy derivates Stilbene derivates Cyanobiphenyl derivates | 7-alkyl-1,8-diazobicyclo[5.4.0]undecenammonium; Chromium carboxylates complexes | nitriles and ureic aromatic acids esters; phenols, aromatic amines; long chain alcohols | <i>Others:</i> Epoxy-resin; polyamidic resin; alkylphenyl-esters; poly-oxyethyl glycol; fluorinated polymers |

Tab 3.4 Classification of surface-active molecules inducing homeotropic orientation in nematic liquid crystals [extrapolated from: J. Cognard, "Alignment of nematic liquid crystals", Gordon&Breach, (1987)]

References

1. Y. Hiroshima et al., *Japan. J. Appl. Phys.*, 21, L791 (1982).
2. L.T. Greagh and A.R. Kmetz, *Mol. Cryst. Liq. Cryst.*, 24, 59 (1973).
3. I. Haller: *Appl. Phys. Lett.*, 24, 349 (1974).
4. T. Uchida et al., *Mol. Cryst. Liq. Cryst.*, 60, 37 (1980).
5. J. Cognard, *Mol. Cryst. Liq. Cryst.*, 78, Supl.1.1, (1982).
6. L.T. Greagh and A.R. Kmetz, *Mol. Cryst. Liq. Cryst.*, 24, 59 (1973).
7. F. Kahn et al., *Proc. IEEE*, 61, 823 (1973).
8. T. Uchida, *Mol. Cryst. Liq. Cryst.*, 123, 15 (1985).
9. C. Mauguin: *Bull. Soc. Fr. Min.* 34, 71 (1911).
10. K. Takatoh et al., *Alignment technologies and applications of liquid crystal devices*, Taylor&Francis, p. 48, (2005).
11. M. Nishikawa, Y. Matsuki, N. Bessho, Y. Imura, S. Kobayashi, *J. Photopolymer Sci. and Tech.* 8, 233, (1995).
12. A.J. Pidduck, G.P. Bryan-Brown, S.D. Haslam, R. Bannister, *Liq. Cryst.* 21,759 (1996).
13. J. M. Geary, J.W. Goodby, A. R. Kmetz, J. S. Patel, *J. Appl. Phys.* 62, 4100, (1987).
14. D.W. Berreman: *Phys. Rev. Lett.* 28, 1683 (1972).
15. W. Chen, M. B. Feller, and Y. R. Shen: *Phys. Rev. Lett.* 63, 2665 (1989).
16. A.J. Pidduck, G.P. Bryan-Brown, S.D. Haslam, et al., *J.Vac. Sci.Technol. A14*, 1723 (1996).
17. M.S. Toney, T.P. Russel, J.A. Logan, H. Kikuchi, et al., *Nature* 374, 709, (1995).
18. H. Furue, Y. Imura, H.Hasebe, H.Takatsu, S.Kobayashi: *IDW'97*, 73, (1997).
19. J. Janning: *Appl. Phys. Lett.* 21, 173, (1972).
20. D. Flanders, D. Shaver, H. Smith: *Appl. Phys. Lett.* 32, 15, (1978).
21. H. Aoyama, Y. Yamazaki, N. Matsuura, et al., *Mol. Cryst. Liq. Cryst.* 72, 127 (1981).
22. Y.Toko, B.Y. Zhang, T. Sugiyama, K. Katoh, et al., *Mol. Cryst. Liq. Cryst.* 304, 1985, (1997).
23. K. Kawahara, Y. Nakajima, T. Udagawa, H. Fuji, H. Morimoto: *Proc. 14th IDRC*, 180, (1994).
24. K. Ichimura, Y. Suzuki, T. Seki, A. Hosoki, K. Aoki, *Langmuir*, 4, 1214, (1988).
25. W. Gibbons, P. Shannon, S. Sun, B. Swetlin, *Nature* 351, 49, (1991).
26. M. Schadt, K. Schmitt, V. Hozinkov, V. Chigrinov, *Jpn. J. Appl. Phys.* 31, 2155 (1992).
27. T. Yoshida, T. Tanaka, J. Ogura, H. Wakai, and H. Aoki: *SID '97 Digest*, 841, (1997).
28. M. Hasegawa and Y. Taira: *J. Photopolymer Science and Technology* 8, 241, (1995).
29. Y.-K. Jang, H.-S. Yu, J. K. Song, B. H. Chae, K.Y. Han: *SID '97 Digest*, 703 (1997).
30. M. Oh-e, M. Ohta, S. Aratani, K. Kondo, *Proc. 15th IDRC (Asia Display '95)*, 577 (1995).
31. N. Kishida and S. Kikui, *Appl. Phys. Lett.* 40, 541 (1982).

32. K. Hiroshima, T. Maeda, T. Furihata, *Proc. 12th IDRC(Japan Display '92)*, 831, (1992).
33. K. Ishikawa, K. Hashimoto, H. Takezoe, A. Fukuda, E. Kuze, *Jpn. J. Appl. Phys.* 23, L211, (1984).
34. S. Hachiya, K. Tomoike, K. Yuasa, S. Togawa, T. Sekiya, K. Takahashi, K. Kawasaki: *J. Soc. Inf. Disp.* 1, 295, (1993).
35. Y. Toko, B.Y. Zhang, T. Sugiyama, K. Katoh, T. Akahane, *16th ILCC Abstracts, BIP53*, (1996).
36. N. Yamada, S. Kohzaki, F. Fukuda, and K. Awane: *SID '95 Digest*, 575 (1995).
37. P. Chaudhari, J. A. Lacey, S.-C. A. Lien, and J. Speidell: *Jpn. J. Appl. Phys.* 37, L55, (1998).
38. T. Suzuki, J. Matsushima, Y. Sasaki, *High Image Quality Panel Technology - Ion Beam Alignment, NEC Technical Journal, Vol.1 No.3/2006*.
39. A. Lien, M. Angelopoulos, K. W. Lee, et al., *Asia Display '95*, 593, (1995).
40. P. Chaudhari, et al., *Nature*, Vol. 411, p.56 (2001).
41. D. N. Stoenescu, et al., *Mol. Cryst. Liq. Cryst.*, Vol. 351, p.427 (2000).
42. M. Kimura, *EKISHO (Liquid Crystals)*, Vol., 10, p.95 (2006).
43. W. Gibbons, P. Shannon, S. Sun, and B. Swetlin: *Nature* 351, 49 (1991).
44. M. Schadt, K. Schmitt, V. Hozinkov, V. Chigrinov: *Jpn. J. Appl. Phys.* 31, 2155 (1992).
45. K. Ichimura, Y. Suzuki, T. Seki, A. Hosoki, K. Aoki, *Langmuir* 4, 1214, (1988).
46. M. Hasegawa, Y. Taira: *Proc. 14th IDRC*, 213, (1994).
47. Y. Kawanishi, T. Takimiya, K. Ichimura: *Polym. Mater. Sci. Eng.* 66, 263, (1992).
48. E. Endo, T. Shinozaki, H. Fukuro, Y. Iimura, S. Kobayashi: *Proc. AMLCD '96*, 341, (1996).
49. K. Lee, A. Lien, J. Stathis, S. Paek: *SID '96 Digest*, 638, (1996).
50. M. Hasegawa, H. Takano, A. Takenaka, et al., A. Lien, *SID '96 Digest*, 666, (1996).
51. K. Lee, A. Lien, J. Stathis, and S. Paek: *SID '96 Digest*, 638 (1996).
52. J. L. Janning: *Appl. Phys. Lett.* 21, 173 (1972).
53. H. Ikeno et al., *Japan. J. Appl. Phys.*, 27, 827 (1988).
54. H. Ikeno et al., *SID Digest*, p. 45, (1988).
55. S. Matsumoto, M. Kawamoto, N. Kaneko, *Appl. Phys. Lett.* 27 (5) 268 (1975).
56. S. Matsumoto, *Chemistry and Chemical Industry* 32 (10) 753 (1979).
57. J. Cognard, , *Alignment of nematic liquid crystals* , Gordon & Breach, (1987).
58. Takahashi et al, *4-aminopyridinium compound*, US Patent n°7193087 B2, (2007).
59. K. Binnemans, *Ionic liquid crystals*, *Chemical reviews*, vol. 105, no11, 4148-4204, (2005).
60. J. Cognard: *Mol. Cryst. Liq. Cryst. Suppl. Ser. (1)* 1(1982).

CHAPTER 4: Impurities characterization in the bis{4-[(6-acryloxy)hexyloxy]benzoate}-1,4-phenylene (C6H) LC monomer

4.1 Introduction

Many scientific groups, in the last years, have developed different sythetic procedures for the obtainment of polymerizable LC molecules, useful in the realization of composite films (PSLC, PDLC etc..) to be employed in electrical controlled light shutters ⁽¹⁾ ⁽²⁾. In particular, liquid crystals monomers with twopolymerizable groups have rised interest as starting materials for the production of anisotropic networks ⁽³⁾ ⁽⁴⁾.

Bireative monomers can be used in situ photopolymerization: ⁽⁵⁾, ⁽⁶⁾ a technique that involves the macroscopic orientation of LC molecules with reactive end groups, such divinylethers, diepoxydes or diacrylates, followed by UV irradiation ⁽⁷⁾. In this way the molecular orientation within the system becomes fixed , due to the creation of the three-dimensional anisotropic network.

One advantage of the photopolymerization, when compared with thermally activated polymerization, is the temperature indipendence of the photopolymerization process. The temperature can be chosen in the range of the mesomorphic state, and the polymerization proceeds with a greater degree of conversion. In this way the degree of order and consequently the anisotropic properties of the network can be adjusted as desired.

In the production of anisotropic networks various reactive liquid crystals molecules were synthetized ⁽⁸⁾. Such molecules can be schematically represented in three parts:

- central mesogenic group
- reactive end group
- flexible spacers.

Each of these group plays an important role in determining the thermal properties, the liquid crystalline phase and the optical properties in the monomeric state. They also influence the polymerization behaviour and infer particular properties to the obtained anisotropic network ⁽⁹⁾.

Another important aspect of the production of optical shutters (but not only), is the process of alignment in the liquid crystal devices. This influences the cost, time and technology required for the production of composite systems, like PDLC and PSLC, and LC displays.

Authors like Cognard ⁽¹⁰⁾ and, recently, Takatoh ⁽¹¹⁾, report a considerable collections of methodologies to get macro-aligned LC systems (see chapter 3 of this thesis).

A font of inspiration for this thesis was Ohgawara work ⁽¹²⁾ regarding the alignment of Liquid crystal molecules on various surfaces. This author used the Liquid Crystal Chromatography, to observe the true orientation properties of the mesogenic molecules, getting free from the influence of impurities contained in the LC materials. It was found that “all nematic LC of Schiff base-, biphenyl-, ester-, PCH-, and azoxy- compounds aligned parallel to the surfaces on In₂O₃, Al₂O₃, soda-lime glass, SiO₂, etc. On the other hand, some of these LC such as MBBA, 5CB have been known to have a tendency to align perpendicular to surface like In₂O₃. Then, the reason of this discrepancy was also investigated and it was found that impurities produced by hydrolysis of these LC had amphiphile characteristic which induced perpendicular alignment of these liquid crystals.”

4.2 The history of our interest for C6H

The LC monomer 4 - [(6-acryloxy) hexyloxy] benzoate - 1,4-phenylene, also called C6H ⁽¹³⁾ is a liquid crystal diacrylate monomer, very useful to make ordered polymer networks and is very good in the preparation of PDLC systems.

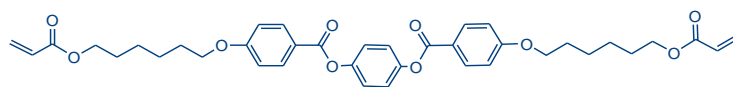


Fig 4.1 bis{4-[(6-acryloxy)hexyloxy]benzoate}-1,4-phenylene (C6H).

Common phase transitions /°C: Cr-115-N-155-I)

The starting point of this work was the observation that the C6H, synthesized through a synthesis scheme developed at Calabria University⁽¹⁴⁾, spontaneously align homeotropically when supported on glass. The above synthesis was different from that classical brought in literature⁽¹⁵⁾, but according to the process given by Boer⁽¹⁶⁾.

On the other hand, the same monomer when synthesized with a different reaction scheme, at the laboratories of Professor R. Dabrowski (*Military Technical Academy, Warsaw, Poland*) (called “commercial C6H” in this thesis) did not show any spontaneous alignment property.

It was therefore hypothesized⁽¹⁷⁾, that the alignment of the system was due to the formation of some impurities deriving from the particular reaction scheme adopted by Cassano et. al. (defined as *CU synthesis* in the following).

This chapter is centered on the characterization of intermediate, sub-products occurring in the CU synthesis of the C6H monomer. The effect of further purification of the C6H monomer obtained in CU synthesis was also investigated.

4.3 Synthesis of bis{4-[(6acryloxy)hexyloxy]benzoate}1,4-phenylene(C6H)⁽¹⁴⁾

The complete CU synthesis pathway for C6H can be summarized in the following steps:

- Step 1 (formation-attachment of the spacers, Fig 4.2):

the 4-hydroxyethyl-benzoate react with 6-Chloro-1-hexanol. After basic hydrolysis is obtained the carboxylic acid that is washed and recrystallized.

- Step 2 (acylation, Fig 4.2):

The second step involves the acylation of the acid 4-[6-hydroxyHexyl)oxy]benzoic with the acryloyl chloride, in presence of N,N dimethylaniline.

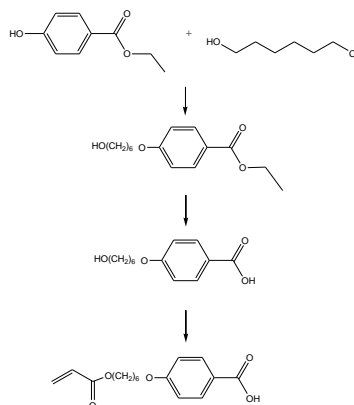


Fig 4.2 Step 1-2 of the CU Synthesis of C6H (synthesis of acid 4-[6-(acryloxy)hexyloxy]benzoic)

– Third step (Fig 4.3):

the acid 4-[6-(acryloxy)hexyloxy]benzoic, synthesized in this way and purified by recrystallization, is used to obtain the desired monomer in a reaction with the Hydroquinone, in presence of DMAP, according to the scheme.

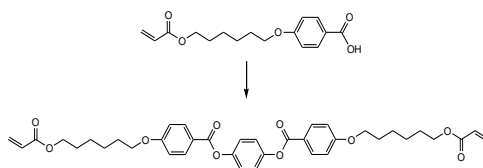


Fig 4.3 Step 3 of the CU Synthesis of monomer C6H (formation of C6H LC monomer)

The monomer and intermediates of this three-step synthesis were characterized by spectroscopic methods and studied by mean of optical microscopy with crossed polarizers, in order to check the properties of alignment of the monomeric/polymeric film.

Then, the C6H produced by this way was compared with the commercial C6H, produced by a different synthesis pathway (Fig 4.4), that can be resumed in the following scheme:

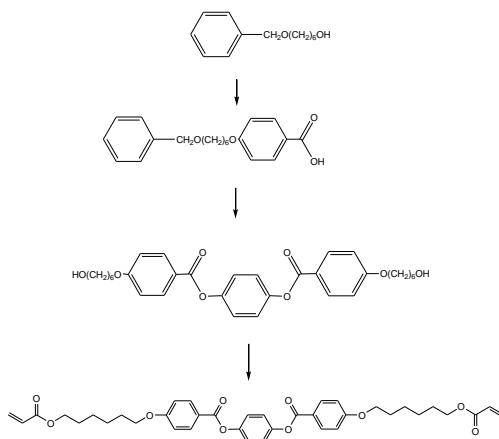


Fig 4.4 Synthesis of the commercial monomer C6H (outlines)

The most important difference between the two synthesis is that for the commercial monomer the synthesis start from the core of the molecule and adds, way by way, the ester groups, the spacers and, as final step, the reactive (acrylate) group. At the contrary, the CU synthesis starts from the formation of the end “acrylic” acid unities, which are then joined together by a central quinonic core.

4.4 Characterization of the monomer

The CU synthesis C6H products as well as the intermediates at each of the above mentioned steps, and after several recrystallizations, were analyzed by ¹H-NMR and FTIR, to check their chemical structure and impurities, on the basis of reference data taken from Ref^{(18) (19)}

The temperatures of phase transition of C6H were determinate by differential scanning calorimetry (DSC) (par 4.4.1). The optical microscopy with crossed-polarizers was used to study the homeotropic self-alignment of the compounds, cycling trough the Isotropic- nematic and nematic- crystal phase transitions by means of an appropriate heating stage.

Chromatographic separation (par 4.4.2) was done to estimate the amount of sub-products present and to isolate them from the principal compound.

SEM-EDS (par 4.4.3) qualitative microanalysis was also used in order to get information on the impurities and in particular to check the presence of nitrogen, sulfur and chlorine in the synthesis impurities.

Qualitative MS (par 4.4.4) analysis was made. In this case the molecular peak was not registered, but the combination of the other peaks confirmed that the appropriate compound was synthesized.

GC-MS analysis was not achieved because was not possible to vaporize the monomer, due to the very high molecular weight

All the spectroscopic data confirmed that C₆H compound was appropriately synthesized, but they also showed the presence of little quantities of other molecules, similar to the C₆H. The relevant data and results for the performed analysis will be given in the following.

4.4.1 DSC

The differential scanning calorimetric unit (Setaram DSC-131 by courtesy of prof L. Coppola, Chemistry Department of Calabria University) was calibrated by melting indium. 3mg of sample were weighed in Al crucibles of 30 μ L capacity. DSC runs were performed on CU synthesized C₆H and on Commercial C₆H at 3 $^{\circ}$ C/minute from 25 $^{\circ}$ C to 180 $^{\circ}$ C. The peaks at 106 $^{\circ}$ C and 153 $^{\circ}$ C indicate respectively the Crystal-Nematic and the nematic-isotropic transition, in agreement with the literature dates for the C₆H. The of 5 degree lowering observed in nematic to isotropic phase transition of the CU synthesized C₆H compound as well as the enlargement of the pick at the nematic to crystal phase transition indicate the presence of not negligible amount of impurities in the CU synthesized C₆H.

| Transition temperatures: | Commercial C6H | CU Synthesized C6H | Literature values (ref) |
|--------------------------|----------------|--------------------|---------------------------|
| T(solid/nematic) | 106 | 106 | 108 |
| T(nematic/isotropic) | 153 | 148 | 155 |

Table 4.1 DSC measurements of the synthesized monomer, reference C6H compared with the literature values.

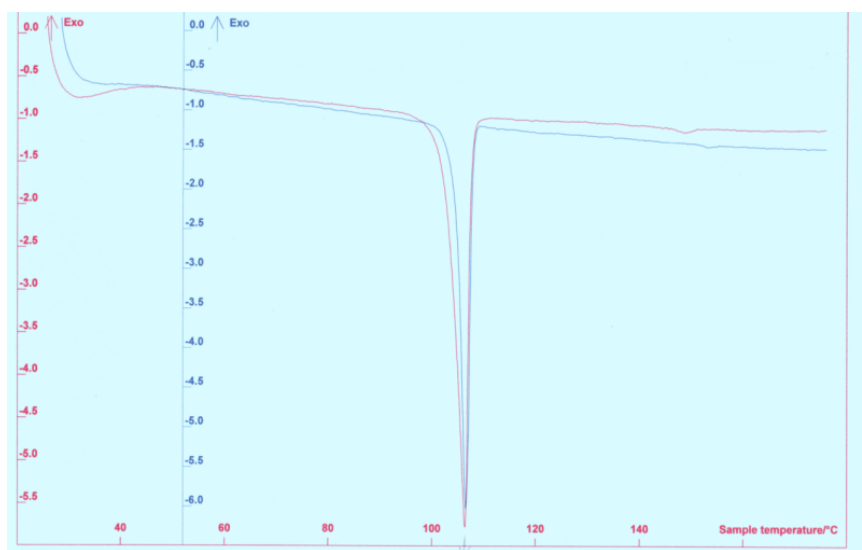


Fig 4.5 DSC curves of commercial C6H (blue line) and CU Synthesized C6H (red line)

4.4.2 TLC

The chromatographic separation was done by TLC, to evaluate the presence of synthesis sub-products. Then column and preparative TLC was used, to isolate and recovery the different fractions for the spectroscopic analysis ⁽²⁰⁾.

The TLC chromatogram obtained from the CU synthesis product, after a single recrystallization) has been compared with the chromatograms of:

- the commercial C6H;
- bi-recrystallized CU Synthesized C6H;
- pure reactants;
- intermediate compounds obtained at each of the synthesis steps.

This investigation showed that most of the spots obtained in the Cu synthesized C6H are identifiable as reagents or intermediates of the second reaction step, but some of the stain, appearing as strips (see bottom of fig. 4.6), could not be identified both by direct comparison and by subsequent spectroscopic analysis due to their negligible amount

The used TLC-plates were: silica gel 60 F254, on glass, by Merck; the best solvent system (eluent mix) in our case was: CH₂Cl₂/MeOH 9/1 (or CH₂Cl₂/EtOH 9,5/0.5). Analogue solvent system was used for the column chromatography.

The developed TLC plates were observed by UV light (254 nm) and after in a iodine chamber to best evaluate the presence of extended pi-systems, amine and thiols.

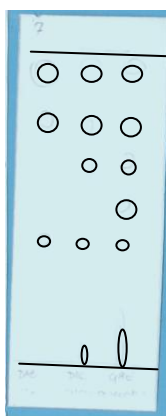


Fig 4.6 TLC of (from the left) commercial C6H, CU Synthesized C6H recrystallized, C6H without recryst. Solvent system: CH₂Cl₂/MeOH 9/1. The spots

on the starting line, that are not present in the commercial C₆H, undergo oxidation in the time.

4.4.3 SEM/EDS microanalysis

The samples were observed both without metallization and after metallization with gold (preferred respect to the carbon to avoid the overlap of the signals at low keV), on a LEO 420 (LEO Electron Microscopy Ltd. Cambridge, England) at 15 kV, 150-50 pA. Then the microanalysis was carried out using an “INCA-EDS” system (Oxford instruments), at 650 pA and 15kV.

In the CU synthesized C₆H, besides carbon and oxygen, it was found chlorine and nitrogen, that are absent in the commercial C₆H.



Fig 4.7 SEM image of a crystal of CU Synthesized C₆H (Magnification: 50x)

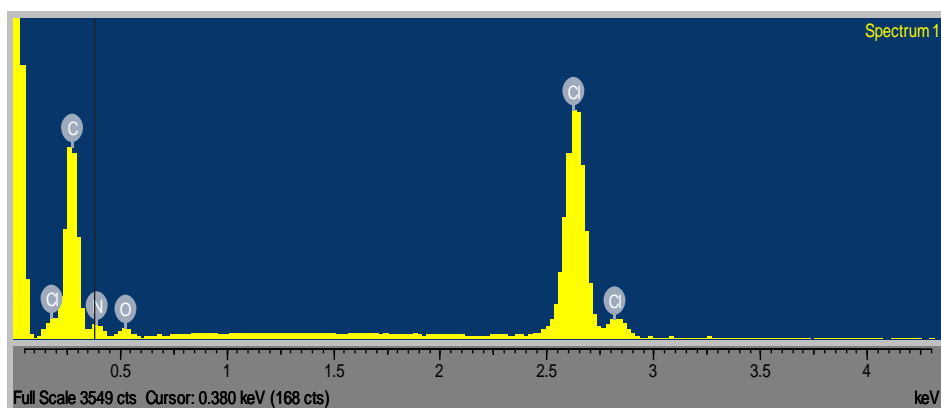


Fig 4.8 EDS spectrum of the CU Synthesized C₆H: The elements found to be present are C, N, O, Cl

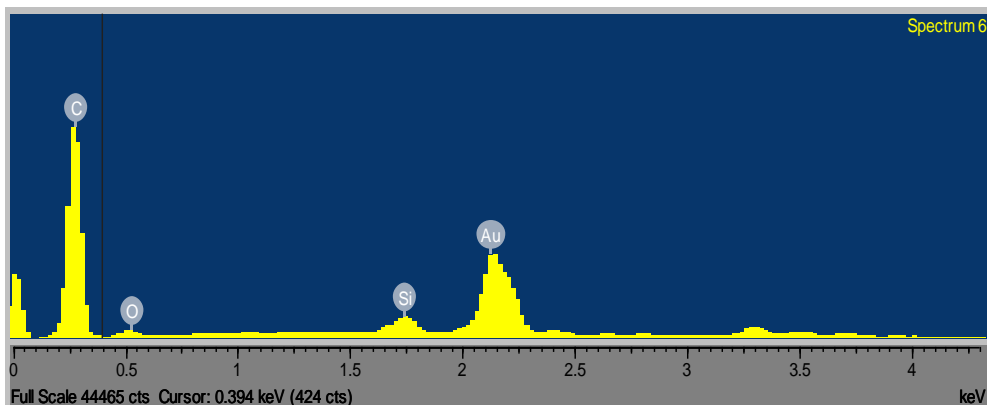


Fig 4.9 EDS spectrum of commercial C6H (Au metallized). Nitrogen was not found.

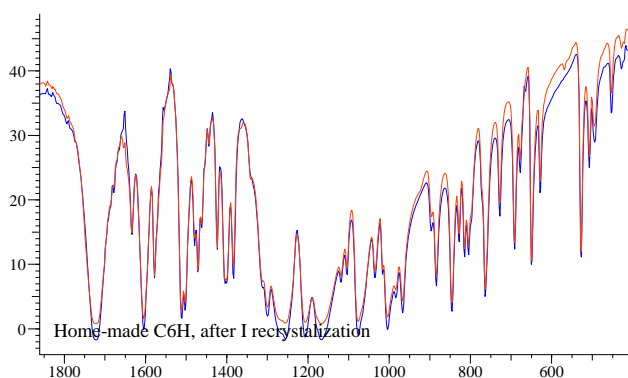
4.4.4 FTIR

Infrared Spectroscopy (FT-IR) spectra were achieved with Jasco 430 and Biorad FTS 6000 spectrometers using KBr disks. 1 mg of monomer was dispersed in a matrix of KBr (100 mg), followed by compression to form disks. All spectra were registered from 4000 to 400 cm^{-1} , with a resolution of 4 cm^{-1} and 64 scans; the background was collected before each spectrum. Each spectrum was repeated three times; these were then averaged and considered as a single measurement. The IR bands were compared with the literature values and through a database search.

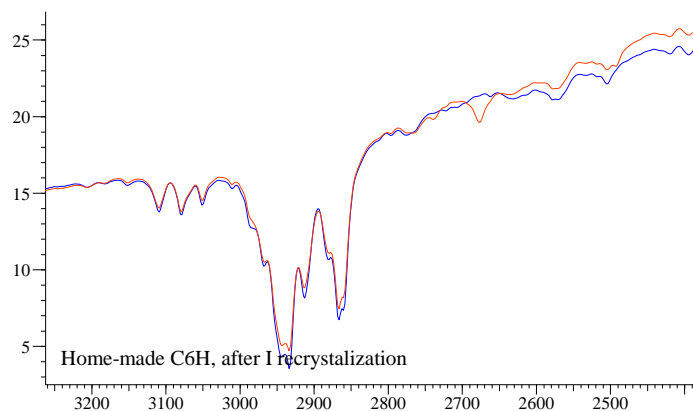
The commercial and CU synthesized C6H appear to be identical, but a small band centered around 2700 cm^{-1} (quaternary ammonium salts: 2700 – 2300 cm^{-1}) which is only present in the CU synthesized C6H (fig 4.10). This band disappear after the second recrystallization of the CU synthesized C6H (fig 4.11). Unfortunately it was not possible to characterize the residue recovered after the second recrystallization of C6H, since this was mainly made by acetonitrile (SR 150, Bio-Rad IR SearchMaster Database), and this indicate that the impurities are in very low percentage.

| CU Synthesized C6H (I recryst) | CU Synthesized C6H (II recryst) | Commercial C6H (I recryst) | Literature values (18) |
|--------------------------------|---------------------------------|----------------------------|--|
| 3431 | 3431 | 3431 | 3434 (vw. OH); |
| 3109, 3078, 3047 | 3109, 3078, 3047 | 3109, 3078, 3047 | 3110, 3080, 3051 (vw, CH ar.); |
| 2965, 2933, 2912, 2866 | 2965, 2933, 2912, 2866 | 2965, 2933, 2912, 2866 | 2944, 2933, 2914, 2867 (w CH al.); |
| <u>2737, 2677, 2492</u> | <u>Not found</u> | <u>Not found</u> | <u>Not found</u> |
| 1720 | 1720 | 1720 | 1725 (s. C=O); |
| 1633 | 1633 | 1633 | 1634 (w, C=C al.); |
| 1605, 1510, 1502 | 1605, 1510, 1502 | 1605, 1510, 1502 | 1605, 1512, 1502 (m, m, w C=C ar.); |
| 1423, 1404 | 1423, 1404 | 1423, 1404 | 1425, 1405 (w, CH=CH); |
| 1312, 1205 | 1312, 1205 | 1312, 1205 | 1311, 1207 (w, m, acrylate); |
| 1300, 1255, 1166 | 1300, 1255, 1166 | 1300, 1255, 1166 | 1298, 1256, 1168 (w, s, vs, C-O); |
| 844 | 844 | 844 | 850, 846 (w, 2H adj); |
| 763 | 763 | 763 | 764 (w, CH ₂ CH ₂); |

Table 4.2 IR bands ($/\text{cm}^{-1}$) of the synthesized, CU Synthesized C6H and the commercial C6H. Comparison with the literature values.



a



b

Fig 4.10 FTIR spectra of CU Synthesized (red) and Commercial (blue) C6H. From the top: a) finger print region; b) region between 2700 e 3250 cm^{-1} (This region, which shows some small differences between the two spectra, correspond to the quaternary amonium salts region).

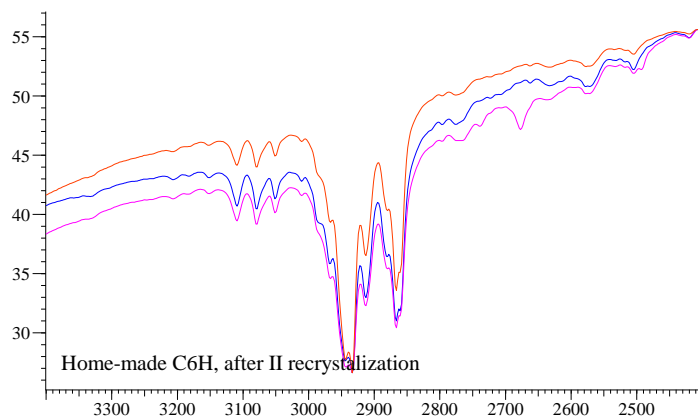
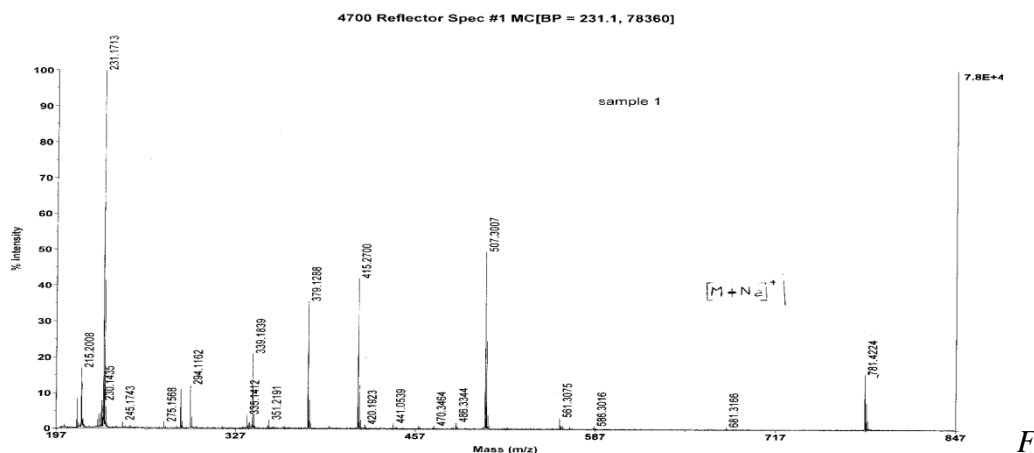


Fig 4.11 Effect of the recrystallization on CU Synthesized C6H. A II recrystallization (red spectrum) determine a lost in the bands between 2800-2300 cm^{-1} , and at the same time the lost in homeotropic alignment capacity respect to the I recrystallized CU Synthesized C6H (pink). The commercial C6H (blue) is shown for comparison.

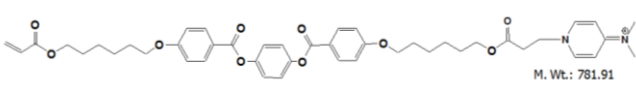
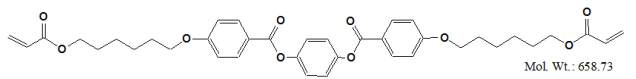
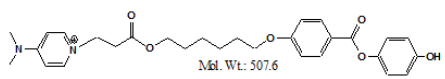
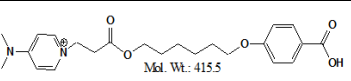
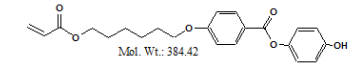
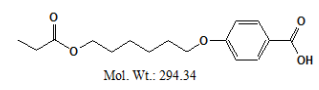
4.4.5 MALDI TOF-MS

The MALDI MS-MS qualitative experiments (by courtesy of prof. Anna Napoli, Chemistry Department Calabria University) were carried out on CU Synthesized C₆H monomer dissolved in MeOH. The molecular peak is not registered but the combination of several molecular ions and fragments allows to make sure that the appropriate compound was synthesized. The second fragmentation (MS-MS spectra) was done on the principal fragments (m/z) found to be present (see tab 4.3). The identification of the fragments was done by the instrument software, taking into account scores, unsaturation numbers, hypothesized chemical formula, and comparison with the literature data ⁽¹⁸⁾ ⁽¹⁹⁾. The fragment 681 m/z was found to be C₃₈H₄₂O₁₀Na and assigned to [M-Na]⁺ while the fragment 781 m/z (formula: C₄₅H₅₃N₂O₁₀) is the result of an addition of DMAP (used in the third step of the CU synthesis) on C₆H.

Unfortunately it is difficult to distinguish between fragments generated during the analytical procedure from the C₆H and those due to the presence of impurities: many of the fragments could derive from the same ion parent but even to be sub-products of the synthesis. However, tanks to the result of this experiment we could acquire the certitude that an impurity resulting from the addition of DMAP (added in the third/final step of our synthesis) to the C₆H acrylate group, is present.



ig 4.12 MALDI MS spectrum of CU Synthesized C₆H. The molecular peak, at 658 m/z was not found.

| m/z | Fragment identified | Structure |
|---------------------|---|---|
| 781.42 | C6H-DMAP ⁺ |  M. Wt.: 781.91 |
| 681.23 | C6H-Na ⁺ | |
| 658.73 Not found | C6H ⁺ |  Mol. Wt.: 658.73 |
| 507.34 | Product of II step of synthesis, with hydroquinone and DMAP |  Mol. Wt.: 507.6 |
| 415.5 | Product of II step of synthesis, with DMAP |  Mol. Wt.: 415.5 |
| 379.09 | Product of II step of synthesis, with hydroquinone |  Mol. Wt.: 384.42 |
| 294.12 | Product of II step of synthesis |  Mol. Wt.: 294.34 |
| 287.25 | DMAP fragm+H ₂ Q | |

Tab 4.3 MALDI MS fragments found by the CU Synthesized C6H soft ionization

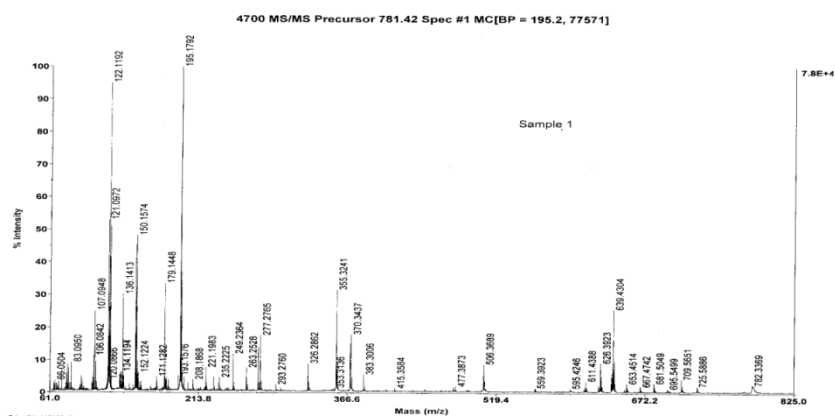


Fig 4.13 MALDI MS-MS spectrum of CU Synthesized C6H. Precursor: 781.42

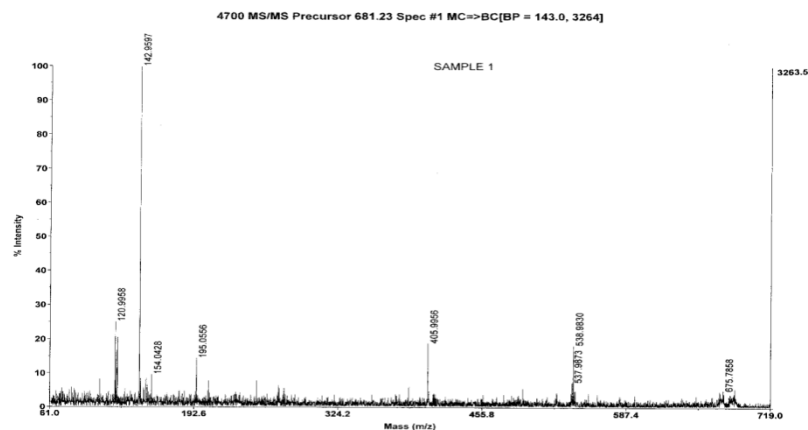
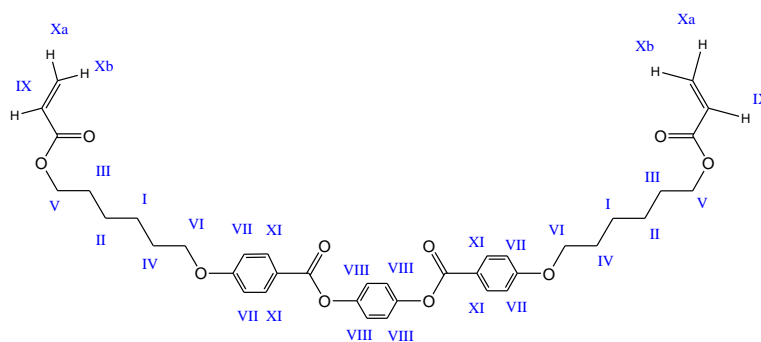


Fig 4.14 MALDI MS-MS spectrum of CU Synthesized C6H. Precursor: 681.23

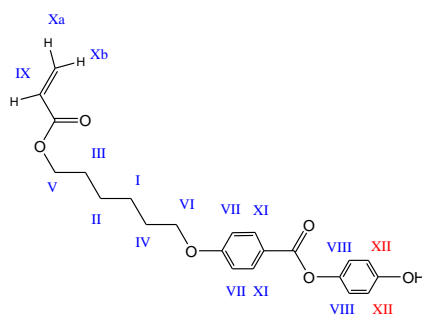
4.4.6 $^1\text{H-NMR}$

^1H NMR spectra of CU C6H synthesized (mono and bi recrystallized) and Commercial C6H show all the C6H expected peaks, with expected integration ratios⁽¹⁸⁾. Data are reported in tab. Nevertheless, a set of low intensity signals, not belonging to C6H, appear. The attribution of these peaks was made taking account the already illustrated, Chromatography, MALDI and EDS results.

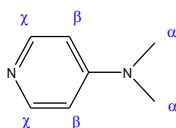
The protons in C6H and of the hypothesized impurities have been labeled as in fig 4.15



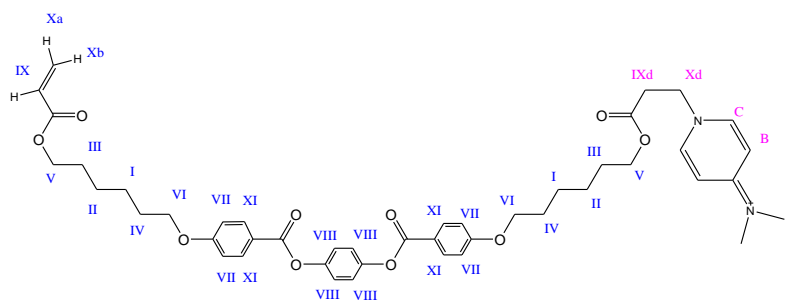
(1)



(2)



(3)



(4)

Fig 4.15 Label assignment of the protons for C6H(1); C6H after hydrolysis of an internal ester group(2); DMAP(3); and C6H-DMAP adduct(4)

The peaks between 8 and 6.6 ppm from C6H (protons labeled XI, VIII, VII) correspond to the aromatic groups. The peaks between 6.5 and 5.5 ppm are from the acrylic group (protons IX, Xa, Xb) while the aliphatic group near to the ether/ester oxygen (V, VI protons) are between 4.5 and 3.5 ppm. Finally, the aliphatic protons are shown between 2.5 and 1 ppm (labels I, II, III and IV).

Minimum amounts of impurities, which disappear after recrystallization, are present even in the commercial C6H. These contain OCH₂CH₃ groups (peaks at 3.08 and 1.39 ppm), as suggested by chromatographic analysis. Fig 4.16 show a

comparison of the Commercial C6H before and after recrystallization and after addition of Hydroquinone (that is commonly added, in low percentage, to prevent spontaneous polymerization of monomers).

The CU synthesized C6H, contains not only the impurities discovered in the commercial C6H, but some other products which generate new small peaks (fig 4.17). These peaks can be attributed in the following way:

- 8.52(d) ppm to the C protons of the C6H-DMAP adduct (4 in fig 4.15.), or to the XI protons of molecule (2) ;
- 7.90 (d) ppm to XI and VIII of molecule (2);
- 6.68 ppm to the B proton of molecule (4) or to XII of molecule (2) ;
- 3.70-3.10 are compatible with the IXd, Xd and IX or X protons in molecule (4) or in polymerized monomers;
- 2.80 ppm multiplet derive from IX, protons in the modified acrylic group.

The interesting aspect to underline is the effect of a second recrystallization on the CU synthesized C6H (fig 4.18), that determine a loss of homeotropic aligning capacity. This result in the disappearing, in the ¹H-NMR spectra, of the signals at 6.68 ppm (the aromatic region of both modified pyridine and hydroquinone) and the signal between 3.70-3.10 ppm (the region attributed to the modified acrylic group). These peaks are recovered in the spectra obtained from the residual of the second recrystallization.

| CU Synthesized C6H (I recryst) | CU Synthesized C6H (II recryst) | Residual after II recryst. of CU Synthesized C6H | Commercial C6H | Commercial C6H with H2Q | Commercial C6H (I recryst) | Literature values for C6H [Guillard], DMAP and H ₂ Q [Aldrich Library] | Labels and multiplicity expected for the protons |
|--------------------------------|---------------------------------|--|----------------|-------------------------|----------------------------|---|--|
| 8.52 d; 8.40 d | 8.40 d | | | | | | C (d) or XI mod |
| | | | | | | 8.22 (d, 2H) of DMAP | γ, d., 2H |
| 8.13 d | 8.13 d | 8.13 d | 8.15 d | 8.15 d | 8.14 d | 8.13(d, 9 Hz, 4H, ar.); | XI d., 4H |
| 7.87 d; 7.52 d | 7.86 d, 7.52 d | 7.90 | | | | | XI (d), VIII mod |
| 7.25 s | 7.25 s | 7.25 s | 7.25 s | 7.25 s | 7.25 s | 7.24 (s, 4H, ar); | VIII s., 4H |

| | | | | | | | |
|--------------------------------------|--------------------------------------|--------------------------------------|--------------------------------------|--------------------------------------|--------------------------------------|--|---|
| 6.97 d | 6.97 d | 6.96 d, 6.92 d | 6.98 d | 6.98 d | 6.97 d | 6.95 (d 8.8 Hz, 4H, ar); | VII d., 4H |
| 6.68 m | (6.69 m)low | 6.76 m | | 6.70 s (H ₂ Q) | | 6.68 (s, 4H) of hydroquinone; 6.48 (d, 2H) of DMAP | H ₂ Q s (m if mod), 4H; β, d., 2H |
| 6.40 dd 6.12 dd 5.82 dd | 6.40 dd, 6.11 dd 5.80 dd | 6.41 dd, 6.15 dd, 5.82 dd | 6.41 dd, 6.13 dd, 5.82 dd | 6.41 dd, 6.13 dd, 5.82 dd | 6.40 dd; 6.12 dd 5.81 dd | 6.38 (dd, 17, 3, 1.5 Hz, 2H, vinyl); 6.11 (dd, 17.3, 10.5 Hz, 2H vinyl); 5.81 (dd, 10.5, 1.5 Hz, 2H vinyl); | Xb d.d., 2H IX d.d., 2H Xa d.d, 2H |
| 4.18 t; 4.05 t | 4.18 t, 4.05 t | 4.19 t, 4.05 t | 4.18 t, 4.05 t | 4.18 t, 4.05 t | 4.18 t, 4.05 t | 4.17 (t, 6.7 Hz, 4H, COOCH ₂); 4.04 (t, 6.6 Hz, 4H, PhOCH ₂); | V t, 4H; VI t, 4H |
| 3.79 t, 3.15 m | | 3.76 t, 3.56 t, 3.10m | | | | | IXd t, Xd t or IX, X mod |
| 3.09 - 2.8 (m) | | 2.92, 2.80 (m) | 3.08 quad | 3.08 quad | | 3.34 (quad, 2H) of O-CH ₂ -CH ₃ for diethyl ether | IX mod |
| 3.00 s | | | | | | 2.99 (s, 6H) of DMAP | α s, 6H, A s |
| 1.84 quint, 1.72 quint; 1.49 m | 1.84 quint, 1.72 quint; 1.48 m | 1.84 quint, 1.73 quint; 1.50 m | 1.84 quint, 1.72 quint; 1.49 m | 1.84 quint, 1.72 quint; 1.49 m | 1.84 quint, 1.73 quint; 1.49 m | 1.83 (q, 6.7 Hz, 4H, COOCH ₂ CH ₂); 1.71 (q, 6.6 Hz, 4H, PhOCH ₂ CH ₂); 1.4-1.57 (m, 8H, inner CH ₂ CH ₂) | III q, 4H IV q, 4H I, II m, 8H |
| 1.37 t | | 1.24 | 1.39 t | 1.39 t | | 1.07 (t, 3H) of OCH ₂ -CH ₃ for diethyl ether | |

Table 4.4 : ¹H-NMR signals (/ppm; 300 MHz, CDCl₃) of the CU synthesized C6H after first and second recrystallization, the residual recovered after II recr., the commercial C6H, the literature values (in blu), and the assignment of the signals to the protons. The impurities signals are writing in green.

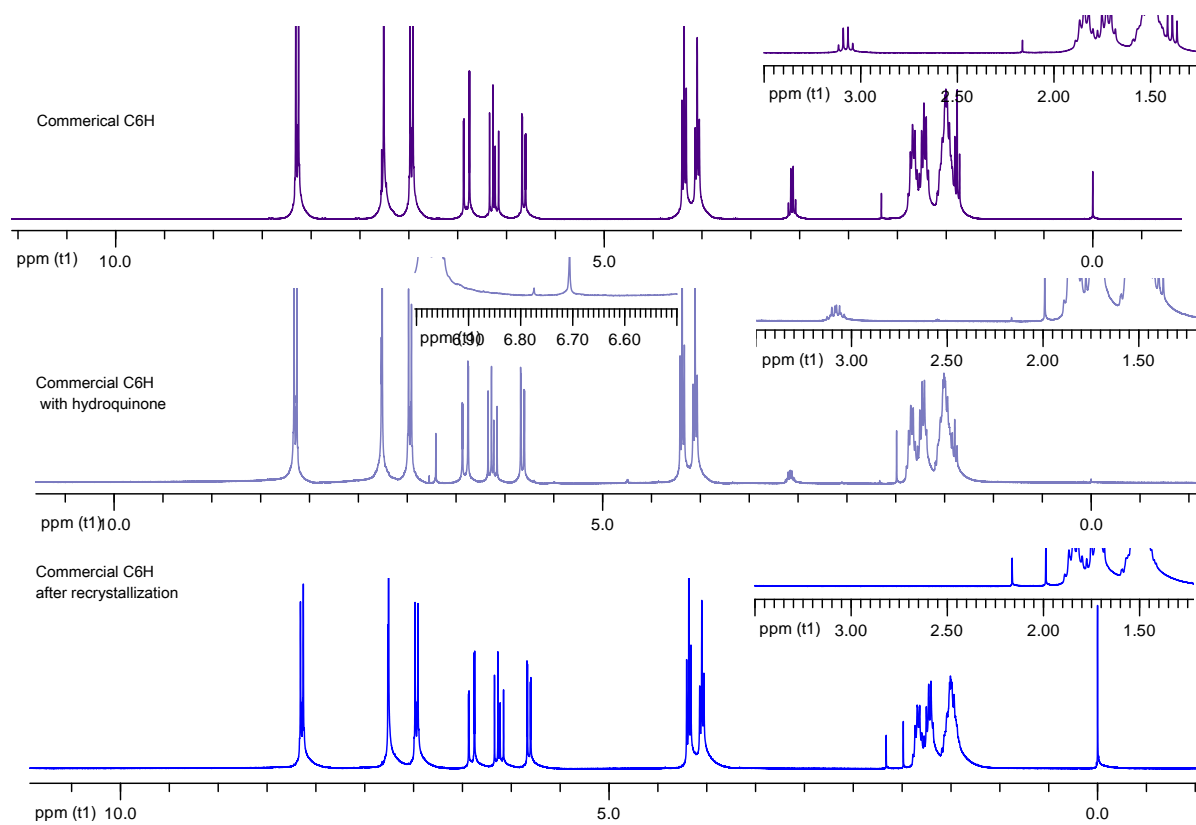


Fig 4.16 $^1\text{H-NMR}$ spectra of (from the top) Commercial C6H, commercial C6H stabilized with Hydroquinone and commercial C6H recrystallized. Enlarged regions indicate the impurity of OCH_2CH_3 (peaks at 1.41 and 3.07 ppm) and the region of the hydroquinonic peak (at 6.69 ppm).

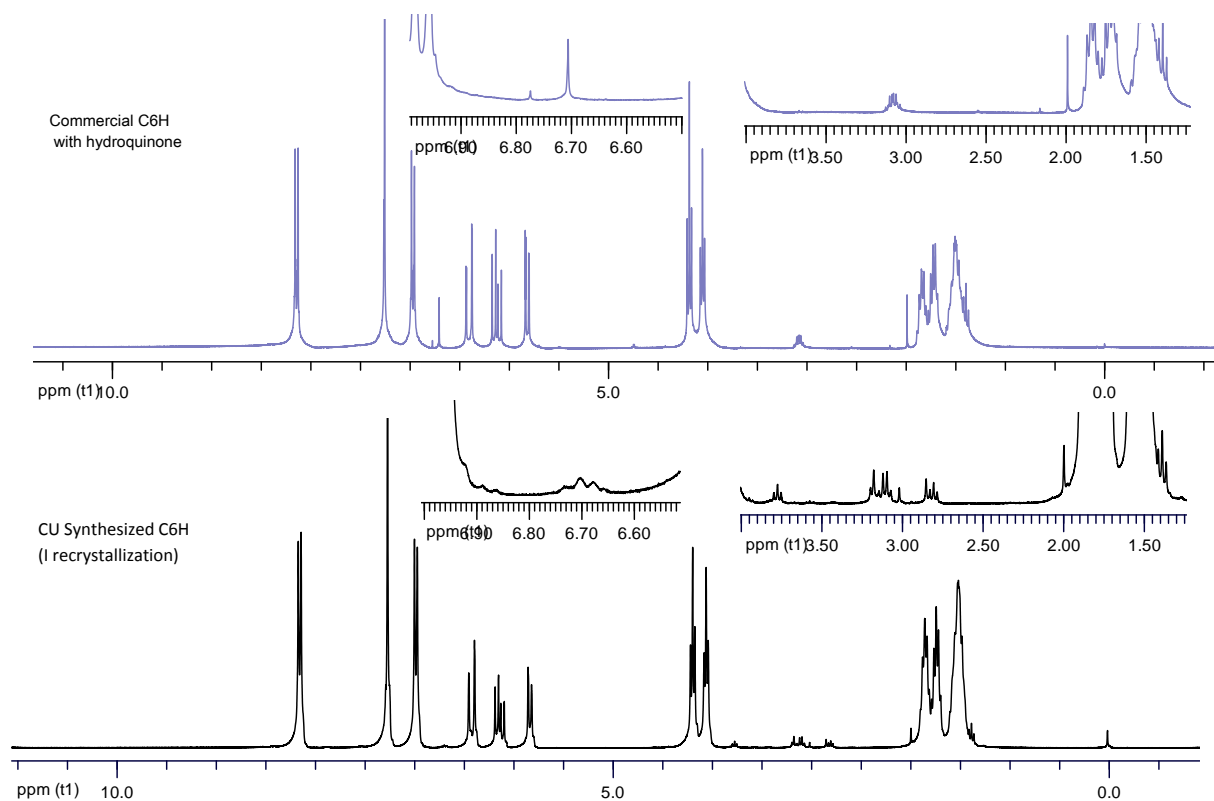


Fig 4.17 $^1\text{H-NMR}$ spectra of Commercial C6H, stabilized with hydroquinone (top, indigo); bottom and CU Synthesized C6H (bottom, black). The enlarged region between 1.25 and 4 ppm shows the new signals found in CU Synthesized C6H (see text)

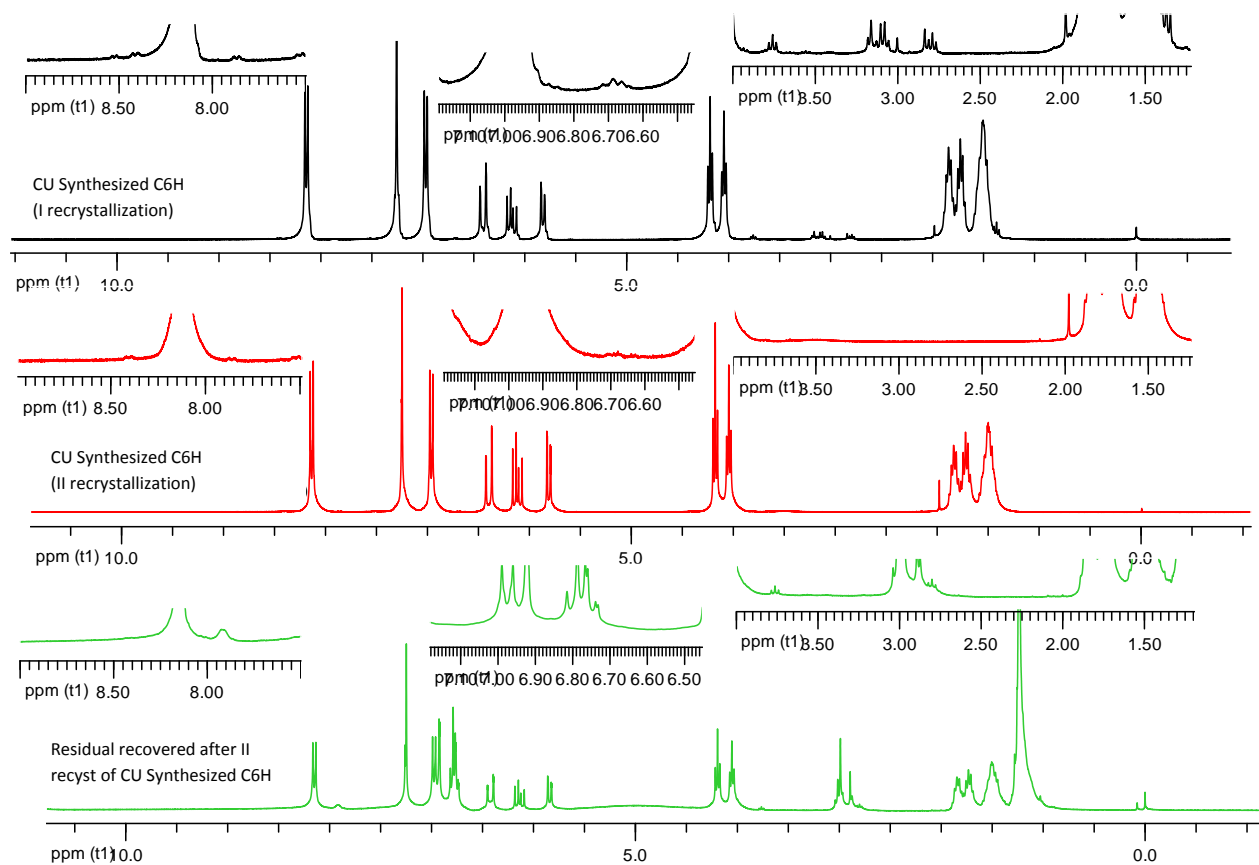


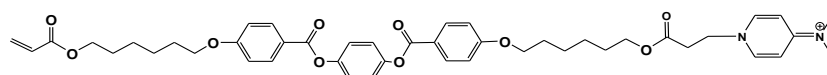
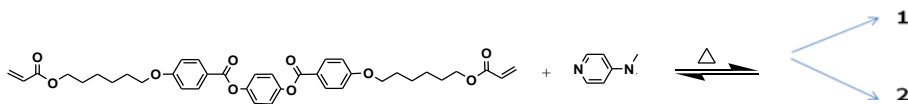
Fig 4.18 $^1\text{H-NMR}$ spectra of CU Synthesized C6H after I recrystallization (black spectrum), CU Synthesized C6H after II recrystallization (red) and Residual recovered after the II recrystallization (green). Enlarged regions at 1.25 – 4 ppm, at 6.45 – 7.20 ppm (the hydroquinonic type proton) and 7.5 – 9 ppm are also showed.

4.5 Impurities generation mechanisms

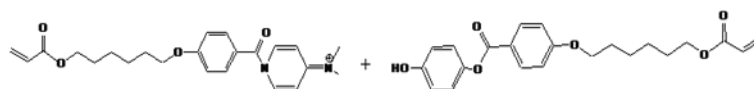
The spectroscopic analysis above illustrated of the CU synthesized C6H, indicate the formation of several sub-products, like fragment of C6H and an acrylate formed by an “asymmetric” mono-addition to the hydroquinone in the third step of our synthesis, with formation of molecules with a phenolic tail. Literature work indicate the possibility of formation alcoholic fragments, by hydrolysis of C6H ester groups⁽²¹⁾ due substituted amines chemical attac . This suggests that the formation of the “self-aligning” impurities in the CU C6H synthesis could be mainly related to the reactions of dimethylaminopyridine (DMAP) with the C6H, used in the third CU synthesis step.

Further, recently, a synthesis method⁽²²⁾ to prepare LC pyridine salts, which induce homeotropic alignment in nematic LCs, it was performed. The procedure consists of a multi-step synthesis, comprising addition of pyridines to a chloride intermediate, in low temperature conditions. Other works report the addition of tertiary amines to acrylic acid, in equilibrium conditions⁽²³⁾ with formation of quaternary ammonium salts⁽²⁴⁾.

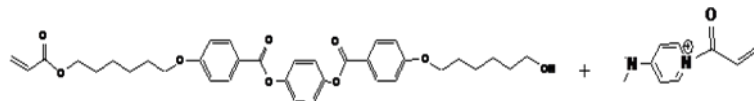
ON these basis, the Michael addition of DMAP (added in the third step of the CU C6H synthesis to facilitate the addition of hydroquinone) to acrylate group (showed in fig 4.19 a), could hypothesized, in such a way to generate aligning impurities. Other possible reactions such as the addition of hydroquinone at a carbonyl group in the C6H, or/and aminolysis, with formation of amides and alcohols, could be also taken into consideration. In the case of an aminiolysis two site can react (see fig 4.19 b, c).



(a. Michael synthesis, i.e. the 1,4-addition of primary and cyclic secondary amines to esters of α,β -unsaturated α -unsubstituted carboxylic acids)



(b. aminolysis on the internal groups ester)



(c. aminolysis on the external groups ester)

Fig 4.19 Probable reactions responsible for the formation of interest impurities during the third step of CU synthesis of C6H: (1) Product (*molecule a*) of a like Michael addition; (2) Aminolysis products at the (b) internal or (c) external ester groups.

4.6 Reproduction of aligning “impurities” in C6H monomer

To test the above hypothesis, a set of experiments have been performed. Commercial C6H and DMAP have been mixed and brought at the a suitable temperature, in order to favor the adduct formations between these two molecules. The reaction products have been investigated and the Homeotropic alignment capacity of the resulting mixtures have been studied by optical microscopy under crossed polarization.

The reactions between DMAP and C6H, were conducted for different ratio of reactants, at different times and in several solvent, like DMSO, DMF and chloroform and, further, without solvent. The chloroform was found to be the best solvent, because of its affinity for both the reactant and easiness in removal.

We define as “standardized conditions for the reaction” (s.c.) the following conditions: chloroform as solvent, 80°C (reflux) for 1 hour.

The same experiment was repeated by changing conditions (different temperatures, times, molar ratio of reactants).

Table 4.5, summarize the conditions used in the performed experiments.

| C6H : DMAP mol/mol | | solvent | Temperature | Time of reaction |
|--------------------|---|-------------------|-------------------------|------------------|
| 10 | 1 | CHCl ₃ | 80°C (reflux) | 1 h |
| 5 | 1 | CHCl ₃ | 80°C (reflux) | 1 h |
| 4 | 1 | CHCl ₃ | 80°C (reflux) | 1 h |
| 3 | 1 | CHCl ₃ | 80°C (reflux); 40°C; | 1 h; 2 h |
| | | CHCl ₃ | Room Temperature | 1 h |
| | | CHCl ₃ | R.T | 3 days |
| | | CDCl ₃ | 50°C | 24 h |
| | | DMSO-d6 | 110°C | 24 h |
| 2.5 | 1 | CHCl ₃ | 80°C (reflux) | 1 h |
| 1 | 1 | CHCl ₃ | 80°C (reflux) | 1 h |
| 1 | 3 | CHCl ₃ | 80°C (reflux) | 1 h |
| 1 | 5 | CHCl ₃ | 80°C (reflux) | 1 h |

Tab 4.5 experimental conditions achieved for the reaction of commercial C6H with DMAP

The 3:1 C6H: DMAP, (on CHCl₃ 80 ° C reflux, 1h) gave the best aligning mixture. A TLC chromatographic investigation of this mixture, was made to monitor the product formation, to recover the different products from reagents mixture, and finally to perform their characterization.

The better solvent mixture, for compounds separation, was found to be: CH₂Cl₂/EtOH = 9.8/0.2 on silica (fig 4.20). A more marked separation was achieved with a two-dimensional TLC (CHCl₃, and CH₂Cl₂/EtOH 9.5:0.5). For convenience the stains resulting from the bidimensional TLC were labeled, from the top, as **a**, **b**, **c** and **d** (see fig 4.21).

The amount of compound recovered after the separation, even in this case, was very low, hence the corresponding spectroscopic analysis give poorly results. Two compounds, as expected, were found to be the C6H and partially polymerized C6H The DMAP was not recovered after the separation.

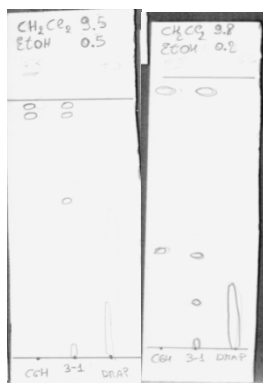


Fig 4.20 TLC of C6H:DMAP 3:1 mol/mol compared with C6H and DMAP with different solvent mixtures.

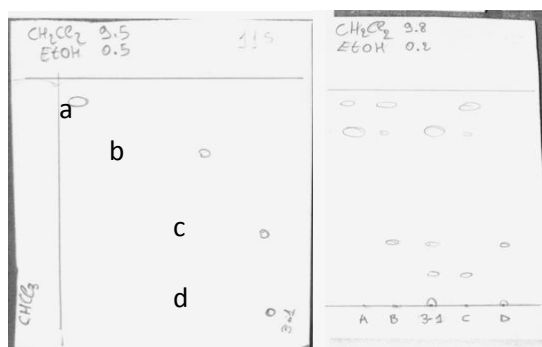


Fig 4.21 Left: Bidimensional TLC of C6H:DMAP 3:1 mol/mol (solvent mixture: CHCl_3 and $\text{CH}_2\text{Cl}_2/\text{EtOH}$ 9.5:0.5); Right: TLC of recovered stains, compared with the starting compound.

A cold extraction of the product was carried out in $\text{H}_2\text{O}/\text{chloroform}$, in acid conditions (HCl 0.5% v / v), to remove the residual DMAP, also monitored by TLC.

The product thus recovered shows an alignment more clean and homogeneous, while the NMR spectrum shows some fragmentation of the products of departure (see par 4.7.3).

Finally, the products, extracted and not, were recrystallized. This causes a total loss of homeotropic aligning capacity, like in the CU Synthesized C6H.

4.7 Characterization of the products of reaction between commercial C6H and DMAP

The compounds obtained after reaction between commercial C6H and DMAP have been characterized by spectroscopic and chromatographic methods. The better compound obtained, resulting from the reaction of C6H:DMAP 3:1 mol/mol, was also characterized after recrystallization, acid extraction and chromatographic separation.

4.7.1 FTIR

Some information, concerning possible adduct formation in the reaction between C6H and DMAP, comes out from FTIR spectra analysis.

The first comparison was made between the spectra of product of the C6H:DMAP 3:1 mol/mol, reacted mixtures and spectra of the pure reactants.

As expected, there is a little change in the fingerprint region for the 3:1 mixture respect to the commercial C6H (fig 4.22). But more interesting is the region between 2400-3600 cm^{-1} , where the spectra of the C6H:DMAP reacted mixture is still very similar to that of the C6H except for a more marked –OH band (fig 4.23).

The CU Synthesized C6H and the C6H:DMAP 3:1 compound (fig 4.24) shows the same difference in the FP region, and the –OH band is more evident in the latter, but we expect an hydrolysis of the ester groups while the CU Synthesized C6H is more similar to the commercial compound (showed for comparison).

The IR spectra of the C6H:DMAP 3:1 mixture, taken before inducing between the two components, is a simple superposition of those of the two reactants (see spectrum of 3:1 not reacted). After the reaction, the mixture, shows a change in the fingerprint region, that remains almost the same even after acid extraction. (Fig 4.25)

The spectrum of the recrystallized 3:1 compound, that shows a loss in the homeotropic aligning capacity, returns to be like that of the commercial C6H.

Indeed the recrystallization brings to a reduction of the –OH band, that become similar to that of the not aligning commercial C6H. (fig 4.25)

Finally, comparing the synthesis products made by C6H:DMAP on different ratios (fig 4.26) there are not relevant differences. As expected, the amine band is more intense in the 1:5 compound, indicating a large excess of DMAP respect to the monomer.

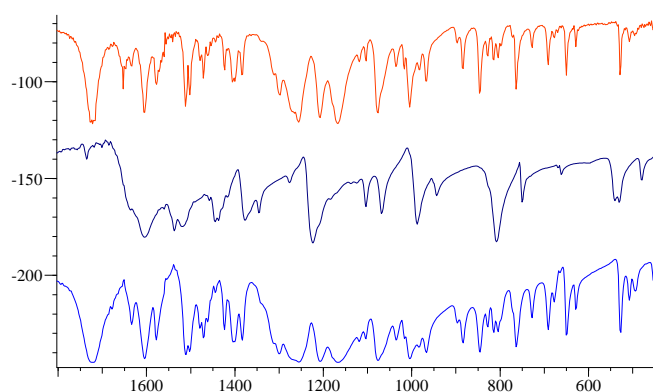


Fig 4.22 FTIR spectra of: C6H-DMAP 3-1 mol/mol (red), DMAP (dark blue), commercial C6H (blue) (FP region)

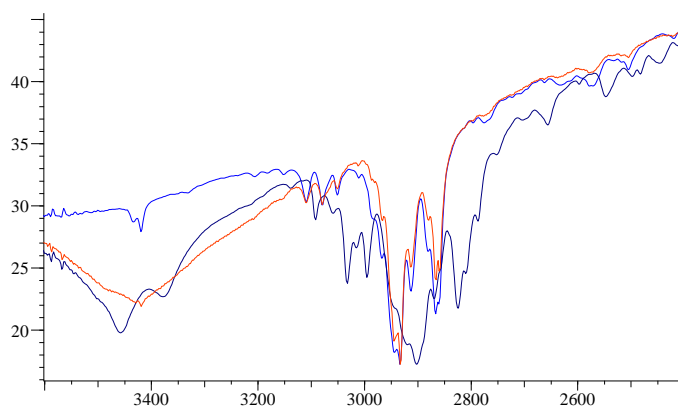


Fig 4.23 FTIR spectra of: C6H-DMAP 3-1 (red), DMAP (dark blue), commercial C6H (blue) (3600-2400 cm⁻¹ region)

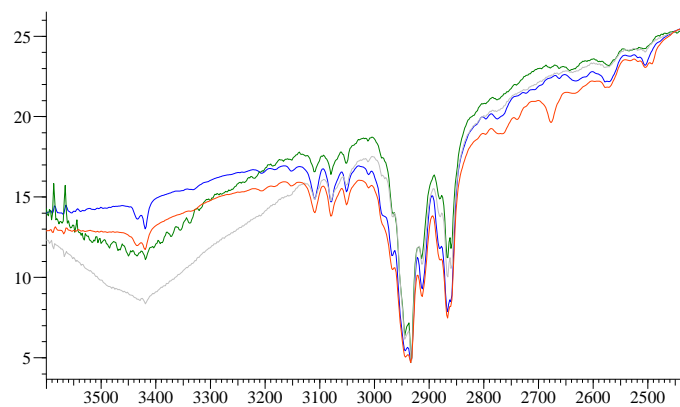


Fig 4.24 FTIR of: CU Synthesized C6H (red), 3-1 (gray), 3-1 extracted (green), commercial C6H (blue) (3600-2400 cm^{-1} region)

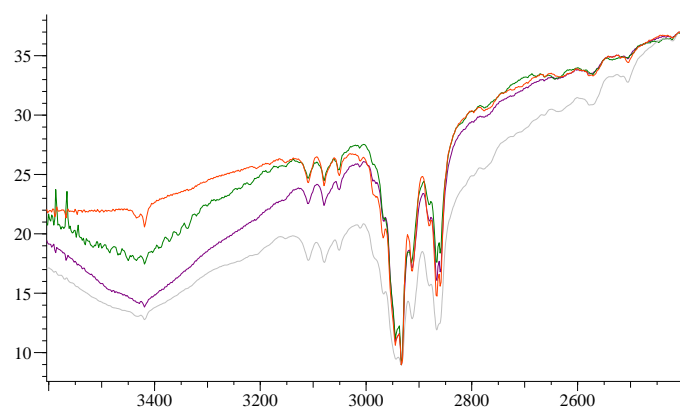


Fig 4.25 FTIR of: C6H:DMAP 3:1 mol/mol not reacted (gray), after reaction (violet), after acid extraction (green), and after acid extraction and recrystallization (red) (3600-2400 cm^{-1} region)

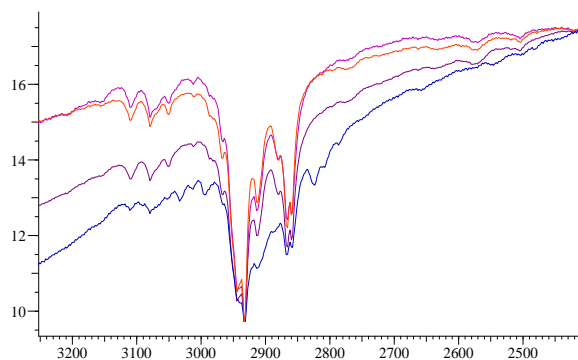


Fig 4.26 FTIR spectra of: C6H-DMAP 1-5 mol/mol (blu), 1-1 (purple), 3-1 (violet), 5-1 (red) (Overlay in the region 2400-3250 cm^{-1})

4.7.2 MALDI MS-MS experiments

The MALDI spectrometry was used to characterize the resulting product, after the reaction of C6H: the DMAP 3:1 mol/mol mixture. The MALDI MS spectrum is shown in fig 4.27.

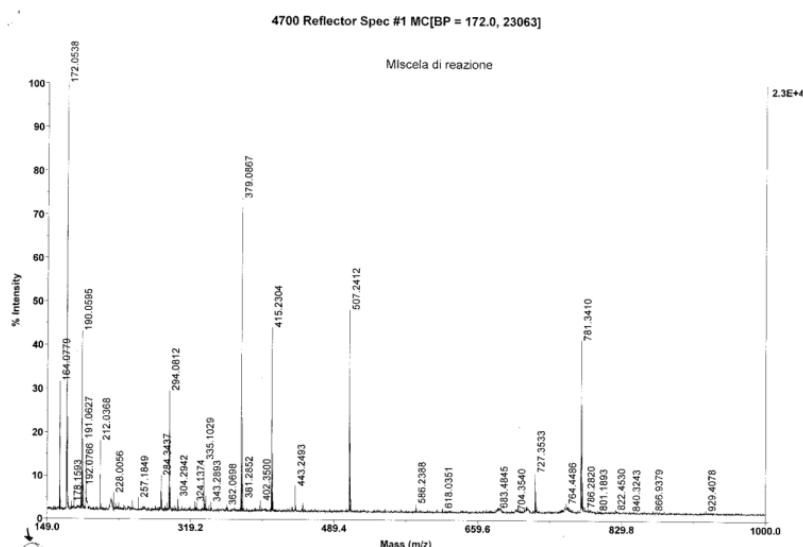
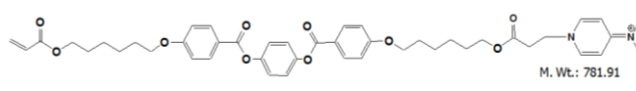
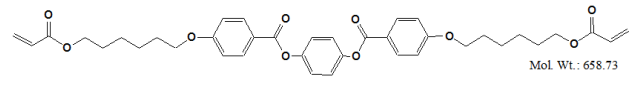
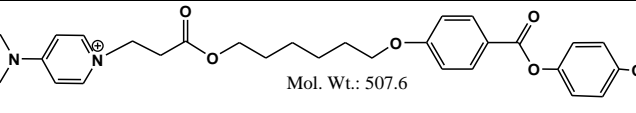
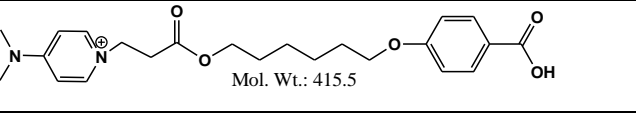
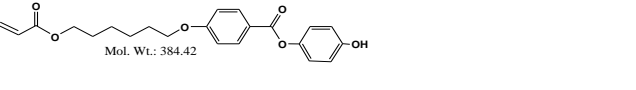
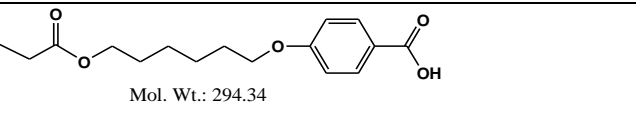





Fig 4.27 Mass soft ionization of product of C6H:DMAP 3:1 mol/mol reaction

The fragmentation is very similar to that of our CU Synthesized C6H (see fig 4.12, par 4.4.5). The most relevant fragments identified, by MS-MS analysis, are listed in tab. 4.26 and in fig 4.28 are shown the principal fragmentations for the hypothesized C6H-DMAP adduct.

| m/z | Fragment identified | Structure |
|---------------------|---|--|
| 781.42 | C6H-DMAP ⁺ |  M. Wt.: 781.91 |
| 658.73 Not found | C6H ⁺ |  Mol. Wt.: 658.73 |
| 656 | C6H after cyclization and elimination of 2H | |
| 507.34 | Product of II step of synthesis, with hydroquinone and DMAP |  Mol. Wt.: 507.6 |
| 415.5 | Product of II step of synthesis, with DMAP |  Mol. Wt.: 415.5 |
| 384.02 | Product of II step of synthesis, with hydroquinone |  Mol. Wt.: 384.42 |
| 294.12 | Product of II step of synthesis |  Mol. Wt.: 294.34 |
| 195.24 | Fragment of DMAP bonded on acrylate group |  Mol. Wt.: 195.24 |
| 178 | Fragment of Dmap+acrylate |  Mol. Wt.: 177.22 |
| 172 | Lateral chain with acrylate group |  Mol. Wt.: 172.22 |

Tab 4.26 Principal fragments identified for Mass soft ionization of product of C6H:DMAP 3:1 mol/mol reaction

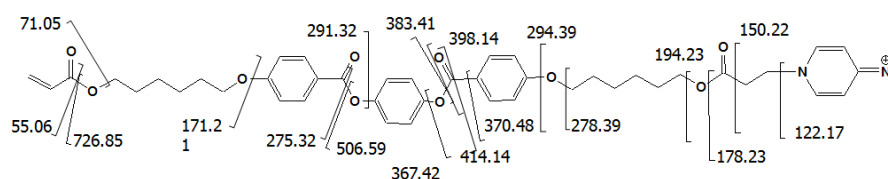


Fig 4.28 Fragmentations for the hypothesized C6H-DMAP adduct

Another analysis was performed by adding and mixing the reactants directly on the MALDI matrix (fig 4.29). This, unexpectedly, give the same fragmentation spectrum obtained by the previously reacted molecules (fig 4.30 and fig 4.31).

This observation can be explained by the effect of the laser on the, very reactive, acrylate system. This effect make it difficult to distinguish among adducts produced by the laser, fragmentation products and molecules resulting from the reaction. But the presence of the fragment of 195 m/z, that derive from the addition of DMAP to the acrylate system, allow us to say that the reaction has be done.

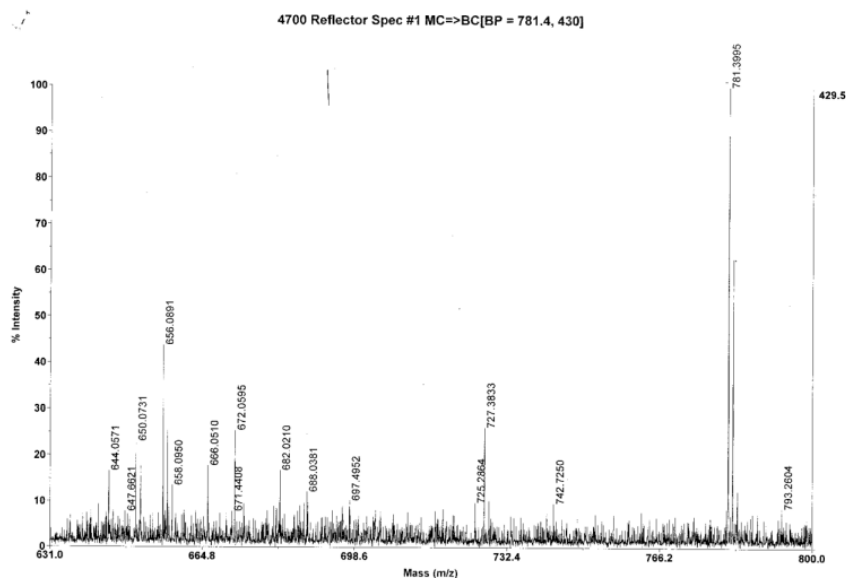


Fig 4.29 MALDI MS spectrum of C6H:DMAP directly mixed on matrix

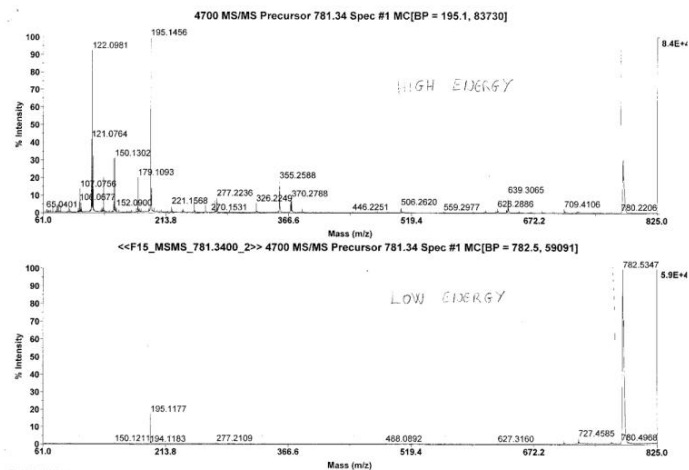


Fig 4.30 MALDI MS spectrum at high (upper) and low energy(down) of $C_6H:DMAP$ after reaction

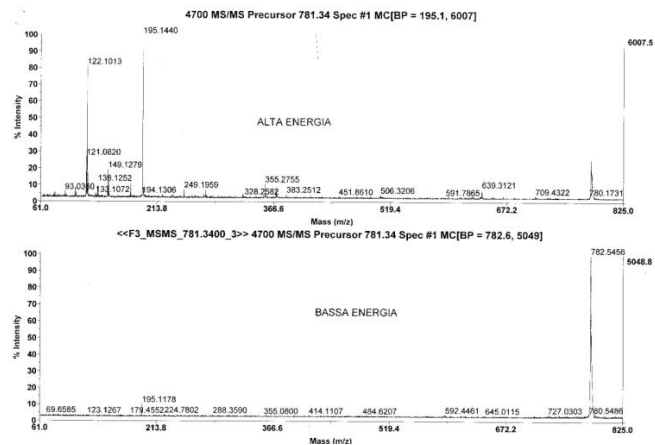


Fig 4.31 MALDI MS spectrum at high (upper) and low energy(down) of $C_6H:DMAP$ directly mixed on matrix

4.7.3 ^1H -NMR

The ^1H -NMR spectroscopy was used to analyze the C6H:DMAP reacted mixture, to monitor the appearance of new signals and the change in intensity of those present in the reactants: mainly those of the pyridinium ring (2.99 (s), 6.48 (d), 8.19 (d) ppm) of the unsubstituted DMAP. The acrylic group protons, may be less informative, since of the C6H possible spontaneous polymerization.

The signal of TMS signal was used as reference. The experiments were performed with an Avance 300 spectrometer (Bruker). CDCl_3 was used as solvent.

NMR spectra were taken from sample prepared from:

- Different ratios of C6H:DMAP reacted (s.c.) mixtures;
- C6H:DMAP 3:1 (s.c.), after acid extraction;
- Analysis of TLC stains obtained from C6H:DMAP 3:1 reacted (s.c.) mixtures;
- C6H:DMAP 3:1 reacted in other conditions (different solvent, time, temperature)
- C6H:DMAP 3:1, at 50°C monitored in the time (the first 24h)

For the assignment of the ^1H NMR signals, protons were labeled as in fig 4.15, while the peaks position (ppm) are compared with the literature values in tab 4.27 and 4.28. The corresponding spectra are shown in the following (fig 4.32 to 4.37)

Fig 4.32 shows the ^1H -NMR spectra from reacted C6H:DMAP with 1:5, 1:1, 3:1, 5:1 molar ratios. In all the cases we can correlate the formation of new species with the appearance of new signals with respect to those of C6H and DMAP [3.22 (s), 6.86 (d), 8.77 (d), 4.67 (m)].

In fig 4.33 the integral area of a new signal (the singlet at 3.2 ppm, is plotted versus the C6H concentration. The increasing in DMAP concentration not influence the concentration of the new peak appeared.

The ^1H NMR spectrum of C6H:DMAP 3:1 after acid extraction to eliminate the excess of DMAP is showed in fig 4.34. The incoming of the signals between 7-8 ppm and the change in the aliphatic region indicate a fragmentation of the original product, probably due to the hydrolysis of the ester groups. The same interest peaks were found in the product of multistep CU Synthesized synthesis (tab 4.4).

A chromatographic separation to isolate and recovery the molecular species induced by the C6H and DMAP reactions was made. The spectra of the four stain isolated by preparative TLC, for the C6H:DMAP 3:1, are showed in fig 4.35. The first two stains (a and b) are essentially composed of C6H, with a loss in the acrylic signals. The DMAP signals are founds only in the stain d (see par 4.6, the stain with the lower Rf), close to the starting line in the TLC plate. This stain was present in the TLC of the CU Synthesized C6H, but was not present in the TLC of the commercial C6H. Due to the small quantities of recovered products, no more information can be obtained from these spectra.

NMR spectra were taken from C6H:DMAP 3:1 mixtures reacted in several experimental conditions, changing solvent, temperature and time of reaction (i.e. high temperature for short times with respect to long times at relatively low temperature). The features of the pyridinium NMR signal appear to be strongly correlated to the variation of the reaction temperature (fig 4.36).

The reaction was also studied by taking spectra at fixed temperature as a function of time (the first 24 hours at 50°C) . by allowing the reaction to occur directly in the NMR probe (fig 4.37) . The corresponding changes in intensity of the DMAP singlet at 2.99 ppm and of the reaction generated signal at 3.22 ppm are plotted in the time, both normalized respect to the TMS signal, in fig 4.38. The reaction, in the first 24 hours show a linear trend, remaining very far from the equilibrium.

| C6H- DMAP 1-5 | C6H- DMAP 1-1 | C6H- DMAP 3-1 | C6H- DMAP 5-1 | C6H- DMAP 3-1 only mixed (time = 0, RT) | Values for C6H ⁽¹⁸⁾ and DMAP [<i>Aldrich Library</i>] | Labels and multiplicity expected for the protons |
|-------------------------------|-------------------------------|-------------------------------|-------------------------------|---|--|---|
| 8.80 d | 8.80 d | 8.77 d | 8.79 d | | | C (d) or XI mod |
| 8.21 d | 8.21 d | 8.20 d | 8.21 d | 8.19 d | 8.22 (d, 2H) of DMAP | γ, d., 2H |
| 8.14 d | 8.14 d | 8.14 d | 8.14 d | 8.14 d | 8.13(d, 9 Hz, 4H, ar.); | XI d., 4H |
| 7.26 s | 7.25 s | 7.25 s | 7.25 s | 7.25 s | 7.24 (s, 4H, ar); | VIII s., 4H |
| 6.97 d | 6.97 d | 6.97 d | 6.97 d | 6.97 d | 6.95 (d 8.8 Hz, 4H, ar); | VII d., 4H |
| 6.86 d | 6.86 d | 6.85 d | 6.86 d | | | B (d) or XI or VIII mod |
| 6.48 d | 6.48 d | 6.48 d | 6.48 d | 6.48 d | 6.48 (d, 2H) of DMAP | β, d., 2H |
| 6.40 dd 6.12 dd 5.81 dd | 6.40 dd 6.12 dd 5.81 dd | 6.40 dd 6.12 dd 5.81 dd | 6.40 dd 6.12 dd 5.81 dd | 6.40 dd 6.12 dd 5.81 dd | 6.38 (dd, 17, 3, 1.5 Hz, 2H, vinyl); 6.11 (dd, 17.3, 10.5 Hz, 2H vinyl); 5.81 (dd, 10.5, 1.5 Hz, 2H vinyl); | Xb d.d., 2H IX d.d., 2H Xa d.d, 2H |
| 4.69 m | 4.66 t | 4.66 t | 4.66 t | | | |
| 4.18 t 4.05 t | 4.18 t 4.05 t | 4.18 t 4.05 t | 4.18 t 4.05 t | 4.18 t 4.05 t | 4.17 (t, 6.7 Hz, 4H, COOCH ₂); 4.04 (t, 6.6 Hz, 4H, PhOCH ₂); | V t, 4H; VI t, 4H |
| 3.66 t | 3.66 t | 3.66 t | 3.66 t | | 3.34 (quad, 2H) of O-CH ₂ -CH ₃ for diethyl ether; about 3.70 for R-CH ₂ -OH | IXd t, Xd t or IX, X mod |
| 3.22 s 2.92quad | 3.22 s | 3.22 s | 3.22 s | | | A (s) |
| 2.99 s 2.76 s | 2.99s 2.76 s | 2.99 s 2.76 s | 2.99 s | 2.99 s | 2.99 (s, 6H) of DMAP | α s, 6H |
| 1.84 q 1.73 q 1.51 m | 1.84 q 1.73 q 1.51 m | 1.84 q 1.73 q 1.51 m | 1.84 q 1.73 q 1.51 m | 1.84 q 1.73 q 1.51 m | 1.83 (q, 6.7 Hz, 4H, COOCH ₂ CH ₂); 1.71 (q, 6.6 Hz, 4H, PhOCH ₂ CH ₂); 1.4-1.57 (m, 8H, inner CH ₂ CH ₂) | III q, 4H IV q, 4H I, II m, 8H |
| 1.26 t | | | | | 1.07 (t, 3H) of OCH ₂ -CH ₃ for diethyl ether; About 1.70-1.50 for R- CH ₂ - CH ₂ OH | |

Tab 4.27 NMR signals in the C6H/DMAP reacted mixtures. Incoming signals [3.22 (s), 6.86 (d), 8.77 (d), 4.67 (m)] are in green.

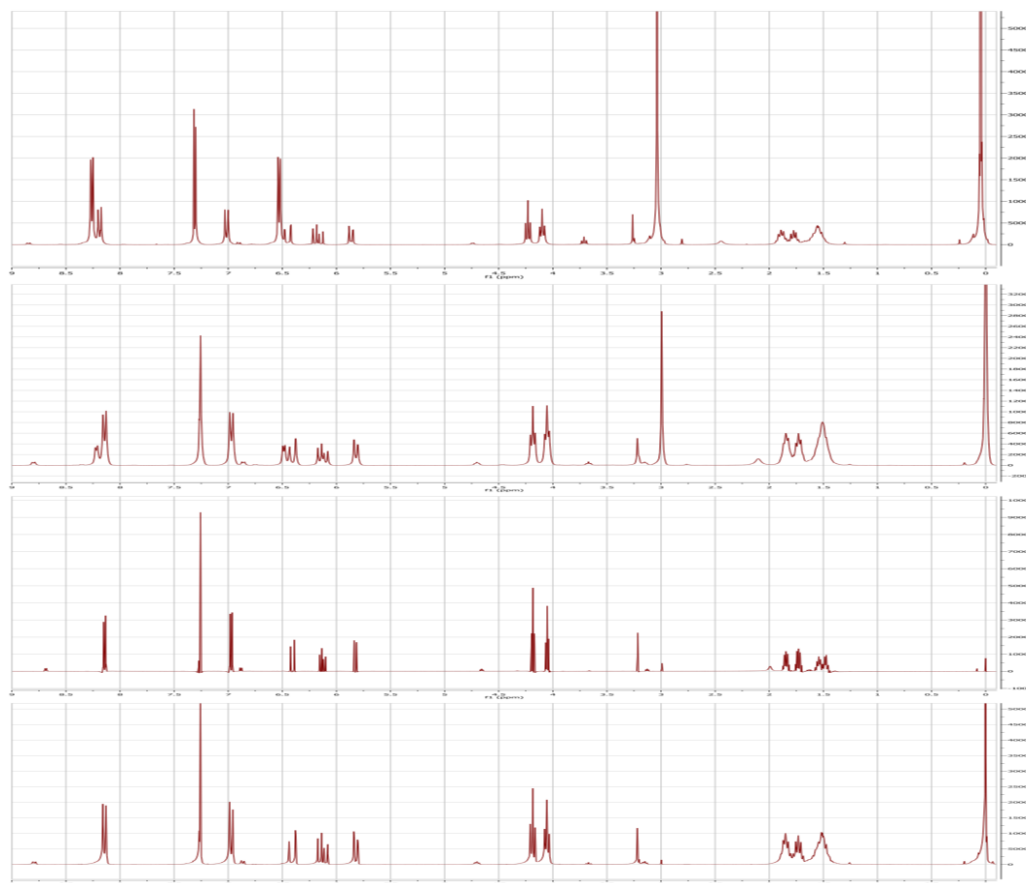


Fig 4.32 ^1H -NMR spectra of C6H:DMAP ratios of, from the top, 1:5, 1:1, 3:1, 5:1. In all the cases, signals at 3.22 (s), 6.86 (d), 8.77 (d), 4.67 (m) appear

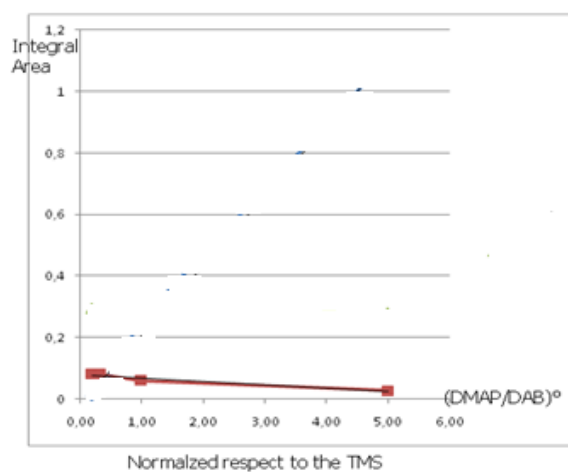


Fig 4.33 Integral area of the new emerging signal singlet at 3.22 ppm as a function of the DMAP concentration. The signal has been measured 2 hours of reaction time.

| C6H- DMAP 3-1 | Stain A | Stain B | Stain C | Stain D | After extraction 3-1 | Values for C6H (see tab 4...) and DMAP [Aldrich Library] | Labels and multiplicity expected for the protons |
|-------------------------------|-----------------------------------|-------------------------------|----------------------------------|---|--|--|---|
| 8.77 d | | | | | 8.70 d | | C (d) or XI mod |
| 8.20 d | | | | 8.23 | | 8.22 (d, 2H) of DMAP | γ d., 2H |
| 8.14 d | 8.15 d | 8.15 d | 8.15 d | | 8.14 d | 8.13(d, 9 Hz, 4H, ar.); | XI d., 4H |
| 7.25 s | 7.25 s | 7.25 s | 7.61 s 7.25 s | 7.61 s 7.26 s | 7.26 s | 7.24 (s, 4H, ar); 7.26 CHCl ₃ | VIII s., 4H |
| 6.97 d | 6.98 d | 6.97 d | 6.97 d | NO | 6.97 d | 6.95 (d 8.8 Hz, 4H, ar); | VII d., 4H |
| 6.85 d | | | 6.90 s | 6.91 s | 6.88 d | | B (d) or XI or VIII mod |
| 6.48 d | | | | | | 6.48 (d, 2H) of DMAP | β d., 2H |
| 6.40 dd 6.12 dd 5.81 dd | 6.40 dd 6.12 dd 5.81 dd | 6.40 dd 6.12 dd 5.81 dd | | | 6.40 dd 6.12 dd 5.81 dd | 6.38 (dd, 17, 3, 1.5 Hz, 2H, vinyl); 6.11 (dd, 17.3, 10.5 Hz, 2H vinyl); 5.81 (dd, 10.5, 1.5 Hz, 2H vinyl); | Xb d.d., 2H IX d.d., 2H Xa d.d, 2H |
| 4.66 t | | | 5.34 | 5.35 | 4.66 m | | |
| 4.18 t 4.05 t | 4.18 t 4.05 t | 4.18 t 4.05 t | 4.05 | 4.05 quad | 4.18 t 4.05 t | 4.17 (t, 6.7 Hz, 4H, COOCH ₂); 4.04 (t, 6.6 Hz, 4H, PhOCH ₂); | V t, 4H; VI t, 4H |
| 3.66 t | 3.72 q | 3.68 t | 3.68 t | 3.73 quad | 3.66 t | 3.34 (quad, 2H) of O-CH ₂ -CH ₃ for diethyl ether; about 3.70 for R-CH₂-OH | IXd t, Xd t or IX, X mod |
| 3.22 s | | | 2.54? | 3.09 s | 3.22 s | | A (s) |
| 2.99 s 2.76 s | 2.29 t 2.17 s | 2.29 m 2.17 s 2.00 m | 2.28 2.01 s | 2.29 m 2.17 s 2.00 m | | 2.99 (s, 6H) of DMAP | α s, 6H |
| 1.84 q 1.73 q 1.51 m | 1.84 q 1.73 q 1.51 m | 1.84 q 1.73 q | 1.84 m | | 1.84 q 1.73 q 1.51 m | 1.83 (q, 6.7 Hz, 4H, COOCH ₂ CH ₂); 1.71 (q, 6.6 Hz, 4H, PhOCH ₂ CH ₂); 1.4-1.57 (m, 8H, inner CH ₂ CH ₂) | III q, 4H IV q, 4H I, II m, 8H |
| | 1.62 s q,25 m 0.85 quad? | 1.56 1.25 s 0.85 m | 1.56 s 1.25 s 0.87 quad | 1.59 s o m 1.25 m 0.86 quad 0.20 s | 1.48 m 1.26 s 1.11 s 0.88 m 0.72 m | 1.07 (t, 3H) of OCH ₂ -CH ₃ for diethyl ether; About 1.70-1.50 for R- CH ₂ - CH ₂ OH | |

Tab 4.28 Proton signals for recovered stain after chromatographic separation of reacted C6H:DMAP 3:1 mol/mol and after acid extraction.

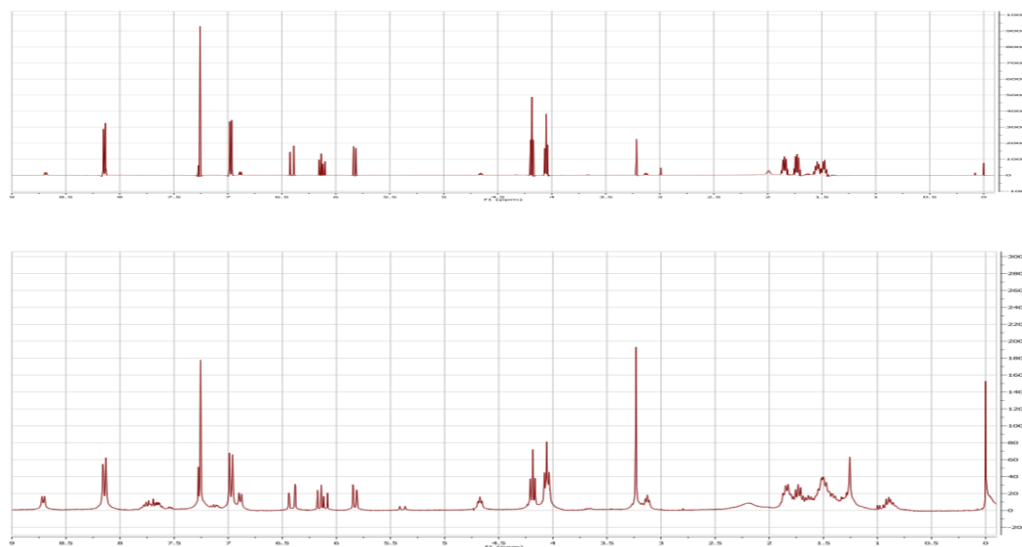


Fig 4.34 ^1H NMR spectrum of C6H:DMAP 3:1 after acid extraction to eliminate the excess of DMAP (the upper spectrum, of the compound before the extraction is showed for comparison). The emergence of the signals between 7-8 ppm and the change in the aliphatic region indicate a fragmentation of the product.

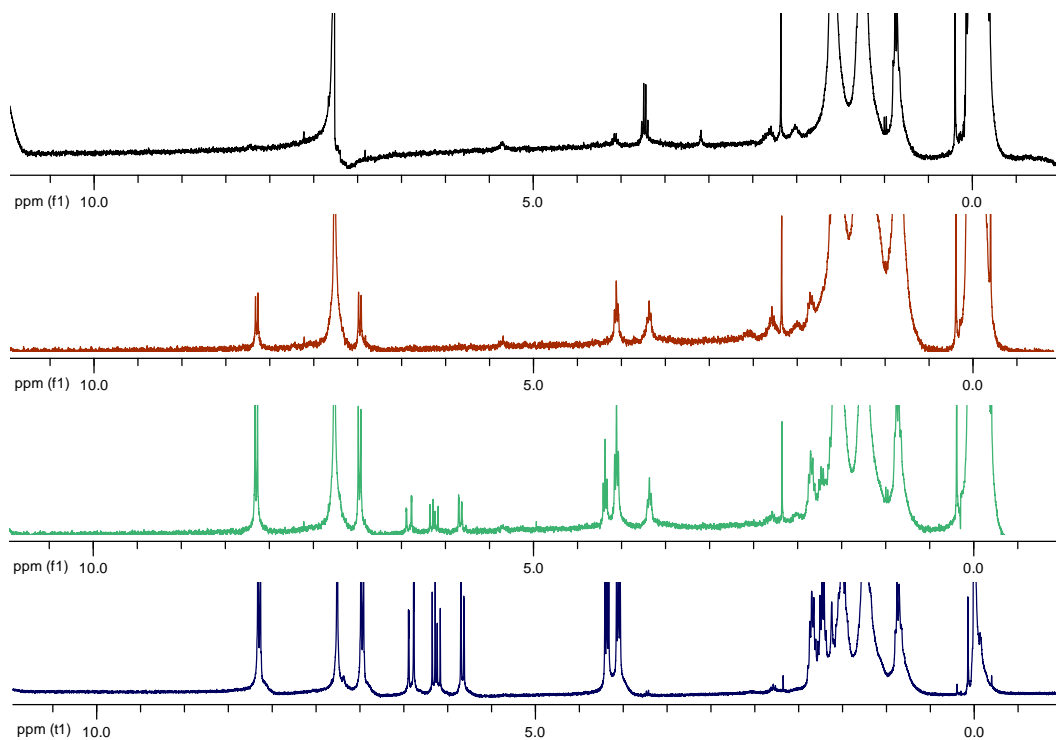


Fig 4.35 Staked ^1H -NMR spectra of the recovered stains after chromatographic separation of reacted C6H:DMAP -3:1 (from the top: stain d, c, b and a) The intensity of the spectra b, c, d was enhanced to overcome the low intensity of the signals.

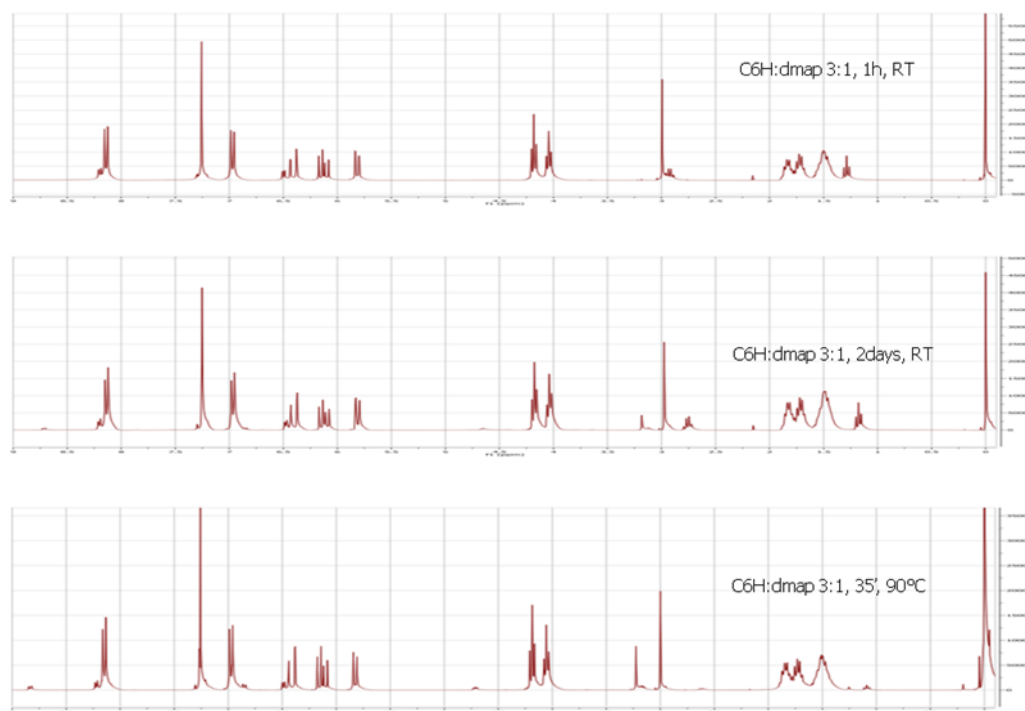
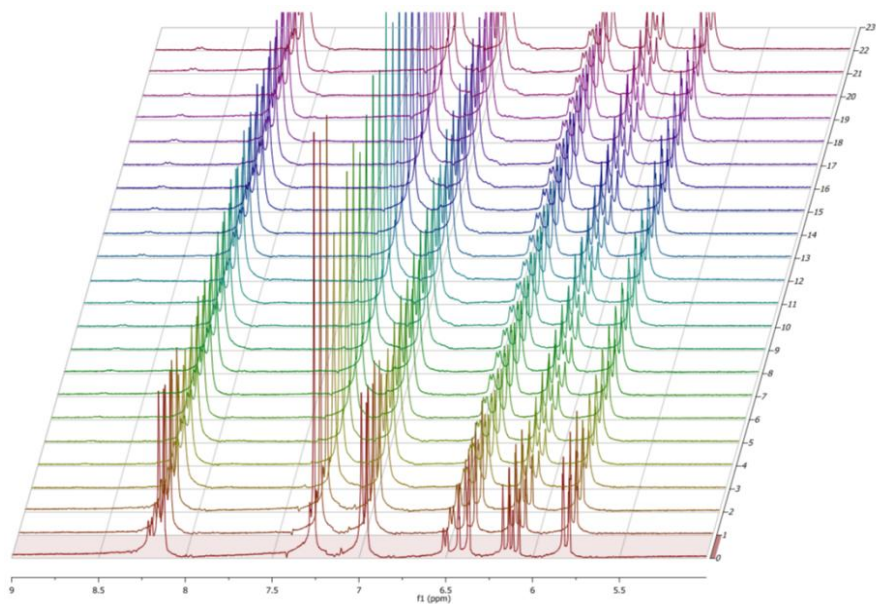
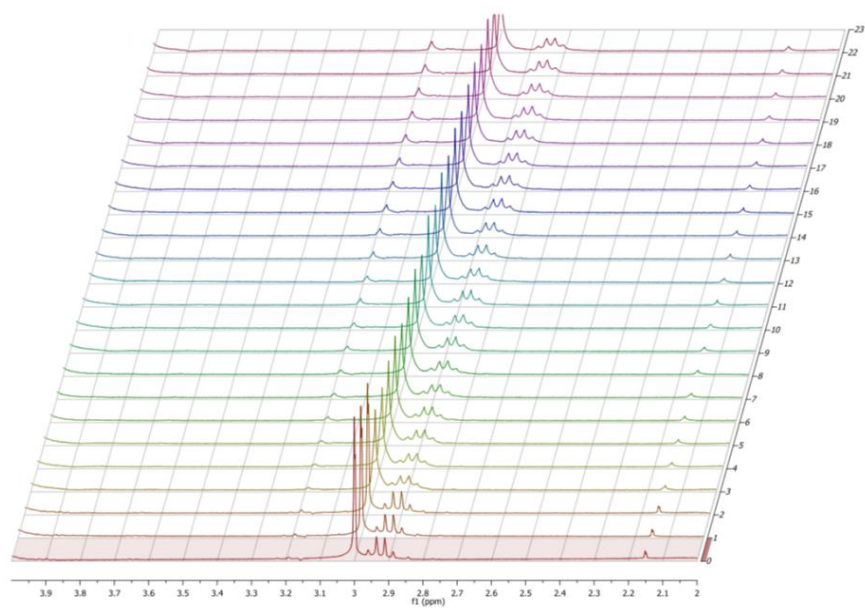


Fig 4.36 $^1\text{H-NMR}$ spectra of the reaction of $\text{C}_6\text{H}:\text{DMAP}$ 3:1 mol/mol at different reaction conditions. High temperature or long times are both correlated to the formation of the interest peaks (the “substitued pyridine signals”). At room temperature the reaction need long times.



a



b

Fig 4.37 Enlarged region of 5-9 ppm(a) and 2-4ppm (b). The peak at 8.70 ppm and the singlet at 3.2 ppm appear and increase in intensity in the time

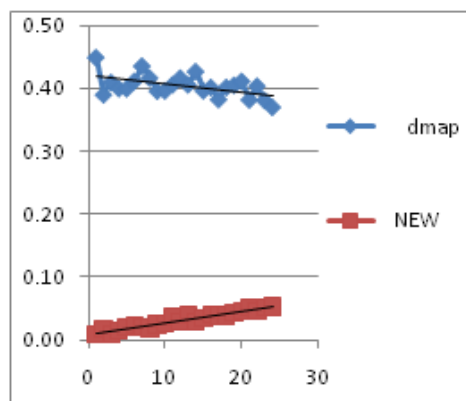


Fig 4.38 Plot of the DMAP (singlet at 2.99 ppm) and the new signal appeared (singlet at 3.2 ppm) in the time/h. All integrals are normalized respect to the TMS signal. (Reaction of C6H:DMAP 3:1 mol/mol; 50°C, CDCl₃)

4.7.4 ^{13}C - NMR

The ^{13}C -NMR analysis, with broadband decoupling of the protons, was achieved to complete the information by ^1H -NMR about the C6H/DMAP reaction.

As it can be seen from fig 4.40, new sp^3 carbon signals (between 20-70 ppm) related to alkylic chains, probably generated by the external ester group hydrolysis and to a change of hybridization in the acrylic group, appear in the ^{13}C -NMR spectra.

A series of “new” signals (at 143, 107.7, 40.3 ppm). that can be assigned to a “modified pyridine”, appear in the C6H:DMAP reacted system and remain in the spectra even after acid extractions of the reacted mixtures.

Some signals (i.e., 28.8, 61.6 ppm) are not found in product of C6H:DMAP 5:1 while are very evident in the 1:5 product (Fig 4.41) This lead to think that an excess of DMAP favors a fragmentation of the molecule, i.e. the hydrolysis of ester groups.

The Carbon signals are listed in tab 4.29, while the label assignment for the Carbons nuclei is showed in fig 4.39.

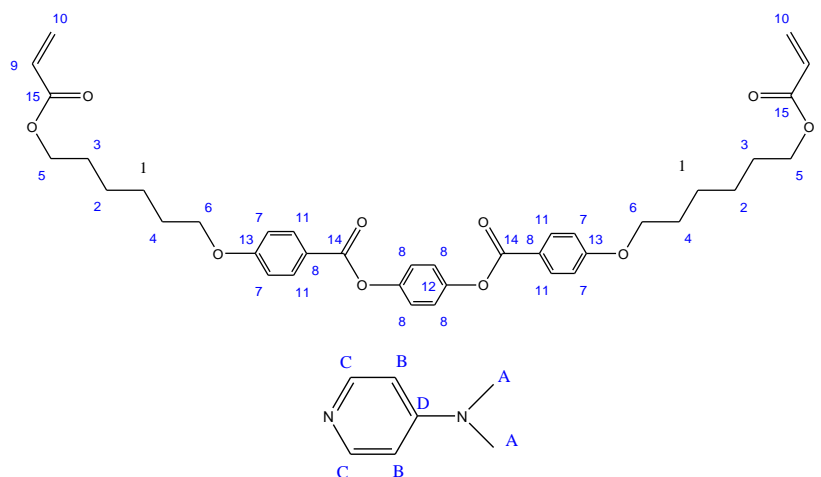
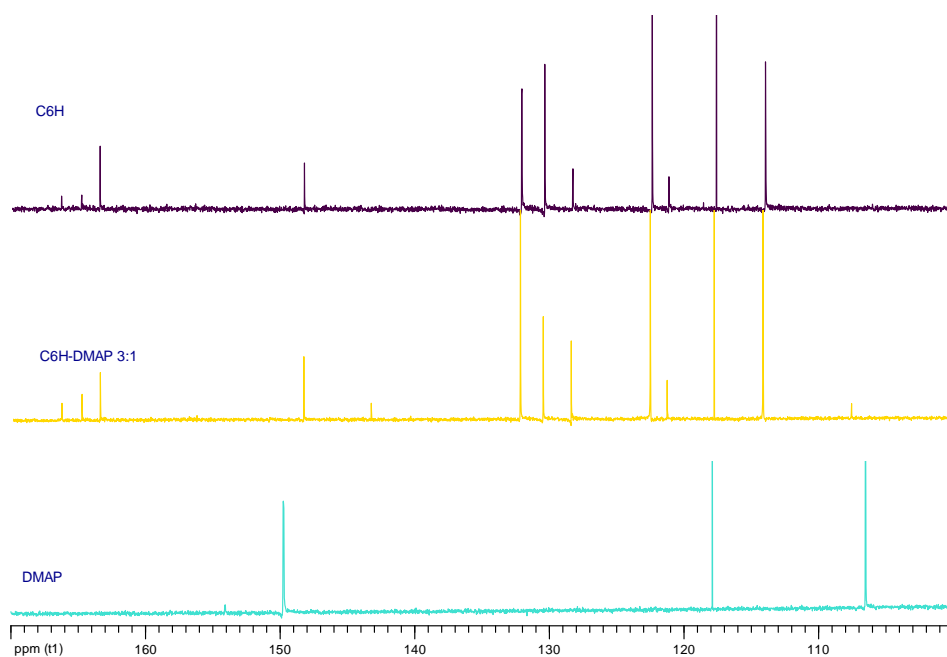


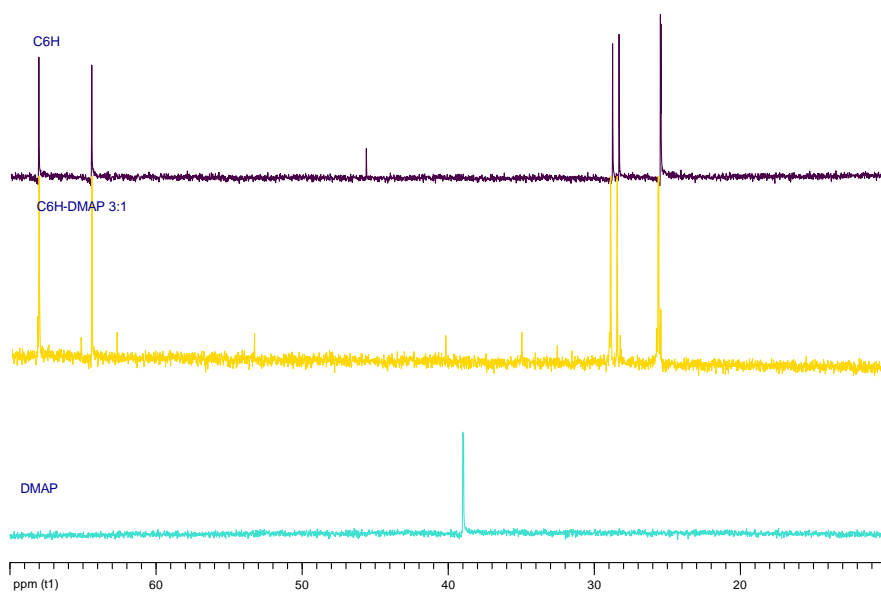
Fig 4.39 label assignment for C6H and DMAP Carbons

| C6H- DMAP 1-5 | C6H- DMAP 1-1 | C6H- DMAP 3-1 | C6H- DMAP 5-1 | After acid extraction 3-1 | C6H- DMAP 3-1 only mixed (time = 0, RT) | <i>C6H and DMAP</i> | Labels for the ¹³ C nuclei |
|---------------------|---------------------|---------------------|---------------------|---------------------------------|---|-------------------------|---|
| - | - | 166.37 | - | 166.361 | 166.288 | 166.36 | 15 |
| 164.869 | 164.8 | 164.879 | 164.8 | 164.87 | 164.801 | 164.868 | 14 |
| 163.504 | 163.44 | 163.518 | 163.44 | 163.508 | 163.439 | 163.51 | 13 |
| | | | | | | 154.11 | D |
| 149.737 | | | | | | 149.77 | C |
| 148.405 | 148.342 | 148.421 | 148.361 | 148.413 | 148.342 | 148.413 | 12 |
| 143.592 | 143.39 | 143.418 | 143.506 | 143.558 | | | C', 12' |
| 142.82 | | | | | | | |
| 132.341 | 132.27 | 132.35 | 132.262 | 132.356 | 132.27 | 132.333 | 11 |
| 130.641 | 130.559 | 130.658 | 130.56 | 130.668 | 130.592 | 130.649 | 10 |
| 130.534 | | | | | | | 10' |
| 128.565 | 128.519 | 128.58 | 128.52 | 128.572 | 128.501 | 128.569 | 9 |
| 122.681 | 122.616 | 122.714 | 122.615 | 122.705 | 122.631 | 122.704 | 8? |
| 121.469 | 121.421 | 121.464 | 121.434 | 121.473 | 121.365 | 121.473 | 8 |
| 114.318 | 114.265 | 114.348 | 114.268 | 114.32 | 114.267 | 114.334 | 7 |
| 107.698 | 107.65 | 107.782 | 107.648 | 107.737 | | | B' |
| 106.596 | | | | | 106.526 | 106.521 | B |
| 68.216 | 68.21 | 68.23 | - | | | | |
| 68.126 | 68.057 | 68.135 | 68.072 | 68.127 | 68.057 | 68.128 | 6 |
| | | 65.263 | 64.98 | 65.25 | | | |
| 64.522 | 64.452 | 64.532 | 64.453 | 64.518 | 64.452 | 64.523 | 5 |
| 62.682 | 62.78 | 62.803 | - | 62.72 | | | |
| | | 53.406 | | | | | 50=10' |
| 40.305 | 40.31 | 40.326 | 40.252 | 40.317 | | | A' |
| 39.091 | | | | | 39.129 | | A |
| 35.12 | 35.1 | 35.128 | 35.104 | 35.16 | | | |
| 32.763 | 32.64 | 32.74 | - | | | | 9' |
| 29.139 | 29.14 | 29.17 | 29.14 | 29.764 | | | 4' |
| 29.047 | 28.979 | 29.035 | 28.981 | 29.05 | 28.962 | 29.049 | 4 |
| 28.605 | 28.539 | 28.596 | 28.539 | 28.609 | 28.521 | 28.608 | 3 |
| 28.387 | 28.32 | 28.398 | 28.32 | 28.83, 28.401 | | | 3' |
| 25.905 | 25.91 | 25.93 | | | | 25.79 | 2 |
| 25.77 | 25.833 | 25.801 | - | 25.791 | 25.686 | 25.759 | 1 |
| 25.65 | 25.689 | 25.7 | 25.73 | 25.70 | 25.43 | | 1' |

Tab 4.29 ¹³C signals for Reaction products of C6H:DMAP obtained for different ratio of the reactant, compared whit the signal of the reactants, and their assignment at the Carbon nuclei

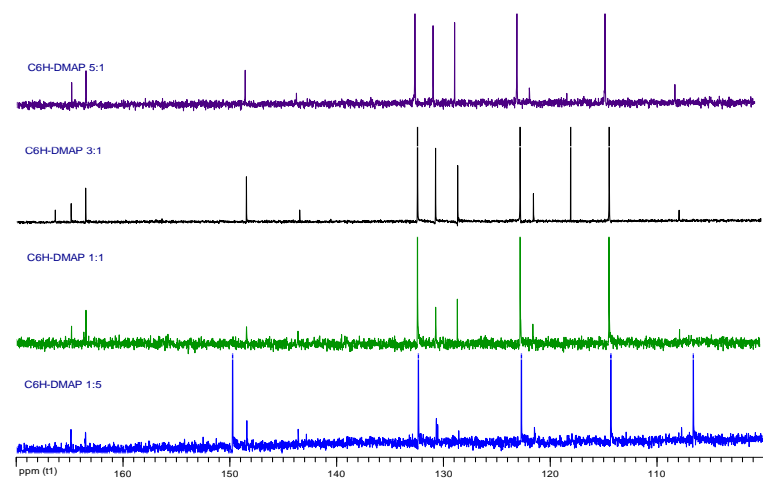


a

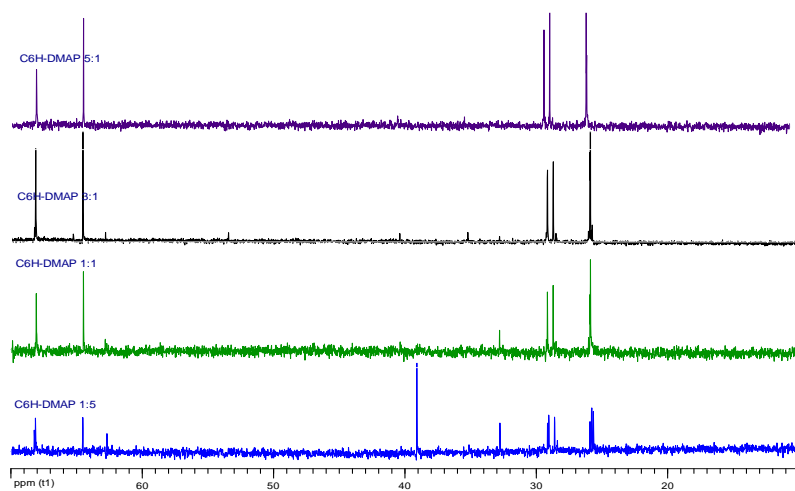


b

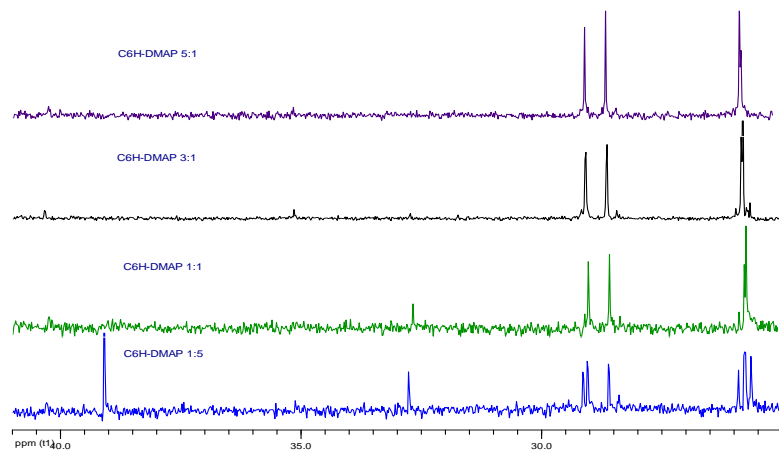
Fig 4.40 ^{13}C spectra of C_6H , $\text{C}_6\text{H}:\text{DMAP}$ 3-1 mol/mol and DMAP. Enlarged regions in the range of 170-100 ppm (a), and)70-10 ppm (b)



a



b



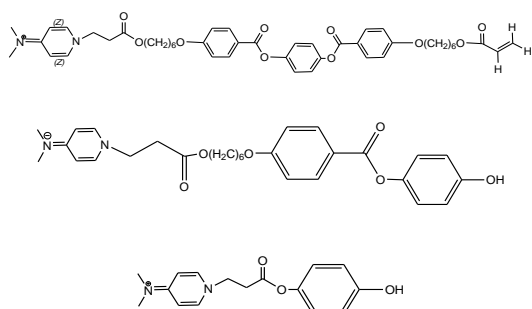
c

Fig 4.41 ^{13}C spectra of $\text{C}_6\text{H}:\text{DMAP}$ reacting mixtures on different molar ratios of the reactant. Enlarged regions in the range of 170-100 ppm(a), 70-10 ppm(b), 41-25 ppm(c).

4.8 Conclusions

The data reported in this chapter lead to the following conclusions, regarding with the possible impurities in the CU synthesis of the self aligning C6H:

- EDS: the elemental analysis indicates the presence, in addition to C and O, of N and Cl, which are not found in Commercial C6H.
- FTIR: Between 2700 - 2300 cm^{-1} impurities bands are present. These are characteristic of quaternary ammonium salts. After a second recrystallization, that determine a loss in the alignment capacity of the compound, these bands disappear and the spectrum become identical to that of the Commercial C6H.
- MALDI MS – MS: The analysis was able to give indications on the presence of the following species and fragments:



- NMR: The peaks around 6.8 ppm confirms the presence of an aromatic ring like hydroquinone but with not equivalent protons; the signals around 3.0 ppm indicate the presence of alkyl groups adjacent to nitrogen or oxygen atoms, and are compatible with the addition of an amine to the acrylate group and/or an hydrolysis of the ester group. The disappearance of these two signals, after the second recrystallization, is associated with progressive loss on aligning capacity of the system.

Fig 4.42 resumes the main impurities in the CU synthesized C6H. literature data confirm they are able to confer homeotropic aligning property to LC on glass substrates. So, we can conclude that the species responsible of CU synthesized

C6H homeotropic alignment can be both C6H- DMPA adducts and hydroquinone substituted products (partially reacted hydroquinone in step 3 or hydrolyzed C6H).

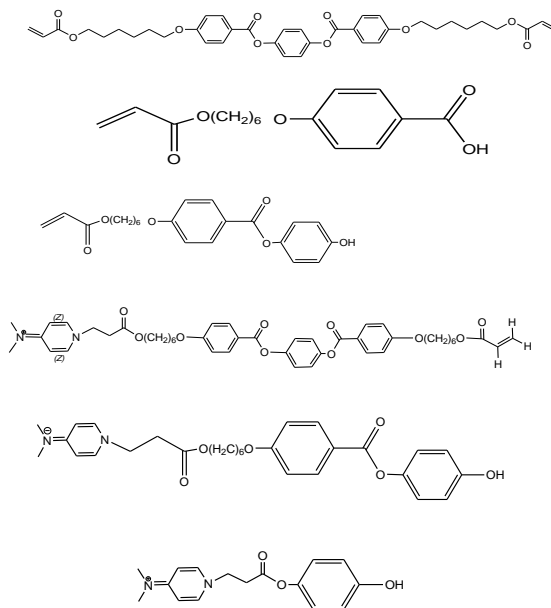


Fig 4.42 Main impurities formed in the C6H CU Synthesized synthesis and responsible of the homeotropic alignment of the C6H.

Significant information for the knowledge of the investigated aligning mechanism were obtained by NMR and other spectrometer and spectroscopic data. The following conclusion can be driven.

- Michael addition and aminolysis of the ester groups can occur between C6H and DMAP (signal-OH in the IR spectrum; fragment 195 m / z in the MALDI spectrum new peaks in the ^{13}C -NMR and ^1H -NMR spectra). The same reaction also occur in the C6H multi-step synthesis.
- We can correlate the formation of the interesting products (the self-aligning monomer) with the appearance of the news picks, that indicate the formation of new species. The same peaks are still present after acid extraction, and are found in the multi steps synthesis product (the CU Synthesized C6H).
- The reaction between C6H and DMAP, in appropriate conditions, is a simple, rapid and low cost method to obtain an "self-aligning" LC acrylate monomer (or, more correctly, an adduct) homeotropic.

References

1. J.W. Doane, G. Chidichimo, N.A. Vaz, *US Patent 4688900*, (1987).
2. P.S. Drzaic, *Liquid Crystal Dispersions*, World Scientific, (1995).
3. D.J. Broer, H.Finkelmann, K.Kondo, *Makromol. Chem*, Vol 189, 1988, 185.
4. D.J. Broer, R.A.M. Hikmet, *Angew. Makromol. Chem*, Vol 183, 3235, (1990) .
5. Y. Ide, T. Chung, *Macromol. Sci. Phys*, Vol B 23, 497,(1984).
6. D.J Broer, *Integration of fundamental of Polymer science and technology*, Elsevier, 669,(1986) .
7. J. Lub, DJ Broer, R.A.M. Hikmet, K.G.J. Nierop, *Liq. Cryst.*, Vol 18, 1995, 319.
8. H. Chain-Shu, C. Hwai-Len, *J. Polym. Sci. A. Polym. Chem.*,Vol. 37, (1999).
9. P.S. Drzaic, *Liquid Crystal Dispersions*, World Scientific, 1995.
10. J. Cognard, *Alignment of nematic Liquid Crystals and their mixtures*, Gordon&Breach, 1982.
12. M. Ohgawara, T.Ukida, M.Wada, *Liquid crystals orientation on various surfaces*, *Mol. Cryst. Liq. Cryst*, 74, 227-242, 1981 .
13. R.A.M. Hikmet, J. Lub, *Anisotropic networks and gels obtained by photo-polymerization in the liquid crystalline state: Synthesis and applications*, *Progress in Polymer Science*, 21, 1165-1209, 1996.
14. R. Cassano, *Synthesis and characterization of liquid crystalline monomers*, PhD thesis, STM3 XVIII cycle, pp 63-64.
15. RAM Hikmet, *Mol Cryst. Liq. Cryst*, vol 146, 1, 1987.
16. D.J. Boer, J. Boven, *Mol. GN. Makromol. Chem*, 190, 2255, 1989.
17. L.Tortora, *Optical shutters by liquid crystal organic dispersions*, PhD thesis, XVI cycle, Unical, 2003-2004.
18. H. Guillard, P. Sixou, L. Reboul, A.Perichaud, *Electrooptical characterization of polymer stabilized cholesteric liquid crystals*, *Polymer* 4, 2, 9753-9762, (2001).
19. D.J. Boer, J Boven, *Mol. GN. Makromol. Chem*, 190, 2255, (1989).
20. Hahn-Deinstrop, *Applied Thin-Layer Chromatography - Best Practice and Avoidance of Mistakes*, 2Ed, Wiley 2007.
21. A. Talvik et al., *Kinetics and mechanism of aminolysis of aliphatic esters in aprotic solvents*”, *J. Of Ph. Org. Chem.*, 1999.

22. Takahashi et al., "4-aminopyridium compound", US Patent 7193087 B2, 2007.
23. A.P. Malyshev, K.V. Shirshin et al., *Effect of reactant association in addition of tertiary amines to acrylic acid*, *Russian Journal of Applied Chemistry*, vol. 79, 10, 1629-1633, 2006.
24. O. A. Kazantsev, K.V. Shirshin, S.A. Kazakov, S.M. Danov, *Quaternization of Methacrylic Monomers Containing Tertiary Amino Groups with Acrylic Acid Derivatives*, *Russian Journal of General Chemistry*, 69, 8, (1999).

Chapter 5: High contrast Reverse Mode PDLC Films: morphologic and electro-optical studies

5.1 Reverse mode PDLC

The PDLC Reverse Mode^{(1) (2)}, proposed in previous work⁽³⁾ and object of this part of study, are formed by photo-polymerization of a homeotropic aligned mixtures containing diacrylate LC monomer and ZLI 4788-000, a low molecular mass liquid crystal with negative dielectric anisotropy (by Merck). In previous studies^{(4) (5)} the diacrylate LC monomer was the C6H, which has been the object of the researches described in the previous chapters.

The ZLI 4788-000 Merck nematic mixture is an appropriate complementary partner (a non polymerizing negative dielectric anisotropy liquid crystal) of C6H, in the starting liquid crystal solution. This product was, when this research started, the only available liquid crystal having a quite large negative dielectric anisotropy ($\Delta\epsilon$ (1 kHz, 20°C) = -5.7) and a very wide temperature nematic range (from -30 to 83 °C).

| <i>Liquid Crystal ZLI-4788-000</i> | |
|---|--------|
| S-N | <-30°C |
| N-I | 83°C |
| $\Delta\epsilon$ (1 kHz, 20°C) | -5.7 |
| $\epsilon_{//}$ (1 kHz, $\pm 20^\circ\text{C}$) | 4.5 |
| ϵ_{\perp} (1 kHz, $\pm 20^\circ\text{C}$) | 10.2 |
| Δn (+20°C, 589 nm) | 0.164 |
| n_0 (+20°C, 589 nm) | 1.486 |
| n_e (+20°C, 589 nm) | 1.650 |
| Viscosity (cSt, 20°C) /mm ² sec ⁻¹ | 35 |
| Viscosity (cSt, -30°C) /mm ² sec ⁻¹ | 155 |
| Rotational viscosity (20°C) /mPa sec | 225 |
| K_3/K_1 (20°C) | 1.49 |
| K /N | 18.9 |

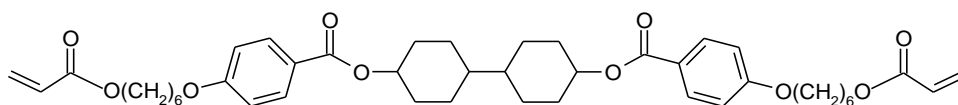
Tab5.1 Physical and chemical characteristics of the liquid crystal ZLI 4788-000

The working principle of the Reverse mode PDLC cell, obtained by the above mentioned mechanism is based on the fact that an incoming beam of light going through the equilibrium configuration of the film compares the n_0 refractive index of the ZLI with the n_0 refractive index of the polymer, which should be the more possible similar. The film in this conditions will appear transparent. If an electric field, big enough to give a 90° tilt of the ZLI director, is applied to the cell, the light beam will compare the extraordinary refractive index n_e of the fluid liquid crystal with the ordinary index of the polymer. When a relevant difference between these indices occurs the film is shifted in an opaque state as a result of the strong light scattering introduced, by the refractive index mismatching, on the incoming light.

These devices are easy to prepare thanks to the “self-aligning” property of the CU synthesized C6H monomer (see discussion in chapter 4 of this thesis).

A preliminary investigation of the electro-optical and morphology properties of reverse-mode PDLC films obtained by processing a mixture of C6H with the ZLI 4788-000 liquid crystal, has been recently presented ⁽³⁾. The electro-optical responses has been correlated to the changes in the morphology induced by the different UV curing powers. In these studies a matching of the n_0 indices of the two separate phases composing the film could be only approximately made thanks to the big quantity of ZLI which remained trapped into the polymer matrix, due the a very highly polymerization rate of the film. This could be obtained by using a quite strong UV irradiation, which on the other hand raises up the film conductivity due to the UV induced molecular fragmentation into the film.

A part of the thesis work was dedicated to match the refractive indices of the two phases composing the PDLC film, by using the C6H monomer in combination with another diacrylate LC monomer having a much lower refractive n_0 index with respect to that of C6H. As a new partner of the system: the UNICAL synthesized monomer bis{4-[6-(acryloxy)hexyloxy]benzoate}-4,4'-bicyclohexyl (AHBB) was chosen. In fact, the AHBB, which chemical structure is shown below, having two cyclohexyl rings in the molecular framework, was expected to have a much lower n_0 refractive index with respect to C6H ⁽⁵⁾.



Different mixtures of the above monomer with C6H were used in PDLC formulation. The uniform homeotropic orientation of PDLC precursor mixture was obtained by using the commercial C6H, previously reacted with the DMAP, as described in Chapter 4. Other PDLC cell have been prepared by aligning the LC precursor solution by pre-treating the support glass surfaces with [3-(trimethoxysilyl)propyl]octadecyl-dimethylammonium chloride (DMOAP).

5.2 Films preparation methodology

ZLI 4788-000 was supplied by Merck, while the commercial C6H monomer was supplied by Poland Synthesis Group led by prof. Roman Dabrowski.

The PDLC precursor mixtures were prepared mixing the ZLI with monomers C6H and AHBB (the relative ratio of the two monomers AHBB/C6H was varied in the range from 100/0 to 0/100). About 2% of photoinitiator, Irgacure 651 (supplied by Ciba-Geigy, for the monomer matrix polymerization) was added to the precursor mixtures.

The full composition of the investigated PDLC film was:

- 16% of monomer component, 82% of ZLI, 2% Irgacure (w/w);
- 20% monomer component and 78% of ZLI, 2% Irgacure (w/w).

After mixing and stirring of the appropriate amounts of the components, the mixtures were heated above the nematic-isotropic transition temperature, at about 120°C. The isotropic solution was introduced by capillarity into home-made cells, whose thickness was set about 25 μm , by means of glass spheres.

The cell walls had an indium tin oxide (ITO) conductive substrate, which was 120 nm thick.

For inducing the homeotropic orientation in PDLC with 100% AHBB monomer and in those with not-aligning C6H, cells pre-treated with a DMOAP solution (Fluka), according to standard procedure ⁽⁶⁾, has been used.

The sample was cooled until it reached an homeotropically aligned nematic state, and it was cured at 65°C for 10 minutes, using an UV Lamp at uniform power of about 0.5 mW/cm².

| sample | Name Mixture | ZLI 4788-000 wt% | Total Monomer wt% | Monomer fraction | | DMOAP treated glasses |
|--------|--------------|---------------------|-------------------------|------------------|------------|-----------------------------|
| | | | | AHBB wt% | C6H wt% | |
| 1 | 16%AHBB-0* | 82 | 16 | 0 | 100 | No |
| 2 | 16%AHBB-40* | 82 | 16 | 40 | 60 | NO |
| 3 | 16%AHBB-50* | 82 | 16 | 50 | 50 | No |
| 4 | 16%AHBB-60* | 82 | 16 | 60 | 40 | NO |
| 5 | 16% AHBB-70* | 82 | 16 | 70 | 30 | No |
| 6 | 16% AHBB-90* | 82 | 16 | 90 | 10 | No |
| 7 | 16% AHBB-100 | 82 | 16 | 100 | - | Yes |
| 8 | 16% AHBB-90 | 82 | 16 | 90 | 10 | Yes |
| 9 | 16% AHBB-70 | 82 | 16 | 70 | 30 | Yes |
| 10 | 16% AHBB-0 | 82 | 16 | -0 | 100 | Yes |
| 11 | 20% AHBB-100 | 82 | 20 | 100 | 0 | Yes |
| 12 | 20% AHBB-90 | 78 | 20 | 90 | 10 | Yes |
| 13 | 20% AHBB-70 | 78 | 20 | 70 | 30 | Yes |
| 14 | 20% AHBB-0 | 78 | 20 | 0 | 100 | Yes |
| 15 | 20% AHBB-90* | 78 | 20 | 90 | 10 | No |
| 16 | 20% AHBB-70* | 78 | 20 | 70 | 30 | No |
| 17 | 20%AHBB-0* | 78 | 20 | 0 | 100 | No |

Tab 5.2 *Formulation Of the investigated PDLC. (*) indicates that the samples contained the spontaneous aligning C6H monomer and no surface treatment was used. The remaining to % of the chemical formulation was Irgacure.*

5.3 Electro-optical measurements

The electro-optical properties of the reverse-mode films were measured at room temperature using the experimental setup, shown in Figure 5.1, made up of a He-Ne Laser (632.8 nm), as light source, with a power of 2 mW.

The light beam goes through the chopper rotating disk, and enters a diaphragm able to eliminate reflections. Later, the ray is directed through beam expander in order to correct the intrinsic laser divergence. This yields a collimated beam that goes through a second diaphragm, which reduces the dimension of the laser beam incident on the film. Transmitted light is collected by a detector, converted in an electrical signal and sent to a lock-in-amplifier, controlled by the reference chopper signal.

The output signal is then sent to a computer and recorded. The applied voltage is controlled by a Digital Analogical Converter (DAC).

Measurements were performed using an alternating signal at a frequency of 1 KHz.

The intensity of the incident light measured with no sample in place was assumed to be the full-scale intensity.

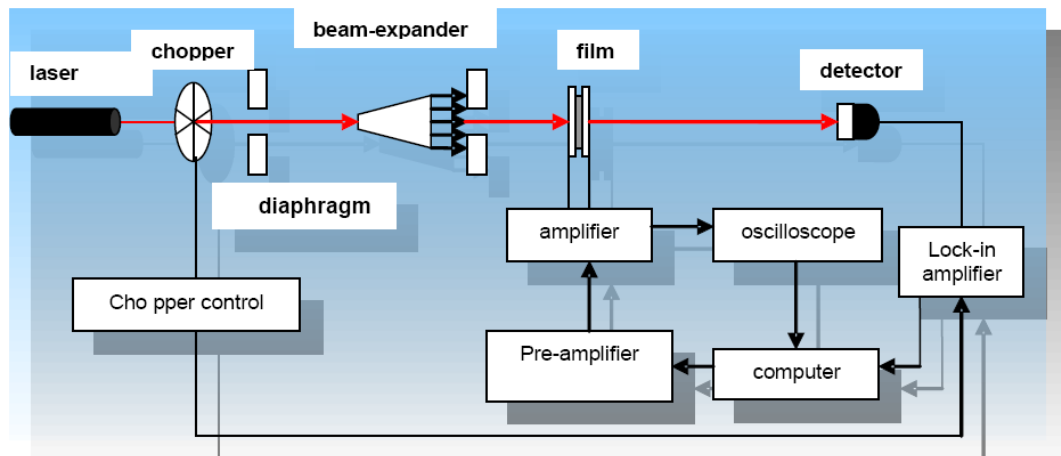
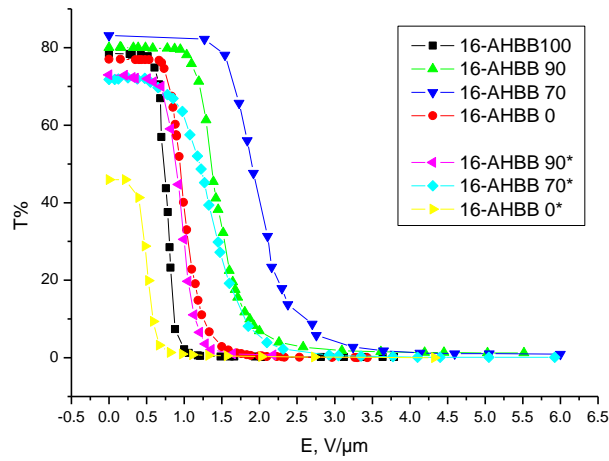


Fig 5.1 Schematic drawing of the experimental setup.

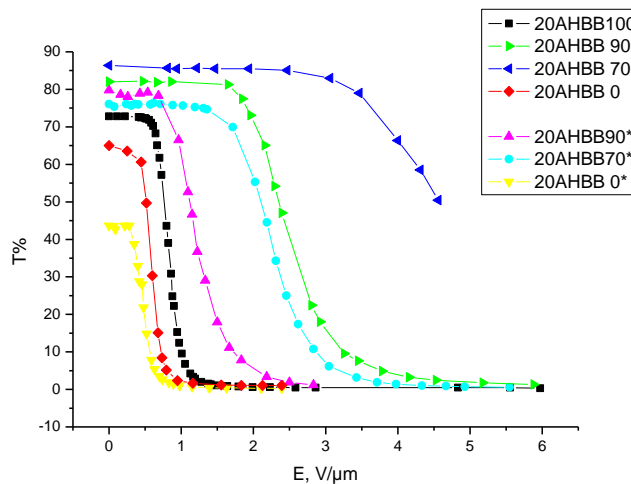
The electro-optical properties of the samples were as investigated by determining their optical transmittance as a function of the applied electric field.

Figure 5.2 shows the electric field dependent transmittance through PDLC films containing different amounts of the monomer AHBB. For simplicity we divided the samples on four groups, taking account of the total monomer weight percent in the film (16 or 20%) and of the method used to obtain the homeotropic alignment (glass pre-treated with DMOAP or use of aligning C6H (=*))

To illustrate the general trends, the experimental data have been plotted in several ways in order to put in evidence the different factor influencing the main operational parameters of the PDLC cell, that is to say, the switching voltage and optical response.



A



B

Fig.5.2 Comparison between electro-optical responses of surface treated and spontaneously aligning (*) samples. The total amount of polymer in the film was 16% for

A and 20% for B.

Data compared in Fig 5.2 shows three important results: a) the optical transparency of the film in the off state reaches a maximum value when the polymer part of the film contains 70% of AHBB; b) The operational field increases at higher polymer content; c) the operational field increases dramatically for sample with pretreated glass surface. In the case of sample 20HABB-70 (Fig.5.2 B) the full switch of the sample could not be reached since the field increased too much and the sample would be destroyed for further increase of the applied voltage. This effect is mainly due to fact that part of the applied voltage drops to the sides of aligning layers deposited on the glass surfaces. It is not easy to account for his effect since the lack of reproducibility of surface coating treatments.

Another effect is well pointed out with the help of the next fig. 5.3.

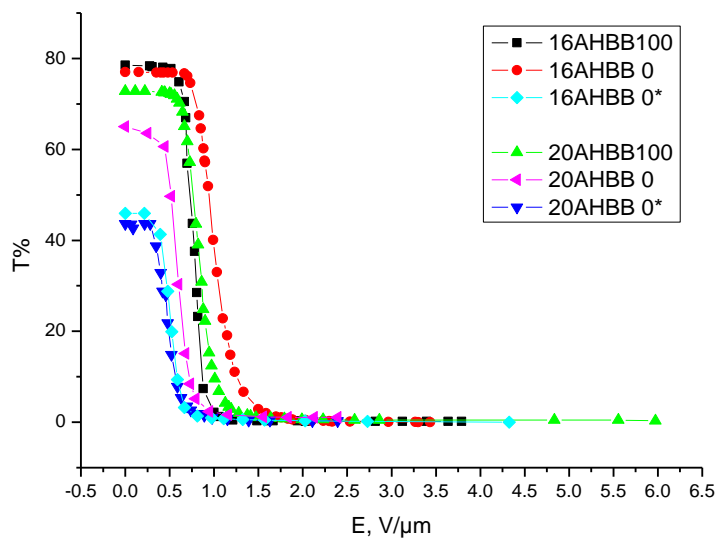


Fig.5.3 Comparison between electro-optical responses for mixtures containing only AHBB or C6H monomer. Note that All the samples show low operational voltages

This figure shows clearly that the threshold field remains around 1 volt/micron when only one monomer is used, almost independently from the type of monomer used. So is the mixing of the two different monomers to create a large spread, or more precisely a big increase, at parity of other conditions, in the threshold field.

The morphologic analysis shown in the following will furnish a possible interpretation of this phenomena.

The next figure 5.4 gives a further contribute to the discussion. Here the electro optical response of 16% polymer samples, obtained by using the spontaneous aligning properties of the C6H monomer, is reported as a function of the gradual increase of the AHBB monomer with respect to C6H one.

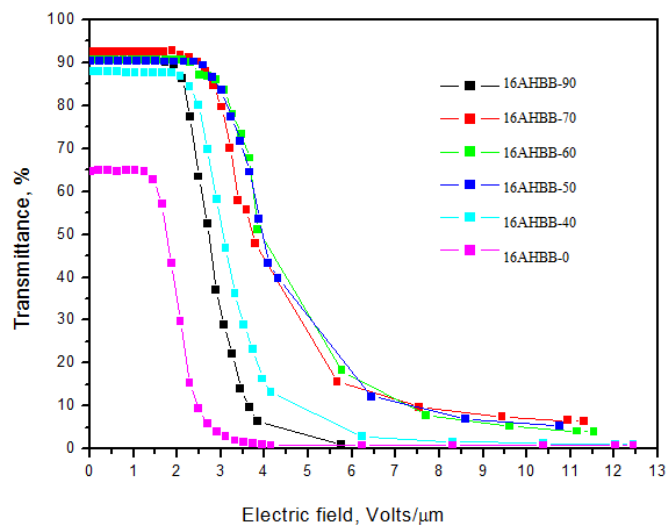


Fig. 5.4 Comparison between electro-optical responses of PDLC films as a function of the gradual increase in AHBB concentration.

Data shown in fig 5.4 are not affected by surface treatment of the cells, so they allows a reliable interpretation of the electrooptical response, in terms of morphologic models. For this reason the discussion will be limited to these data in the next. optical contrast (ratio between T_{off} and T_{on}) has been calculated, by data reported in fig.5.4. Results are shown in the next fig. 5.5, together with the T_{off} and T_{on} transmittance. The best sample from the point of view of the optical contrast is the sample 16 AHBB-90.

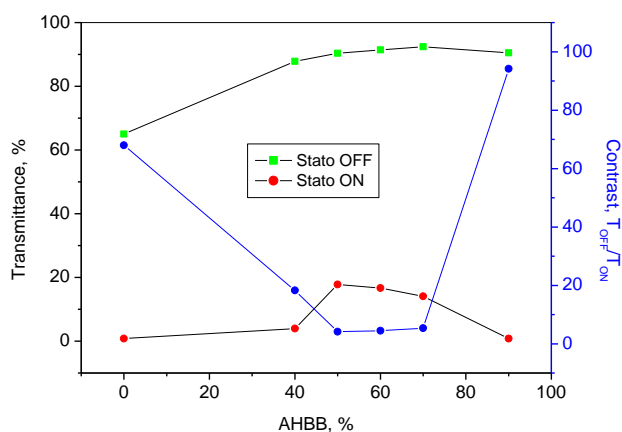


Fig. 5.5 OFF and ON state transmittances and contrast ratio as functions of AHBB weight percentage, with respect to the total monomer composition

A further characterization of our PDLC film was made by measuring the response time, i.e. the rise and decay times.

Rise time (t_{rise} or t_{on}) is the time needed so that film transmittance decreases to 10% by application of a suitable electric field, and the decay time t_{off} is the time in which the film, starting from an opaque ON state, reaches the 90% of its OFF state (max) transmittance, after field removal.

A suitable driving voltage of 1 kHz was applied for the measurements.

Results for t_{off} are shown in the next fig.5.6, for samples which electrooptical response is illustrated in fig 5.4. In the same figure the threshold field, of the Fréedericksz transition, for the same samples, are also reported for completeness. The threshold fields, E_{th} , here is defined as the electric field required to reach 90% of the maximum transmittance, as the AHBB concentration increases, increase up to a maximum, corresponding to the 70% of AHBB, and then decrease. The four groups of mixtures exhibit identical behaviour.

The decay time (t_{off}), i.e. the necessary time for the homeotropic realignment of the liquid crystal molecules, after the field removal, ranges from 0.5 to 8 msec. These data confirms that the 16AHBB-90 formulation is also very good from the point of view of the operational parameters. It has a very fast response (about 2 ms) and a reasonable threshold field (about 2 volts/micron)

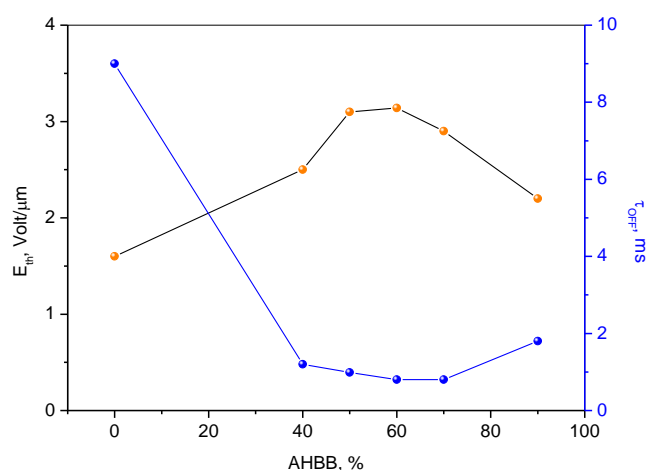


Fig.5.6 Threshold electric field, E_{th} (orange) and decay time, τ_{OFF} (bleu), as a function of AHBB wt%, with respect to total monomer composition.

Data reported in fig. 5.6 have been interpreted in terms of a simple model which will be presented in the following after the discussion of morphologic data.

5.4 Morphologic analysis of PDLC films

To have a complete analysis of the samples, the morphological analysis of the reverse-mode films, with 16% monomer content, was performed by a Leica Leo 420 scanning microscope (SEM). The post elaboration was achieved by the “Image J” software.

Polymerized films were cut after immersion in liquid nitrogen, and fixed on microscope stubs. The samples were left under vacuum at 10^{-3} Torr for several hours in order to extract the liquid crystal; successively they were gold coated, and finally examined.

Both the samples with 70 and 90% of AHBB appear to be made by fractured polymeric structures separated by “void channels“, regions which were full of ZLI liquid crystal. This type of morphology was observed, in single monomer film, only for high UV irradiation power, about 100 mW/cm^2 .

The long range spatial heterogeneity (large voids separated by polymer dense regions) of the film it is strongly linked to the presence of two different monomers having a

different reactivity with respect to the polymerization reaction, and is compatible with a spinodal decomposition during the polymerization process (see par 2.6)

The voids have an almost regular elliptic shape, with a little tendency, as shown in the SEM images of the sections, to a “triangle” shape, depending on the different UV power feels at the two opposite glasses of the cell.

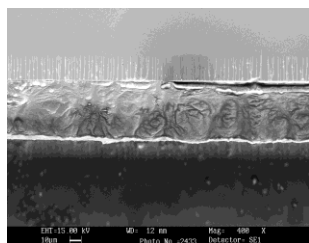
The lost of scattering efficiency of the film in ON state in the range of film composition of 70 and 90 AHBB wt% could be explained by this morphology:

Large channels having an elliptic shape, where the minor transversal dimension is around 5 microns do not efficiently scatter light. The structure of the void channels is better illustrated in figures.

This effect is almost absent in samples of AHBB-100 and AHBB-0, where the void volume fraction is reduced.

Further, the inner surfaces of voids (see fig 5.9), progressive increasing of magnification) appear to be made by elongated polymer filaments developing perpendicularly to the film surface, while the central part of the polymer network contains smaller voids. These features suggest that a good model to apply to have a quantitative interpretation of the electro optical response (threshold voltage and decay time) can assume that the liquid crystal, remained more finely entrapped into the polymer structure, is dispersed as a multitude of elongated elliptic droplets, according to the SEM images, where the nematic director, in the off state, is parallel to the major axis.

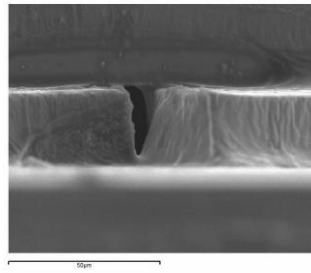
From the SEM images, the fraction of volume occupied by the void channels seems much greater in sample AHBB-70, respect to the AHBB-90 on both the samples with pre-treating of the glasses.



a

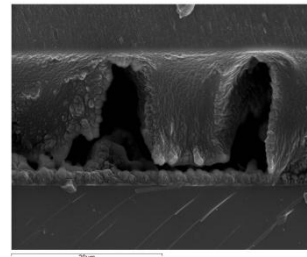
pre-treated with DMOAP

16% AHBB-100



b

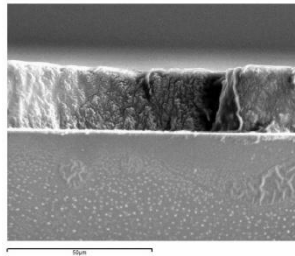
with DMOAP,



c

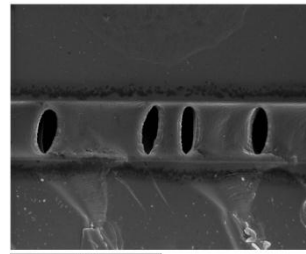
*with C6H**

16% AHBB-90



d

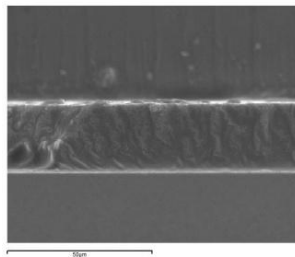
with DMOAP,



e

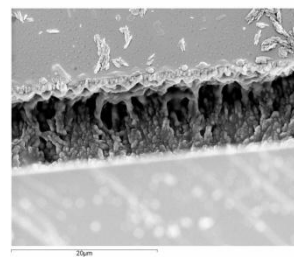
*with C6H**

16% AHBB-70



f

with DMOAP,

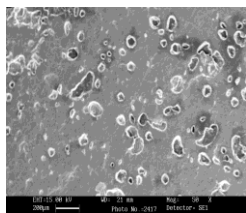


g

*with C6H**

16% AHBB-0

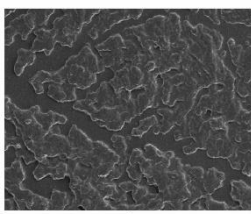
Fig 5.7 SEM images of film section of 16-AHBB-100, -90-70,-0 samples



h

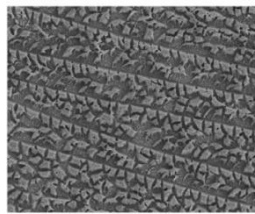
cell pre-treated with DMOAP

16% AHBB-100



i

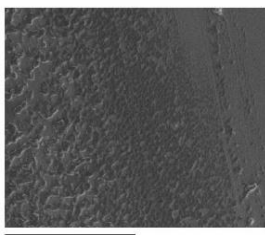
with DMOAP,



l

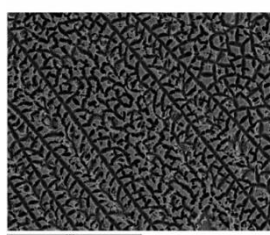
with C6H self-aligning

16% AHBB-90



m

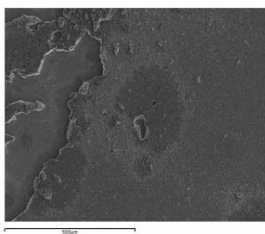
with DMOAP,



n

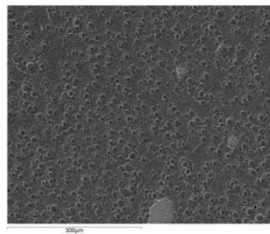
with C6H self-aligning

16% AHBB-70



o

with DMOAP,



p

with C6H self-aligning

16% AHBB-0

Fig 5.8 SEM images of in plane film of 16-AHBB-100, -90-70,-0 samples

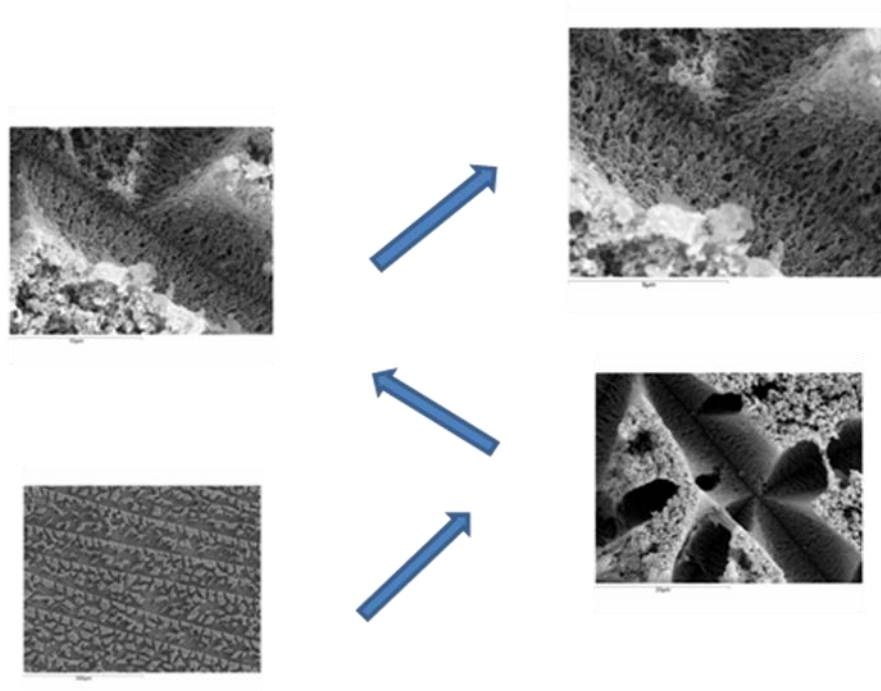


Fig 5.9 SEM images illustrating the progressive increasing in magnification. The channels appear made of elongated polymer filaments developing perpendicularly to the film surface and leading smaller voids.

5.5 Model for E_{th} and response times t_{off}

A competition between the applied field and the elastic and viscous torques of the LC govern the response times and switching voltage of this kind of device.

Useful equations to model the threshold voltage and the decay time for elliptic droplets PDLC have been derived time ago in the case of normal mode PDLC films ^{(7) (8)}.

We model the domain of the nematic director by ellipses of dimensions a and b (semi-major and semi-minor axis)

In this case the threshold voltage needed to reorient the nematic director along the semi-minor axis ($\Delta \epsilon$ is negative in our case), and the time required to turn the director back on equilibrium configuration, after removing the electric field, are given by the following equations:

$$E_{th} = F(\rho_p, \rho_{CL}, r_p, r_{CL}) \cdot \frac{1}{a} \cdot \left(\frac{K \cdot (l^2 - 1)}{\Delta \epsilon} \right)^{\frac{1}{2}} \quad (1)$$

$$\tau_{OFF} = \frac{\gamma \cdot a^2}{K(l^2 - 1)} \quad (2)$$

The term $\frac{1}{a} \cdot \left(\frac{K \cdot (l^2 - 1)}{\Delta \epsilon} \right)$ in equation 1 is the critical field required into the elliptic droplet to balance the torque exerted by the elastic force on tilting the nematic director.

K is the elastic constant

a, b are the length of the ellipsis major and minor axis

l is the aspect ratio of the nematic ellipsoid: $l = a/b$

γ is the rotational viscosity of the liquid crystal.

The function F represents a scalar factor between the external threshold field and the critical field acting in the droplet. This is due to a pure electric effect and depends on:

- the polymer and liquid crystal resistivity (ρ_p and ρ_{CL})

➤ the relative thickness r_P and r_{CL} (the ratio between the average thickness of each material with respect to the full film thickness) of the polymer and liquid crystal mixed in the film.

In order to have an idea of the order of magnitude of the F function value, we can estimate it on the basis of a simple model, assuming that the film, from an electric point of view, can be assimilated to a couple of resistors. Having defined the meaning of ρ_p , ρ_{cl} , r_p , r_{cl} , on the basis of a simple circuit analysis :

$$F = \left(\frac{\rho_p}{\rho_{CL}} \cdot r_p + r_{CL} \right) \quad (3)$$

When considering equation 2 we need only to remind that γ is the rotational viscosity of the liquid crystal.

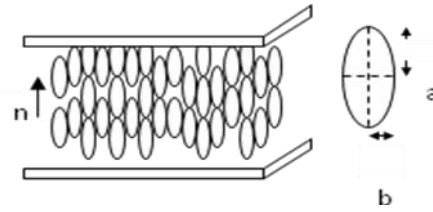


Fig 5.10 Model of liquid crystal distribution into the polymer matrix.

We can further simplify the above written equations by considering that in the present case as it is evident from the SEM analysis of the films $l \gg l$. Then in first approximation equations 1 and 2 can be simplified in the following equations 3 and 4:

$$E_{th} = F \cdot \left(\frac{K}{\Delta \varepsilon} \right)^{\frac{1}{2}} \cdot b^{-1} \quad (3)$$

$$\tau_{OFF} = \frac{\gamma}{K} b^2 \quad (4)$$

According to this simplified model the threshold field and decay time should depend only on the value of the elliptic minor semi axis.

In order to check the proposed interpretation of the electro optical property of the films:

- 1) we derived the value of b using equation 4 and τ_{off} values measured $\gamma = 225 \text{ mPa}\cdot\text{sec}$ and $K=18.9 \text{ N}$ (by Merck)
- 2) we used the b value obtained, to calculate E_{th} , leaving F to vary in order to reach the best fitting of the experimental data.

The calculated parameters are shown together with the experimental in the following tab.5.3

| Sample | τ_{off} <i>ms</i> | b <i>micron</i> | $E_{th (exp)}$ <i>volt/micron</i> | $E_{th (calc)}$ <i>volt/micron</i> | $\Delta E_{th} (\%)$ |
|--------|---------------------------|----------------------|--------------------------------------|---------------------------------------|----------------------|
| 1 | 9.00 | 0.90 | 1.60 | 1.50 | +6.0 |
| 2 | 1.20 | 0.33 | 2.50 | 2.54 | - 1,60 |
| 3 | 1.00 | 0.30 | 3.10 | 2.67 | + 16,10 |
| 4 | 0.75 | 0.26 | 3.14 | 2.87 | + 9,40 |
| 5 | 0.75 | 0.26 | 2.90 | 2.87 | + 1,00 |
| 6 | 1.7 | 0.39 | 2.20 | 2.34 | - 5,98 |

Table 5.3 *Experimental and calculated values of E_{th} and τ_{off}*

As it is possible to see from the results shown in Table 5.3 the differences between the calculated and experimental E_{th} values are, on average, of the order of 16% maximum. We consider this result a positive test of the applied model for at least two main reasons. First of all it must be considered that the experimental data are chosen in a very arbitrary way, assuming that the threshold field corresponds to the value of the field required to obtain a reduction of the 10% of the light transmission. As a second point it must be underlined that the model has been chosen on the basis of the morphology characterization of the films containing two different monomeric precursors of the polymer matrix which has

been deeply discussed above. Sample 1 is, instead, obtained from a single monomer (C6H) and the morphology in this case is quite different, as it is shown in Figure 5.7g. The morphology of sample 1 is more next to that of a PSLC systems, where isolated polymer filaments are able to contain the liquid crystal phase without interrupting the continuity of the phase. Then, for sample 1, here reported only for comparison, a different model should be applied: for example that reported by Kossyrev et al. ⁽⁹⁾. In the bi-monomer films, part of the liquid crystal transfers into the large channel, and part remains finely dispersed into the polymer matrix cannot be considered as a PSLC. Another important point to underline is the value of the F function which has been used to calculate the threshold field of Table 5.3. The best fit is actually obtained when F is equal to 1.

This value is the limit value of the function when the thickness ratio of the polymer r_p goes to zero, since contemporaneously r_{CL} goes to 1. This means that even the liquid crystal dominion finely dispersed into the polymer can be considered as an elliptic droplet joining the two opposite surface of the film (a =film thickness). This is an advantage for this kind of systems, since the applied field can reach the liquid crystal without any shield due to the polymer matrix. Nevertheless, the operational voltage is quite high, since the minor axis of the liquid crystal aggregate are quite small and the elastic force require a quite high balancing electric field.

5.6 Conclusions

This part of the thesis work brings to some valuable conclusion with respect to the Reverse mode PDLC system obtained by Phase separating a negative dielectric Liquid crystals, during the polymerization of LC monomers contained, as a minor component, in the precursor mixture. A good homeotropic alignment, of the precursor solution, need to be obtained in order to get a very transparent OFF state film. Here it has been shown that such a good homeotropic alignment can be obtained by using, as polymer precursors, diacrylate LC monomers containing suitable aligning impurities, which nature has been clarified in the previous chapter. This aligning method gives better system, when the threshold

operational field is taken into consideration. In fact much bigger switching fields are required in the case that aligning surface coatings are used.

Another valuable conclusion is that mixtures of diacrylate monomers, with slight different cores, can be used to obtain polymer matrices having the n_o index well matched with the corresponding index of the of the other LC component .

Nevertheless when mixtures of diacrylate monomers are used, the morphology of the final films tends to assume , at least in the investigated system, a conformation where very elongated LC dominium are separated by very tiny polymer walls.

We have shown that very high contrast Reverse Mode PDLC films can be obtained by matching appropriately the refractive indices of the polymer and the liquid crystal.

The morphology investigation has been found very useful to suggest the way to rationalize the factor influencing the operational electro optical parameters. It has been further shown that the morphology is characterized by the presence of two type of liquid crystal segregations: one corresponding to large liquid crystal longitudinal channels and the other to vertical submicron channels, which are responsible of the electro optical contrast of the film. We believe that what reported on this paper opens a new challenging research argument: how to optimize the size and geometrical features of the large channels. It could be interesting to obtain ordered oriented channels in order to get different optical properties and different modulation possibility for these regions. In order to reach this goal, work must be done to understand what are the physical parameters which control the morphology. Of course it is possible to hypothesize that among these parameters a critical role must be paid by the polymerization speed of the monomers, the diffusion coefficient of the reactants and the relative concentration of the components. Investigations will follow on this subject in the next future.

References

1. G. Chidichimo, G. De Filpo, *European Patent n° WO9816865 (1997)*.
2. G. Chidichimo, G. De Filpo, *European Patent n°WO9900464 (1997), U.S. Patent n°6,383,577 B1 (2002)*.
3. G. De Filpo, R. Cassano, L. Tortora, F.P. Nicoletta, and G. Chidichimo, *Liq. Crys.*, 35, 45, 2008.
4. L. Tortora, *Ph.D. Thesis, Optical shutters by Liquid Crystal Organic Dispersions, 2004*.
5. R. Cassano, R. Dabrowski, J. Dziaduszek, N. Picci, G. Chidichimo, G. De Filpo, R. Muzzalupo, F. Puoci, *Tetrahedron Letters*, , 48, 1447, 2007.
6. K.Takatoh et al., “*Alignment technologies and applications of liquid crytal devices*”, Taylor&Francis, 2005.
7. J. Erdmann, J.W. Doane, S. Zumer, and G. Chidichimo; *SPIE Vol.1080, Liquid Crystal Chemistry, Physics and Applications*, 32, 1989.
8. B.Wu, J. Erdmann, J.W. Doane, *Liq. Crys*, 5, 1453, ., 2008.
9. P.A. Kossirev, J.Qi, N.V. Priezjev, R. A. Pelcovits, and G.P. Crawford, *Appl. Phys. Lett.*, 81, 2986, 2002.

Acknowledgments

First of all, I would like to thank Professor Lev Blinov for his precious suggestions and his help during this research work, and the Doctor Alexander Turin who helped me in the interpretation of the scientific articles in Russian;

I would also like to thank professor Anna Napoli for the MALDI analysis and especially for the great willingness and kindness with which give me important suggestions about the organic synthesis mechanisms. I would like to thank professor Luigi Coppola for the DSC analysis and the doctor Amerigo Beneduci that supported me, with great patience, for all the NMR studies.

I am also very grateful to professor Giuseppe Chidichimo, for his critical review of the manuscript, and to all the Research Group for their support.

A heartfelt thanks to the doctor Teresa Cerchiara who, with his friendship and experience, supported me during these long years of work.

Finally, a very endless "thank you" to the "BDG" (Lo and Giò) and to the 'new entry' Andrea, because without them, this work would never come to an end.

Caterina

"Two things fill the mind with ever new admiration and reverence, and increasingly, as often and as long as we reflect on them: the starry heavens above me and the moral law within me"

(I. Kant, Critica della ragion pratica)